**Mohamed Khider University of Biskra**
Faculty of Science and Technology
Department of Electrical Engineering

# MASTER'S THESIS

Science and Technology
Electrotechnics
Electrical Networks

Ref: Enter the document reference

---

Presented and defended by:

***Mezine Sohaib***

On: Wednesday, June 18, 2025

# Optimal management of reactive power by a new metaheuristic technique

---

**Jury:**

| | | | | |
|---|---|---|---|---|
| Dr. | MOHAMED REZIG | MCB | University of Biskra | President |
| Pr. | NAIMI DJEMAI | Professor | University of Biskra | Examiner |
| Dr. | SOUHEIL SALHI | MCB | University of Biskra | Supervisor |

***CLASS OF 2025/2026***

**Mohamed Khider University of Biskra**
Faculty of Science and Technology
Department of Electrical Engineering

# MASTER'S THESIS

Science and Technology
Electrotechnics
Electrical Networks

Ref: Enter the document reference

---

# Optimal management of reactive power by a new metaheuristic technique

On: Wednesday, June 18, 2025

Presented by:

MEZINE SOHAIB

Favorable opinion of the supervisor:

SOUHEIL SALHI

Favorable opinion of the Jury President:

MOHAMED REZIG

Seal and signature

## ملخص:

تتناول هذه المذكرة مشكلة التوزيع الأمثل للقدرة التفاعلية **(ORPD)** في أنظمة الطاقة الكهربائية، باعتبارها إحدى التحديات الهامة لتحسين استقرار الشبكة وتقليل الخسائر وضمان جودة الجهد. تم في هذا العمل مقارنة عدة خوارزميات ميتاهيوريستية، من بينها الخوارزمية الجينية **(GA)** وخوارزمية الذئب الرمادي **(GWO)** بالإضافة إلى الخوارزمية المقترحة **Tunicate Swarm Algorithm (TSA)**.

تم تطبيق هذه الخوارزميات على أنظمة الاختبار ذات سعة 30 و57 حافلة من معيارIEEE ، مع دوال هدف تركز على تقليل فقدان القدرة الفعالة والانحراف الكلي للجهد .(TVD) أظهرت النتائج أن خوارزمية سرب التونيكيت (TSA) توفر توازناً قوياً بين الاستكشاف والاستغلال، محققة أداءً متفوقاً من حيث سرعة التقارب ودقة التحسين مقارنة بالطرق الأخرى.



**الكلمات المفتاحيه**: التوزيع الأمثل للقدرة التفاعلية(ORPD) ، إجمالي ضياعات الاستطاعة الفعالة ($P_{loss}$) ، الانحراف الكلي للجهد (TVD)، خوارزمية سرب التونيكيت (TSA).



## *Abstract*

This thesis addresses the Optimal Reactive Power Dispatch (ORPD) problem in electrical power systems, which plays a key role in enhancing voltage stability, reducing power losses, and improving power quality. Several metaheuristic algorithms were evaluated, including the Genetic Algorithm (GA), Grey Wolf Optimizer (GWO), and the recently proposed **Tunicate Swarm Algorithm (TSA).**

These algorithms were applied to IEEE 30-bus and 57-bus test systems, with objective functions focusing on minimizing active power losses and Total Voltage Deviation (TVD). The results demonstrated that TSA offers a strong balance between exploration and exploitation, achieving superior performance in terms of convergence speed and optimization accuracy compared to the other methods.



**Key words**: Optimal Reactive Power Dispatch (ORPD), Total Active Power Losses ($P_{loss}$), Total Voltage Deviation (TVD), Tunicate Swarm Algorithm (TSA).



## *Résumé*

Ce mémoire traite du problème de répartition optimale de la puissance réactive (ORPD) dans les systèmes électriques, un enjeu crucial pour améliorer la stabilité de tension, réduire les pertes d'énergie et garantir une qualité de service optimale. Plusieurs algorithmes métaheuristiques ont été comparés, notamment l'algorithme génétique (GA), l'optimiseur du loup gris (GWO) ainsi que le nouvel algorithme **Tunicate Swarm Algorithm (TSA)**.

Ces méthodes ont été appliquées sur les réseaux tests IEEE 30-bus et 57-bus, en visant des fonctions objectifs telles que la minimisation des pertes actives et de la déviation de tension totale (TVD). Les résultats ont montré que l'algorithme TSA fournit un bon équilibre entre exploration et exploitation, avec une excellente performance en matière de rapidité de convergence et de précision des résultats.



**Mots clés** : répartition optimale de la puissance réactive (ORPD), pertes totales de puissance active ($P_{loss}$), déviation totale de la tension (TVD), algorithme de l'essaim des tuniciers (TSA).

# *Dedication*

*I extend my deepest gratitude and heartfelt appreciation to my beloved mother Kenza Gherabli, who has always stood by my side throughout every stage of my life, and to my dear father Hassen as well, for his continuous efforts and unwavering support*

*I warmly extend my greetings to my family, especially my brothers Nadjib and Moqim, Mohamed and my dear sister, my maternal aunt*

*I extend my warmest greetings to the entire Ramzi's family*

*I give special thanks to my friends Rashid and Rahim for standing by me during the difficult days.*

*My greetings to my brother's friends, Nayel and Boba.*

# *Acknowledgements*

First and foremost, all praise is due to Allah for this success. I thank and glorify Him with abundant, pure, and blessed praise. My deep gratitude goes to Him, for without His will and guidance, I would not have reached this point.

'Alhamdulillah'

I would like to extend my sincere thanks and gratitude to all the members of the committee: Professor Djamai Naïmi, Dr. Mohamed Rezig, and our supervisor, Dr. Souheil Salhi, for the great honor of their presence at the presentation of our graduation thesis. Their presence on this special day is a great privilege that we deeply appreciate.

All thanks and appreciation go to my supervisor, doctor Mr. Salhi Souheil, for his support and assistance throughout our journey in completing this dissertation.

A special thanks goes to our professor, Professor Djamai Naïmi, for his valuable support and assistance through the knowledge and advice he provided us throughout those periods.

# *SUMMARY*

# SUMMURY

# *List of Figures*

# *Symbol Definitions*

| Symbol | Definition |
|---|---|
| $V$ | Voltage magnitude |
| $P$ | Active power |
| $Q$ | Reactive power |
| $S$ | Apparent power which represents the total power supplied |
| $Z_s$ | Line impedance |
| $X_s$ | Line reactance |
| $\delta$ | Voltage angle difference between the sources |
| $\phi$ | Phase shift angle between active power and apparent power |
| Y | Admittance matrix |
| $b_{ij0}$ | The transverse susceptance |
| $y_{ij}$ | The complex admittance of the branch connecting nodes $i$ and $j$ |
| $f$ | Objective function |
| g(x,u) / h(x,u) | Set of equality constraints/set of inequality constraints |
| $T$ | Transformer tap ratio |
| $Q_C$ | Reactive power of capacitor bank |
| TVD | Total Voltage Deviation |
| $P_{loss}$ | Power Losses |
| $\alpha$ | Random weight parameter in crossover |
| $r_1$, $r_2$ | Random numbers in GWO algorithm |
| $A$, $C$ | Coefficient vectors in GWO algorithm |
| $N_p$ | Population size |
| $\lambda_V$ , $\lambda_Q$ | The penalty factors |
| Max_iteration | Maximum number of iterations |

# *GENERAL INTRODUCTION*

# GENERAL INTRODUCTION

Electrical power systems are among the most critical infrastructures in modern societies, supporting all sectors from daily life to industry and advanced technology. As these systems grow in size and complexity with increased energy demand, network expansions, and the integration of renewable energy sources it becomes essential to manage power flow efficiently to ensure a balance between generation and consumption, while maintaining system stability and reliability. One of the major operational challenges in power networks is reactive power management, which directly affects voltage control, power loss reduction, and overall system performance. This highlights the importance of Optimal Reactive Power Dispatch (ORPD), which seeks to determine the most efficient operating conditions while satisfying technical and operational constraints. Traditional optimization techniques often fall short in solving the highly non-linear and multi-dimensional nature of ORPD problems. Consequently, recent years have witnessed a growing interest in metaheuristic algorithms, known for their ability to find near-optimal solutions within complex search spaces without requiring derivative information.

This thesis aims to introduce and implement the Tunicate Swarm Algorithm (TSA) as a novel metaheuristic for solving the ORPD problem, and to compare its performance with well-established algorithms. Through simulation on standard IEEE test systems which are 30 and 57 bus in different mono objectives active power losses ($P_{loss}$), total voltage deviation (TVD) minimizations. demonstrating TSA's superior convergence speed and the best lowest results in both objectives. this study contributes to advancing optimization strategies in power systems and opens the door for more intelligent and adaptive control mechanisms in future smart grids.

The following is a synopsis of the thesis's structural organization.

Chapter 1: Electrical Grid

It gives a comprehensive foundation of the electrical grid, delineating its models and elucidating the function of power flow analysis in power grids and its formulation.

Chapter 2: Optimal Reactive Power dispatch

This chapter derives the bus admittance matrix for power flow analysis using classical methods, it focuses on Optimal Power Flow (OPF), and the mathematical formulation of Optimal Reactive Power Dispatch, with detailing its objectives (active losses, voltage deviation) and constraints. Furthermore, it sets the stage for metaheuristic techniques.

Chapter 3: The Meta-heuristics

Describes three metaheuristic algorithms as optimization methods: the Genetic Algorithm (GA), the Grey Wolf Algorithm (GWO), and our new metaheuristic Tunicate Swarm Algorithm (TSA), outlining their biological inspirations, modeling, and solution steps.

Chapter 4: Simulation Results and Analysis

In this chapter, the TSA algorithm is applied to IEEE 30 and 57 bus test systems, presenting and analyzing results against other methods to assess its performance and effectiveness in achieving ORPD objectives.

# CHAPTER I

# *CHAPITER 1*

## *Electrical Grid*

### I-1. Introduction

Firstly, the term “electricity system” generally denotes the entire network of electrically interconnected installations responsible for delivering kilowatt-hours to end users, with power generated from primary energy sources such as hydroelectricity, fossil fuels, nuclear fission, direct solar energy, and wind energy.[4]

Additionally, electrical power is generated and consumed at the same time, it is imperative that power of production be continuously adjusted to ensure it aligns with demand [5]. What is more, an electrical network is composed of power lines that function at various voltage levels. These lines are interconnected the function at different voltage levels. These lines are interconnected through the substations. The management of this network is entrusted to four specialized divisions: generation, transmission management, distribution, and the system operator, which implements settings to ensure the stability and reliability of the entire system [6] this integrated system known as electrical grid [5].

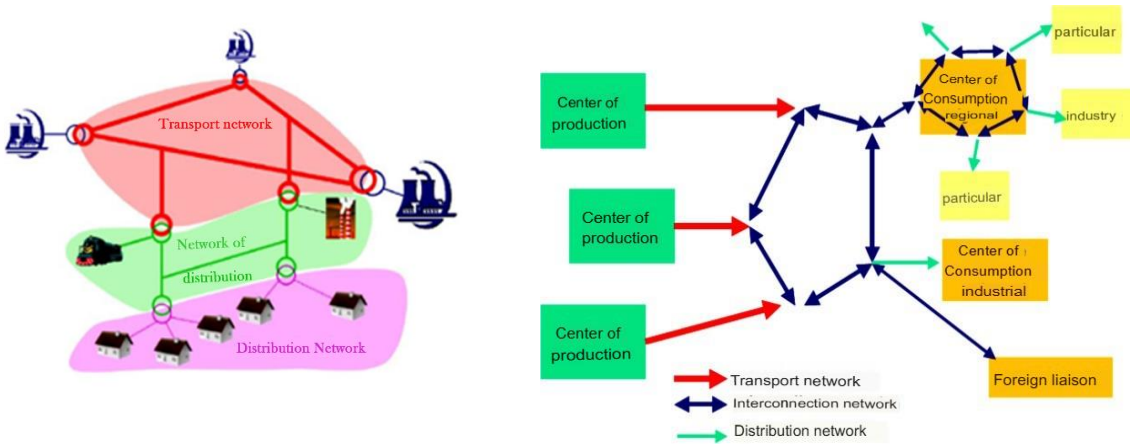


***Figure (I.1)**: general structure of an electrical network*

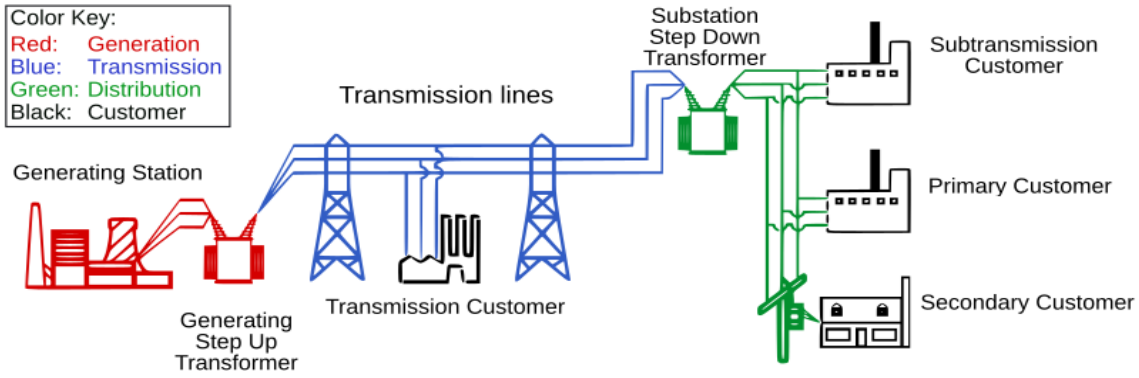


***Figure (I.2)*** *Simplified Diagram of the Electrical Power Grid*

## I-2. Topological Structure of Transmission Networks:

It has been demonstrated that all elements of an electrical network can be organized in different structures, with varying levels of complexity that influence both the availability of electrical energy and the investment cost.

The network must guarantee the secure transfer of electrical energy. The enhancement of supply security can be achieved by:

- Using more robust equipment for the power lines.
- Increasing the number of circuits.[7]

It is important to note that, the choice of architecture for each application is based on the criterion of achieving the optimal technical and economic balance.

### I-2-1. Radial Networks:

These networks originate from a power supply station and consist of multiple branches, each extending outward without reconnecting to a common point. Radial networks have a simple structure and can be managed and protected using basic equipment [8].

Additionally, there are two main configurations to be considered here:

- **Artery-cut structure:** Typical of underground networks, designed for potential loop operation.
- **Tree structure**: These are frequently utilized in rural overhead networks and are incorporating with loop points to ensure medium-voltage backup. As illustrated in Figures (I.3) and (I.4) examples of radial networks.

- ***Advantages:***
  - ✓ Easy to design and construct.
  - ✓ Maintenance operations can be carried out easily by opening the isolating device (disconnector, switch, etc.) at the starting of the network.
- ***Disadvantages:***
  - ✓ A fault at a main outlet affects all secondary outlets and the terminal distribution [6].

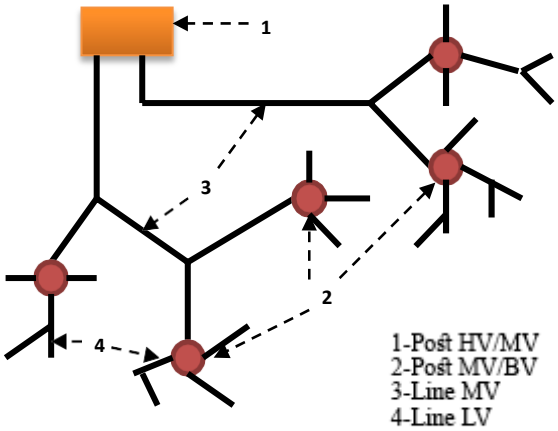


***Figure (I.3):*** *tree structure*

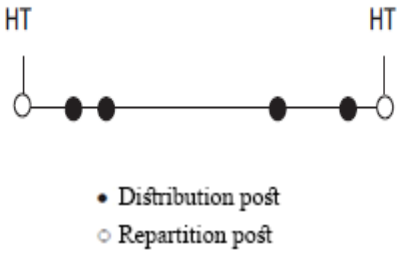


***Figure (I.4):*** *artery cut structure.*

## I-2-2. Looped Networks:

Looped networks are supplied by multiple sources simultaneously, with stations connected through artery cut-offs. This configuration ensures service continuity in the event of a power interruption.

In addition, the presence of multiple parallel sources enhances the reliability of the power supply, particularly in the event of a transformer failure or a fault in one of the loops. In such cases, the damaged section is isolated, dividing the network into two parts.

However, compared to radial networks, looped networks are more complex. Additionally, their control and protection require more advanced and sophisticated devices. [7]

**1**-Post HV/MV
**2**-Line MV
**3**-Post MV/LV
**4**-Line LV

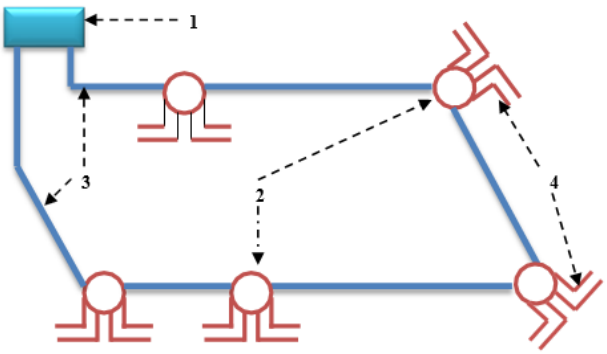


***Figure (I.5)*** *Schematic diagram of a loop network*

- ***Advantages:***
  - ✓ High service continuity
  - ✓ Good performance
  - ✓ Low voltage drop.

- ***Disadvantages*:**
  - ✓ High short circuit currents
  - ✓ More expensive and difficult to operate than radial networks.

### I-2-3. Mesh Networks:

A mesh network features interconnections that form a grid-like topology, providing enhanced supply security, improved service continuity, and reduced voltage drop. However, implementing a mesh network is a complex process that requires significant analysis and costs.[6]

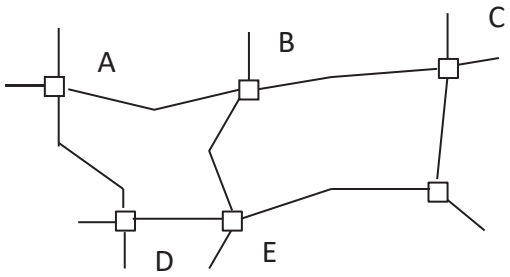


***Figure (I.6)*** *Mesh structure*

- ***Advantages***
  - ✓ Very high reliability and fault tolerance;
  - ✓ Optimized power distribution and load balancing
  - ✓ Lower voltage drops due to multiple pathways.

- ***Disadvantages***
  - ✓ High installation and maintenance costs
  - ✓ Complex control and protection mechanisms
  - ✓ Higher short-circuit currents

## I-3. Interconnection Networks:

Interconnection networks establish connections between power generation centers and facilitate energy exchanges between different regions, and even with neighboring countries.

Furthermore, these networks are designed so that all very high-voltage lines are interconnected through transformer stations, ensuring continuity between lines operating at different voltage levels.[6]

## I-4. Power Transmitted by a Power Line:

In a **DC circuit**, power is calculated as the product of voltage and current:

**P = V* I.**

This also holds true in an **AC circuit** when the voltage and current are in phase, meaning the circuit is purely resistive. However, if the AC circuit contains reactance, a power component is associated with the **magnetic and/or electric fields**. Unlike resistive power, this power is not consumed but rather stored and then discharged as the alternating current and voltage complete their cycles. [9]

Alternating current electrical networks provide **apparent power**, which represents the total power supplied. This power is divided into two components:

- **Active power:** Converted into mechanical energy (work) and heat (losses).
- **Reactive power**: Used to create magnetic fields.

Common consumers of **reactive power** include asynchronous motors, transformers, inductors, and static converters (such as rectifiers).

This leads to another definition:[9]

**Apparent power = Real or Active power (associated with a resistance)**
**+ Reactive power (associated with an inductance or capacitance).**

Using symbols:

$$S = P + jQ \quad \text{(I.1)}$$

### Active Power:

Active power is the power that is actually utilized and consumed for performing useful work in an AC or DC circuit. It is also referred to as **True Power, Real Power, Useful Power,** or **Watt-full Power**. It is denoted by **"P"** and measured in **Watts (W), kilowatts (kW),** or **megawatts (MW)**.

The average value of active power can be calculated using the following formulas:

$$\mathbf{P = V \times I \times Cos\theta} \text{ ... (Single phase AC Circuits)} \quad \text{(I.2)}$$

$$\mathbf{P = \sqrt{3} \times VL \times IL \times Cos\theta} \text{ ... (Three Phase AC Circuits)} \quad \text{(I.3)}$$

**Reactive Power:**

Reactive power oscillates between the source and the load in an AC circuit; it does not deliver network but is vital for maintaining voltage levels and sustaining the magnetic and electric fields. Often termed wattless power, it nonetheless plays a crucial role in power-system operation.

Where, Reactive power is denoted by "Q" and measured in Volt-Ampere Reactive (VAR), kilovolt-ampere reactive (kVAR), or megavolt-ampere reactive (MVAR).[10]

$$\mathbf{Q = V \times I \times Sin\theta} \quad \text{(I.4)}$$

In addition, electrical energy is transmitted through power lines with limited capacity due to the thermal limits of the cables, the applied voltages at the terminals, and the load angle **δ**. The power transmitted by a radial electrical system is given by the following formulas:[11]

Considering **Figure I.7.a**, which represents an electrical line supplying a load (**P + jQ**), and assuming that the line resistance is very low compared to its reactance and impedance, we can express the impedance as: **Zs = jX**.

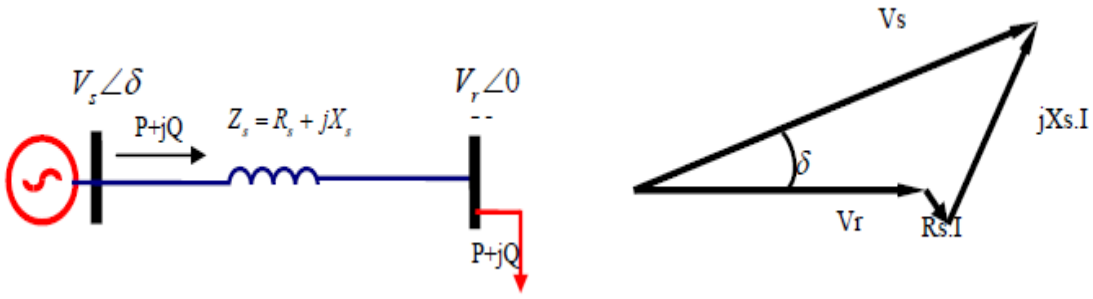


*(a) single-phase transmission line* *(b) single-phase transmission line*

***Fig (I.7)*** *Power line supplying a load*

Taking the voltage at the load terminal as the phase reference as shown in figure.I.7.b and neglecting the resistance Rs, the current will be in phase with Vr. The power required by the load is given by the following equations:[11]

$$S_r = P + jQ = V_r \times I_r^* \; ; \qquad \text{with} \qquad I_r = \frac{V_s - V_r}{Z_s} \tag{I.5}$$

$$P = \frac{V_s \times V_r}{X_s} \sin \delta \tag{I.6}$$

$$Q = \frac{V_s \times V_r}{X_s} \cos \delta - \frac{V_r^2}{X_s} \tag{I.7}$$

**P:** Real power flow

**Q**: Reactive power flow

The sending and receiving end voltages are denoted by **Vs** and **Vr**, respectively.

**Zs**: Line impedance

**Xs**: Line reactance

**$\delta$**: Voltage angle difference between the sources.

## I-5. Voltage Drop:

As current flows through a transmission line, making the voltage at the end of the line lower than at its origin. The greater the power load on the line, the larger the voltage drop. The voltage drop ΔV, derived from the equivalent diagram and the voltage diagram in Figure I.8, is given by the following equation.

$$\Delta V = V_1 - V_2 = Z * I \tag{I.8}$$

formulation:

The vector relation is then written:

$$\bar{V}_1 = \bar{V}_2 + R\bar{I} + jL\omega\bar{I} = \bar{V}_2 + R\bar{I} + jX\bar{I} \tag{I.9}$$

Decomposing into the horizontal (real) and vertical (imaginary) components yields the following two real equations:

$$V_1 \cos\delta = V_2 + RI \cos\varphi + XI \sin\varphi \tag{I.10}$$

$$V_1 \sin\delta = -RI \sin\varphi + XI \cos\varphi \tag{I.11}$$

As well, by squaring and then adding these two expressions, we obtain:

$$V_1^2 = V_2^2 + R^2 I^2 + X^2 I^2 + 2(RV_2 I \cos\varphi + XV_2 I \sin\varphi) \tag{I.12}$$

It is then possible to replace the different terms of this expression by using the powers:

With $P = V_2 I \cos\varphi$ the single-phase active power consumed by the load,

$Q=V_2 I \sin\varphi$ the single-phase reactive power called by the load,

$P_j=RI_2$ the joule losses in the line and $Q=XI^2$ the reactive power consumed by the reactance of the line it comes

$$V_1^2-V_2^2=RP_J+XQ_L+2(RP+XQ) \quad \text{(I.13)}$$

$$(V_1-V_2)(V_1+V_2)=RP_J+XQ_L+2(RP+XQ) \quad \text{(I.14)}$$

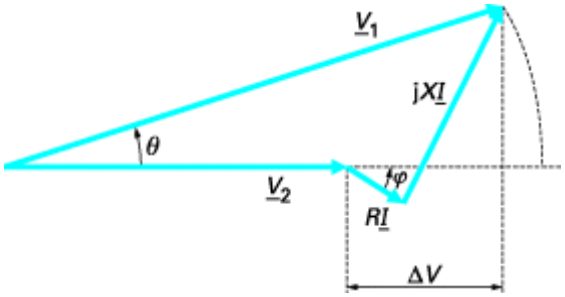


***Figure (I.8)*** *Illustrative diagram of drop voltage and its factors*

Noting V=V1+V2/2 and ΔV=V1-V2 the voltage drop, we obtain:

$$\frac{\Delta V}{V}=\frac{\frac{1}{2}RP_J+\frac{1}{2}XQ_L+RP+XQ}{V^2} \quad \text{(I.15)}$$

In a well-designed power transmission network, Joule losses in the lines typically account for only a small percentage of the total transmitted power. If we consider a case where the reactive power consumption of the line is low relative to the transmitted power, we obtain the following simplified relationship (three-phase):[12]

$$\frac{\Delta V}{V}\cong\frac{RP+XQ}{V^2} \quad \text{(I.16)}$$

Under these conditions, the relationships illustrate the fact that:

• **the voltage drop** depends mainly on the reactive power consumed by the receiving end;

• **the transport angle θ** depends mainly on the transmitted active power.[13]

- **Active losses:**

Active power losses are calculated using the formula:

$$\Delta P = 3RI^2 \quad \text{(I.17)}$$

The current flowing this element is:

$$I = S / \sqrt{3}U \quad \text{(I.18)}$$

$$\Delta U = \frac{R \cdot (P^2+Q^2)}{(U^e)^2} = \frac{R \cdot P^2(1+(Q/P)^2)}{(U^e)^2} \quad => \quad \Delta P = \frac{R \cdot P^2(1+\tan^2\varphi)}{(U^e)^2} \qquad \text{(I.19)}$$

ϕ: Phase shift angle between active power and apparent power, then tan ϕ=Q/P

**Note** : The transit of reactive power leads to an increase in active losses.[12]

## I-6. Modeling of Power Elements in an Electrical Network

The term electrical power grid refers to a network of interconnected components designed to:

- Continuously convert non-electrical energy into.
- Transport electrical energy over long distances.
- Transform electrical energy into specific forms while adhering to well-defined constraints.

In addition, the principal components of a network can be organized into three subsystems:

- **Production** (generators).
- **Transmission, distribution, and dispatch** (power lines).
- **Consumption** (loads).

In summary, to analyze a complex electrical power network, models or equivalent of its key components such as generators, various types of transformers, transmission lines, and loads are developed. [14]

### I-6-1. Power Generator:

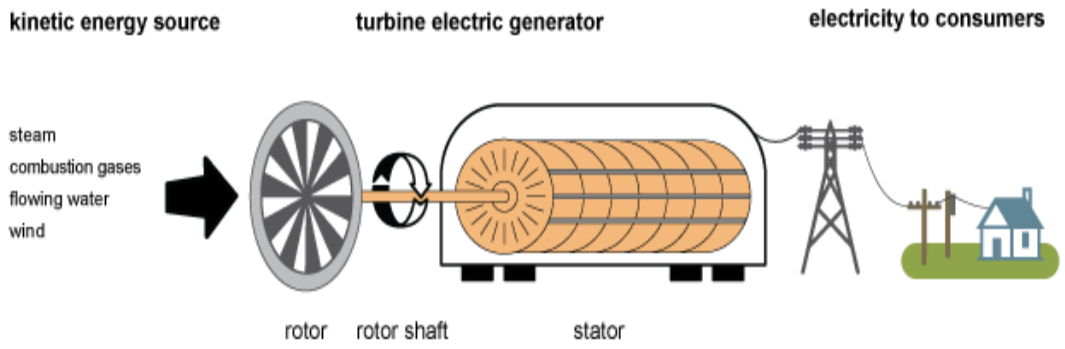


***Figure(I.9) :*** *Electricity generation from electric turbine*

*Source: U.S Energy information administration*

Generators function by converting mechanical energy into electrical energy through electromagnetic induction. This phenomenon is happened when using an electromagnet, created by electricity, along with a rapidly spinning turbine to produce large amounts of electrical current.

The classification of generators can be categorized as follows:

a) **Steam Turbine Generators:** The steam turbine generator is the primary power conversion component in a power plant. Its function is to convert the thermal energy of steam from the steam generator into electrical energy. This process involves two separate components: the steam turbine, which converts thermal energy into mechanical energy, and the generator, which converts mechanical energy into electrical energy. Typically, the turbine is directly coupled to the generator.

b) **Gas Turbine Generators:** Gas turbines are engineered to function within the Brayton cycle framework, which involves the compression of air in conjunction with fuel, followed by its combustion under conditions of constant pressure. The resultant hot gases undergo expansion through a turbine, thereby performing mechanical work [15].

c) **Hydroelectric Generators:** When flowing water turns the blades of a turbine, mechanical energy is generated. The turbine then rotates the generator's rotor, which converts this mechanical energy into electrical energy.[16]

d) **Diesel Generators:** The working principle of a diesel generator is established on the thermodynamics law of energy conversion, following the fundamental laws of thermodynamics.

Additionally, A generator is represented as a constant voltage source that injects active power $P_g$ and reactive power $Q_g$ into the node to which it is connected. The active power $P_g$ remains constant during the calculation, whereas the reactive power $Q_g$ varies within the limits $Q_{gmin} \leq Q_g \leq Q_{gmax}$ to maintain a constant voltage at the generator terminals [17].

This limitation is primarily due to the thermal limits of the stator and rotor windings, as well as the permissible rotor angle constraints [14].

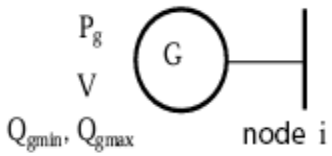


***Figure (I.10):*** *Model of a Generator*

## I-6-2. Transmission Lines

Transmission lines serve the critical function of connecting generating stations to distribution stations. These lines are responsible for the transmission high-voltage electricity from generating stations to primary and secondary transmission stations, as well as to primary and secondary distribution stations.

As well, their primary function is **energy transport** over long distances, ensuring the transmission of electrical energy from production sites to consumers [18].

- **Line Model**

Transmission lines are modeled using the classical π equivalent circuit, as shown in figure I.11 where transverse conductance is neglected .

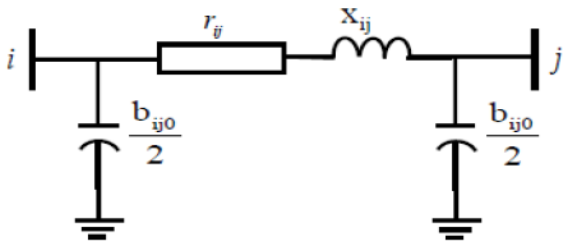


***Figure (I.11)*** *Line model*

The nodal admittance matrix of a line connecting a node i to a node j is given by:

$$\underline{Y}=\begin{pmatrix} y_{ij}+\frac{y_{ij0}}{2} & -y_{ij} \\ -y_{ij} & y_{ij}+\frac{y_{ij0}}{2} \end{pmatrix} \quad \text{(I.20)}$$

Where the series admittance $yij$ is:

$$\underline{y}_{ij} = \frac{1}{r_{ij} + jx_{ij}} = g_{ij} - jb_{ij} \quad \text{(I.21)}$$

$rij$ : The series resistance of the line;

$xij$ : The series reactance of the line

The transverse admittance corresponding to the capacitive effects is written:

$$\underline{y}_{ij0} = jb_{ij0} \quad \text{(I.22)}$$

With:

$b_{ij0}$: The transverse susceptance. [14]

### I-6-3. Power Transformer

Transformers with at least a phase voltage that exceeds 1,000 volts are classified as power transformers. These devices play a pivotal role in the electrical network, facilitating the transmission of electricity over extended distances. Due to their high voltage levels, they must meet specific constraints, particularly in terms of insulation. Their reliability and lifespan must be exceptionally high.[6]

Additionally, A transformer is a device that converts the voltage and current values supplied by an alternative electrical energy source, into a system of voltage and current of different values, but of the same frequency and the same form. It performs this transformation with excellent efficiency [5]. As illustrated in Figure I.12, a transformer power has a capacity of 220 kV.

***Figure (I.12)**: Power transformer for 220 kV floor*

Furthermore, there are two types of transformers to be modeled: the load tap changer voltage regulating transformer and the phase shifting transformer. In power system modeling, tap ratios and phase shifts are typically represented as modifications to the admittance matrix. Figure (I.13) illustrates the equivalent single-line diagram of a three-phase symmetrical transformer with a load tap changer and/or phase shifter.

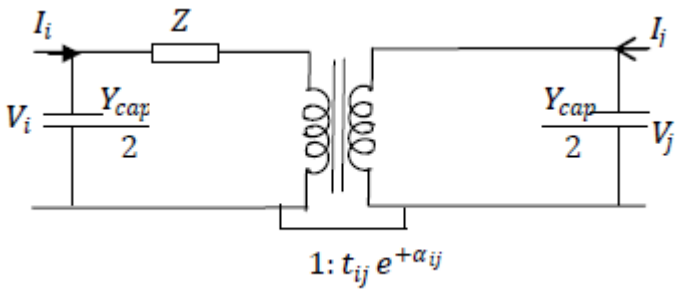


***Figure (I.13)**: Power transformer model*

Where:

***Z***: Represents the Joule effect losses and the transformer leakage inductances referred to the secondary side.

The chosen modeling approach assumes that the losses are equally distributed between the primary and secondary windings.

The parameter ***tij*** represents the on-load voltage regulation ratio.

The parameter ***αij*** represents the phase shift introduced by the transformer between busbars **i** and **j**.

It is important to note that the admittance matrix of the electrical network, which accounts for these variables, will be updated at each iteration.[19]

**Y**: Is the admittance matrix of the transformer, expressed as follows:

$$I = Y \times V \quad => \quad \begin{bmatrix} I_1 \\ I_2 \end{bmatrix} = \begin{bmatrix} y + \frac{Y_{cap}}{2} & \frac{-e^{-j\alpha_{ij}}}{t_{ij}} y \\ \frac{-e^{+j\alpha_{ij}}}{t_{ij}} & \frac{1}{t_{ij}^2} y + \frac{Y_{cap}}{2} \end{bmatrix} \begin{bmatrix} V_1 \\ V_2 \end{bmatrix} \qquad (I.23)$$

### I-6-4. Electrical Loads

The electrical load is frequently modeled as an impedance $Z$ load that consumes constant active power $P_L$ and reactive power $Q_L$ as shown in Figure I.14. It is evident that these loads generally represent distribution substations that supply distribution networks.[14]

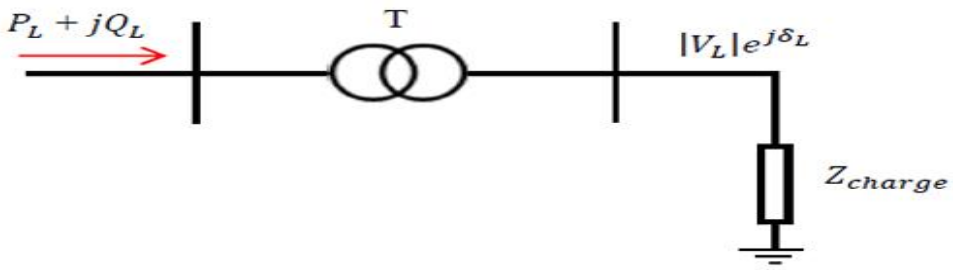


***Figure (I.14):*** *Model of electric charge*

$$S_{Li} = P_{Li} + jQ_{Li} \quad \text{(I.24)}$$

Where

$S_{Li}$: The complex power of the load

$P_{Li}$: The active power

$Q_{Li}$: The reactive power (can be positive or negative depending on whether the load is inductive or capacitive).[20]

### I-6-5. Shunt Elements

Capacitors and inductors are strategically placed at various points in the electrical network to either supply or absorb reactive energy. When $Q_c$ is positive at a given point in the network, the shunt compensator behaves capacitively, supplying reactive energy to that point. Conversely, if $Q_c$ is negative, the shunt compensator is inductive and absorbs the excess reactive energy.

It's important to note that, this step in modeling the line and its elements is crucial for calculating the network's fundamental equations, particularly the nodal admittance matrix [19].

$$\overline{Y}_{i0} = \overline{G}_{i0} + j*\overline{B}_{i0} \quad \text{(I.25)}$$

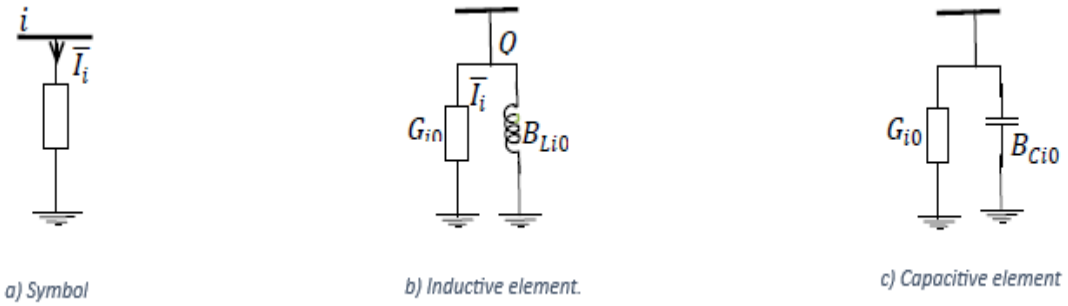


***Figure (I.15)*: *Model of shunt elements***

## I-7. Power Flow

Power flow, or load flow, is widely used in power system operation and planning. The power flow model of a power system is built using the relevant network, load, and generation data. Outputs of the power flow model include voltages at different buses, line flows in the network, and system losses. These outputs are obtained by solving the nonlinear nodal power balance equations. Iterative methods such as Newton-Raphson, Gauss-Seidel, and fast-decoupled methods are typically employed to solve this problem [21].

Where, Power flow is formulated as follows:

$$S = P + jQ = V \cdot I^{*} \qquad (I.26)$$

Power flow is classified into two types:

1. **Real Power**
2. **Reactive Power**

### I-7-1. General Concept of Power Flow

The power flow problem is solved for the steady state determination of the complex voltages at the network busses, from which the active and reactive power flows in each line and transformer are calculated.

Moreover, the set of equations represents the electrical network and is non-linear in nature. In the practical methods of power flow calculation, the configuration of the network and the properties of its equipment are used to determine the complex voltage at each node. On the other hand, the symmetry between the three phases of the three-phase system of the electrical network is perfect**.**

### I-7-2. Objectives of the Power Flow Study

The objective of power flow is to ensure an equilibrium between the generation and consumption of electric energy (the improvement of electricity expenditure, energy production according to need), while respecting operational limits in order to maintain stability and ensure the longevity of equipment, it is necessary to keep the bus-bar voltages between the theoretical limits, using the power control and network planning (from load calculation).Increase the security of operation of networks by a good strategy of power flow before the disturbances [20].

In fact, in power system as we know has four quantities are related with each bus. These are voltage magnitude |V|, phase angle δ, active power P and reactive power Q . In a study of power flow, two out of four are given and the other two quantities are obtained during equations solutions. In addition, Within the domain of power systems, buses are classified into three distinct categories: [22]

***Table (I.1)*** *Type of Buses*

| Bus type | Quantities | |
|---|---|---|
| | Know n | Unkown |
| Load bus<br>PQ bus | P , Q | V , δ |
| Voltage controlled bus<br>Generator bus<br>P-\|V\| bus | P , \|V\| | Q , δ |
| Slack bus (Reference)<br>Swing bus<br>Control bus | V , δ | P , Q |

Where, load flow studies are commonly used to investigate:

(i) Component or circuit loading

(ii) Bus voltage profiles

(iii) Real and reactive power flows

(iv) Power system losses

(v) Proper transformer tap settings

Moreover, load flow is required to be run for the following cases:

(i) In power system planning and monitoring

(ii) In addition or outage of generating unit, transmission lines, or other equipments

(iii) In deciding optimal generation allocations to the generating stations so that the cost of generation is minimal

(iv) When a new load center is established or when the system stays unchanged but load grows

In addition, Power flow solution should have the following solution properties:

(i) Simplicity of the program

(ii) High computational speed

(iii) Flexibility of the problem

(iv) Low computer storage

(v) Reliability [23]

### I-7-3. Conclusion

In summary, we explained electrical networks, their components, and electrical quantities. We also mentioned power flow and its effectiveness in networks. In the next chapter, we will discuss the uses of classical methods in power flow. Furthermore, we will talk about Optimal Power Flow (OPF) and the role of Optimal Reactive Power Dispatch (ORPD).

# CHAPTER II

# *CHAPITER 2*

# *Optimal Reactive Power Dispatch*

## II. Introduction

The continuous evolution of electrical power systems and their increasing complexity have made the accurate study of load flow and power distribution an indispensable aspect of system planning, design, and operation. At the heart of these analyses lies the bus admittance matrix (Y-bus), which provides a compact and systematic representation of the interconnections between different nodes in the network. Through the formulation of this matrix and the application of Kirchhoff's current laws, engineers and researchers are able to model the flow of electrical power across complex systems with precision.

In this chapter, we present the mathematical formulation of the bus admittance matrix and introduce the fundamental iterative methods used in solving load flow equations. Particular attention is given to the Newton-Raphson method, the Gauss-Seidel method, and the Fast Decoupled method, each known for its respective computational efficiency and convergence behavior. Furthermore, the chapter addresses the Optimal Power Flow (OPF) problem, which represents a key challenge in the operation of modern power systems by aiming to determine the most economical and reliable operating conditions under a set of system constraints, and a comprehensive perspective on the optimal reactive power dispatch will be presented [24].

## II-7-3. Nodal Admittance Matrix

The bus admittance matrix, $Y_{bus}$ is an n×n matrix, where n equals the number of nodes in the network constructed from the admittances of the circuit's equivalent elements. Most network elements are represented by a combination of shunt elements (connected between the considered node and the reference node, which is ground) and series elements (connected between two different nodes) [17].

Additionally, the **Bus Admittance Matrix** represents the nodal admittances of the various buses. With the help of the transmission line, each bus is connected to the various other buses. Admittance matrix is used to analyse the data that is needed in the load or a power flow study of the buses. It explains the admittance and the topology of the network. The key advantages of employing the bus admittance matrix are:

1. The data preparation of the bus admittance matrix is very simple.
2. The formation of the bus admittance matrix and their modification is easy.
3. The bus admittance matrix is a sparse matrix thus the computer memory requirement is less.

In nodal analysis, branch admittances are typically used instead of impedances. For the isolated line shown in Figure.II.1, with bus voltages *Vi* and *Vj* at nodes *i* and *j,* respectively, the current flowing from node *i* to node *j* is given by [23]

$$I_{ij} = y_{ij}(V_i - V_j) \tag{II.1}$$

- The complex admittance of the branch connecting nodes *i* and *j* between nodes *i* and *j,* denoted $y_{ij}$ ,is defined as [25]:

$$y_{ij} = \frac{1}{R_{ij}+jX_{ij}} \tag{II.2}$$

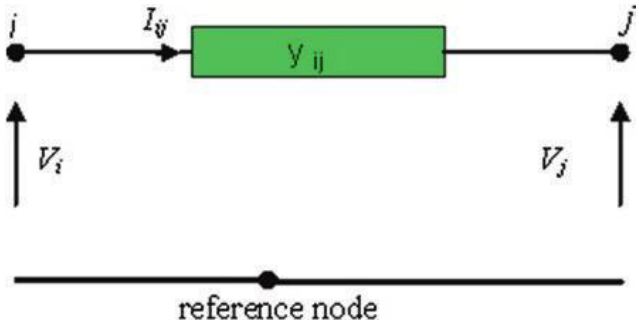


*Figure (**II**.1) Representation of an isolated bus*

Additionally, in a complex network, the nodes being numbered 0,1, 2, …, *n*, where node 0 indicates the reference node, by Kirchoff's current law (KCL), the injected current $I_i$ being equal to the sum of all currents leaving node *i*; thus we can write:

$$I_i = \sum_{j=0}^{n} I_{ij} = \sum_{j=0}^{n} y_{ij}(V_i - V_j) \tag{II.3}$$

It is imperative to consider the three-bus system illustrated in Figure II.2. where node 0 functions as the reference (ground) node. Applying Applying Kirchhoff's Current Law at buses 1 through 3, we have:

$$I_1 = y_{10}V_1 + y_{12}(V_1 - V_2) + y_{13}(V_1 - V_3)$$
$$I_2 = y_{20}V_2 + y_{12}(V_2 - V_1) + y_{13}(V_2 - V_3)$$
$$0 = y_{13}(V_3 - V_1) + y_{23}(V_3 - V_2)$$

The above node equations can be reduced to

$$I_1 = Y_{11}V_1 + Y_{12}V_2 + Y_{13}V_3$$
$$I_2 = Y_{21}V_1 + Y_{22}V_2 + Y_{23}V_3$$
$$I_3 = Y_{31}V_1 + Y_{32}V_2 + Y_{33}V_3$$

Where:

$Y_{11} = y_{10} + y_{12} + y_{13}$

$Y_{22} = y_{20} + y_{12} + y_{33}$

$Y_{33} = y_{13} + y_{23}$

$Y_{12} = Y_{21} = -y_{12}$

$Y_{13} = Y_{31} = -y_{12}$

$Y_{23} = Y_{32} = -y_{23}$

*and*

$I_3 = 0$

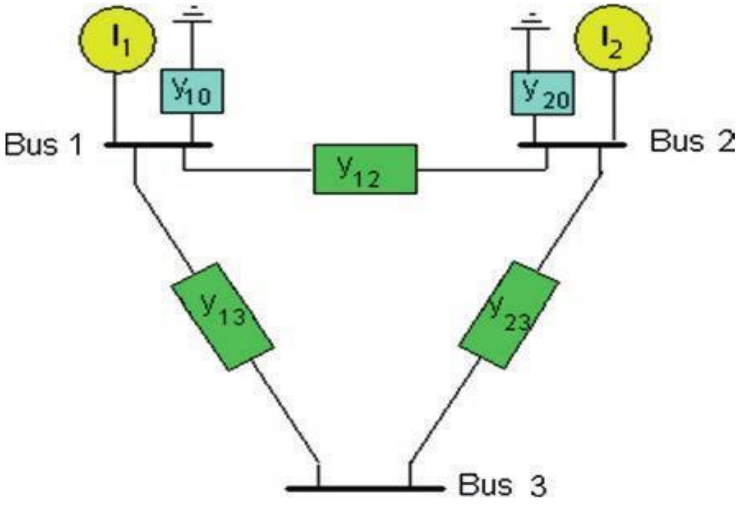


*Figure (**II**.2) Admittance diagram of a 3-bus system*

- These equations for a *n*-bus power network in matrix form can be expressed as follows:

$$\begin{bmatrix} I_1 \\ I_2 \\ \vdots \\ I_n \end{bmatrix} = \begin{bmatrix} Y_{11} & Y_{12} & \cdots & Y_{1n} \\ Y_{21} & Y_{22} & \cdots & Y_{2n} \\ \vdots & \vdots & \cdots & \vdots \\ Y_{1n} & Y_{n2} & \cdots & Y_{nn} \end{bmatrix} \begin{bmatrix} V_1 \\ V_2 \\ \vdots \\ V_n \end{bmatrix} \quad \text{(II.4)}$$

The current injection at a bus can be calculated using the bus-admittance matrix, as shown above.

- In the simplest form, the above matrix can be written as shown below.

$$[I] = [Y_{Bus}][V] \quad \text{(II.5)}$$

where $\boldsymbol{Y}$ is the $N \times N$ bus admittance matrix, $\boldsymbol{V}$ is the column vector of $N$ bus phase voltages, and $\boldsymbol{I}$ is the column vector of $N$ phase currents, the current is positive when flowing towards the bus, and it's negative if flowing away from the bus [26, 27].

The diagonal element $Y_{ii}$ of the bus admittance matrix is equals the sum of all admittances connected to bus i:

$$Y_{ii} = \sum_{\substack{j=0 \\ j \neq i}}^{n} y_{ij} \tag{II.6}$$

- where $y_{ij}$ is the admittance between buses $i$ and $j$ [27]

Furthermore, The off-diagonal element $Y_{ij}$ *of the* bus admittance matrix is known as the mutual admittance or transfer admittance, which is equal to the negative of the admittance between nodes $i$ and $j$ as follows:

$$Y_{ij} = Y_{ji} = -y_{ij} \tag{II.7}$$

## II-8. Power Flow Calculation Methods

The numerical analysis of simultaneous algebraic equations is a fundamental component of computer-aided power system studies, such as load-flow analysis. The first step in performing load flow analysis is to form the *Y*-bus admittance using the transmission line and transformer input data. The nodal equation for a power system network utilizing *Y* bus, bus, can subsequently be expressed as [28]:

$$I = Y_{Bus} \times V \tag{II.8}$$

The nodal equation can be written in a generalized form for an $n$ bus system.

$$I_i = \sum_{j-1}^{n} Y_{ij} V_j \quad for\ i=1, 2, 3, n \tag{II.9}$$

The complex power delivered to bus $i$ is

$$P_i + jQ_i = V_i \times I_i^* \tag{II.10}$$

$$I_i = \frac{P_i - jQ_i}{V_i^*} \tag{II.11}$$

Substituting for $I_i$ in terms of $P_i$ & $Q_i$, the equation gives

$$\frac{P_i - jQ_i}{V_i^*} = V_i \sum_{j-1}^{n} y_{ij} - \sum_{j-1}^{n} y_{ij} V_j \quad j \neq i \tag{II.12}$$

- The above equation uses iterative techniques to solve load flow problems. Hence, it is necessary to review the general forms of the various solution methods.

In addition, An iterative method involves the repeated refinement of initial, arbitrary estimates of unknown variables, leading to the identification of a solution for an equation or system of equations.

Furthermore, Convergence is achieved when the absolute deviation between current and previous estimates falls below a pre-specified accuracy index 'ϵ' (the convergence criterion) for all variables. Solving simultaneous nonlinear power flow equations necessitates iterative techniques, even for the simplest power systems.

There are several methods for solving nonlinear equations, such as:

- Newton-Raphson
- Gauss Seidel
- Fast Decoupled [29]

### II-8-1. Newton-Raphson Method

The Newton-Raphson method, which was developed by British mathematician Isaac Newton and British engineer Joseph Raphson, was first introduced in the late 1960s. This iterative technique involves the linearization of a set of nonlinear equations through the application of a first-order Taylor series expansion. The method has found extensive application in load flow analysis due to its robust convergence properties and reliability, particularly in scenarios where alternative methods may prove ineffective. While the convergence rate is rapid when initial estimates are close to the actual solution, it may require a longer time if the initial estimates are far off.

The admittance matrix is used to write equations for currents entering a power system. Equation (9) is expressed in a polar form, in which $j$ includes bus $i$

$$I_i = \sum_{j-1}^{n} |Y_{ij}| \, |V_i| < \theta_{ij} + \delta_j \qquad \text{(II.13)}$$

The real and reactive power at bus i is

$$P_i - jQ_i = V_i^* \, I_i \qquad \text{(II.14)}$$

Substituting for $I_i$ in Equation (13) from Equation (14)

$$P_i - jQ_i = |V_i| < -\delta_i \sum_{j=1}^{n} |Y_{ij}| \, |V_j| < \delta_{ij} + \delta_j \qquad \text{(II.15)}$$

The real and imaginary parts are separated [28]:

$$\left.\begin{aligned} P_i &= \textstyle\sum_{j-1}^{n} |V_i| \, |V_j| |Y_{ij}| \cos\left(\theta_{ij} - \delta_i + \delta_j\right) \\ Q_i &= \textstyle\sum_{j-1}^{n} |V_i| \, |V_j| |Y_{ij}| \sin\left(\theta_{ij} - \delta_i + \delta_j\right) \end{aligned}\right\} \Rightarrow i = 1, 2. \ldots n \qquad \text{(II.16)}$$

After developing Pi and Pi in TAYLOR series around the first approximation:

$$P_i = P_i^{(0)} + \left(\frac{\partial P_i}{\partial \delta_2}\right)^{(0)} \Delta\delta_2^{(0)} + .. + \left(\frac{\partial P_i}{\partial \delta_n}\right)^{(0)} \Delta\delta_n^{(0)} + \left(\frac{\partial P_i}{\partial |V_2|}\right)^{(0)} \Delta|V_2|^{(0)} + ... + \left(\frac{\partial P_i}{\partial |V_n|}\right)^{(0)} \Delta|V_2|^{(0)}$$

$$Q_i = Q_i^{(0)} + \left(\frac{\partial Q_i}{\partial \delta_2}\right)^{(0)} \Delta\delta_2^{(0)} + .. + \left(\frac{\partial Q_i}{\partial \delta_n}\right)^{(0)} \Delta\delta_n^{(0)} + \left(\frac{\partial Q_i}{\partial |V_2|}\right)^{(0)} \Delta|V_2|^{(0)} + ... + \left(\frac{\partial Q_i}{\partial |V_n|}\right)^{(0)} \Delta|V_2|^{(0)} \quad \text{(II.17)}$$

Based on the relation of $\left[\frac{\Delta P}{\Delta Q}\right]$ with $\Delta P_i^{(0)} = P_i - P_i^{(0)}$ , $\Delta Q^{(0)} = Q_i - Q_i^{(0)}$ (II.18)

The two equation systems (II.17) and (II.18) give:

$$\begin{bmatrix} \Delta P_2^{(0)} \\ \vdots \\ \Delta P_n^{(0)} \\ \Delta Q_2^{(0)} \\ \vdots \\ \Delta Q_n^{(0)} \end{bmatrix} = \begin{bmatrix} \left(\frac{\Delta P_2}{\partial \delta_2}\right)^{(0)} & \cdots & \left(\frac{\Delta P_2}{\partial \delta_n}\right)^{(0)} & \left(\frac{\Delta P_2}{\partial |V_2|}\right)^{(0)} & \cdots & \left(\frac{\Delta P_2}{\partial |V_n|}\right)^{(0)} \\ \vdots & \ddots & \vdots & \vdots & \ddots & \vdots \\ \left(\frac{\Delta P_n}{\partial \delta_2}\right)^{(0)} & \cdots & \left(\frac{\Delta P_n}{\partial \delta_n}\right)^{(0)} & \left(\frac{\Delta P_n}{\partial |V_2|}\right)^{(0)} & \cdots & \left(\frac{\Delta P_n}{\partial |V_n|}\right)^{(0)} \\ \left(\frac{\Delta Q_2}{\partial \delta_2}\right)^{(0)} & \cdots & \left(\frac{\Delta Q_2}{\partial \delta_n}\right)^{(0)} & \left(\frac{\Delta Q_2}{\partial |V_2|}\right)^{(0)} & \cdots & \left(\frac{\Delta Q_2}{\partial |V_n|}\right)^{(0)} \\ \vdots & \ddots & \vdots & \vdots & \ddots & \vdots \\ \left(\frac{\Delta Q_n}{\partial \delta_2}\right)^{(0)} & \cdots & \left(\frac{\Delta Q_n}{\partial \delta_n}\right)^{(0)} & \left(\frac{\Delta Q_n}{\partial |V_2|}\right)^{(0)} & \cdots & \left(\frac{\Delta Q_n}{\partial |V_n|}\right)^{(0)} \end{bmatrix} \begin{bmatrix} \Delta\delta_2^{(0)} \\ \vdots \\ \Delta\delta_n^{(0)} \\ \Delta\left|V_2^{(0)}\right| \\ \vdots \\ \Delta\left|V_n^{(0)}\right| \end{bmatrix} \quad \text{(II.19)}$$

Thus, we can write the system as follows:

$$\begin{bmatrix} \Delta P^{(0)} \\ \Delta Q^{(0)} \end{bmatrix} = \left[J^{(0)}\right] \begin{bmatrix} \Delta\delta^{(0)} \\ \Delta|V|^{(0)} \end{bmatrix} \quad \text{(II.20)}$$

$$\begin{bmatrix} \Delta\delta^{(0)} \\ \Delta|V|^{(0)} \end{bmatrix} = \left[J^{(0)}\right]^{-1} \begin{bmatrix} \Delta P^{(0)} \\ \Delta Q^{(0)} \end{bmatrix} \quad \text{(II.21)}$$

We recall that

$$\Delta\delta^{(k)} = \delta_i^{(k+1)} - \delta_i^{(k)} \quad \text{(II.22)}$$

$$\Delta|V_i|^{(k)} = |V_i|^{(k+1)} - |V_i|^{(k)} \quad \text{(II.23)}$$

The adaptation (II.21) with (II.22) and (II.23) gives:

$$\begin{bmatrix} \delta_i^{(k+1)} \\ |V|^{(k+1)} \end{bmatrix} = \begin{bmatrix} \delta^{(k)} \\ |V|^{(k)} \end{bmatrix} + \begin{bmatrix} \Delta\delta \\ \Delta|V| \end{bmatrix} \quad \text{(II.24)}$$

$$\begin{bmatrix} \delta_i^{(0)} \\ |V|^{(k+1)} \end{bmatrix} = \begin{bmatrix} \delta^{(k)} \\ |V|^{(k)} \end{bmatrix} + \left[J^{(k)}\right]^{-1} \begin{bmatrix} \Delta P^{(k)} \\ \Delta Q^{(k)} \end{bmatrix} \quad \text{(II.25)}$$

By substituting the expression of equation (II.20) into the above equation, we obtain [17]:

$$\begin{bmatrix} \Delta P \\ \Delta Q \end{bmatrix} = [J] \begin{bmatrix} \Delta \delta \\ \Delta |V| \end{bmatrix} \quad \text{(II.26)}$$

with

$$J = \begin{bmatrix} J_1 & J_2 \\ J_3 & J_4 \end{bmatrix} \quad \text{(II.27)}$$

$J_1$, $J_2$, $J_3$, and $J_4$ are the submatrices of the Jacobian.

Such that [19] : $J_1 = \frac{\partial P_i}{\partial \delta_k}$ ,$J_2 = \frac{\partial P_i}{\partial V_k}$ ,$J_3 = \frac{\partial Q_i}{\partial \delta_k}$ ,$J_4 = \frac{\partial Q_i}{\partial V_k}$

Where $\Delta P$ and $\Delta Q$ respectively denote the deviations between specified and calculated active powers, and the deviations between specified and calculated reactive powers;

$\Delta\delta$ and $\Delta V$ respectively represent the deviations between specified and calculated angles, and the deviations between specified and calculated voltages, while J is the Jacobian matrix.

For generator buses, the voltage magnitudes are known. Consequently, if *m* buses in the system are generator nodes, *m* equations involving *Q* and *V* and the corresponding columns of the Jacobian matrix are eliminated. As a result, there are (*n – 1*) active power constraints and (*n - 1 - m*) reactive power constraints, and the Jacobian matrix has an order of *(2n – 2 - m) × (2n – 2 - m)*.

- $J_1$ has an order of *(n - 1) × (n - 1)*,
- $J_2$ has an order of *(n - 1) × (n - 1 - m)*,
- $J_3$ has an order of *(n - 1 - m) × (n - 1)*,
- $J_4$ has an order of *(n - 1 - m) × (n - 1 - m)*.[29]

**The Jacobian submatrices $J_i$**

The diagonal and off-diagonal elements of $J_1$ :

$$\frac{\partial P_i}{\partial \delta_i} = \sum_{j \neq i} |V_i| \, |V_j| |Y_{ij}| \, sin(\theta_{ij} - \delta_i + \delta_j) \quad \text{(II.28)}$$

$$\frac{\partial P_i}{\partial \delta_j} = -|V_i| |V_j| |Y_{ij}| \, sin(\theta_{ij} - \delta_i + \delta_j) \quad i \neq j \quad \text{(II.29)}$$

The elements on the diagonal and off-diagonal of $J_2$ :

$$\frac{\partial P_i}{\partial |V_i|} = 2|V_i||Y_{ii}| \cos\theta_{ii} + \sum_{j \neq i} |V_j| |Y_{ij}| \cos(\theta_{ij} - \delta_i + \delta_j) \quad \text{(II.30)}$$

$$\frac{\partial P_i}{\partial |V_j|} = |V_i| |Y_{ij}| \cos(\theta_{ij} - \delta_i + \delta_j) \quad i \neq j \quad \text{(II.31)}$$

The elements on the diagonal and off-diagonal of $J_3$ :

$$\frac{\partial Q_i}{\partial \delta_i} = \sum_{j \neq i} |V_i||V_j||Y_{ij}| \cos(\theta_{ij} - \delta_i + \delta_j) \quad \text{(II.32)}$$

$$\frac{\partial Q_i}{\partial \delta_j} = - |V_i||V_j||Y_{ij}| \cos(\theta_{ij} - \delta_i + \delta_j) \quad i \neq j \quad \text{(II.33)}$$

The elements on the diagonal and off-diagonal of $J_4$ :

$$\frac{\partial Q_i}{\partial |V_i|} = - 2|V_i||Y_{ii}| \sin\theta_{ii} - \sum_{j \neq i} |V_j||Y_{ij}| \sin(\theta_{ij} - \delta_i + \delta_j) \quad \text{(II.34)}$$

$$\frac{\partial Q_i}{\partial |V_j|} = - |V_i||Y_{ij}| \sin(\theta_{ij} - \delta_i + \delta_j) \quad i \neq j \quad \text{(II.35)}$$

The terms $\Delta P_i^{(k)}$ and $\Delta Q_i^{(k)}$ represent the difference between the specified and calculated values, given by:

$$\Delta P_i^{(k)} = P_i^{sch} - P_i^{(k)} \quad \text{(II.36)}$$

$$\Delta Q_i^{(k)} = Q_i^{sch} - Q_i^{(k)} \quad \text{(II.37)}$$

$\Delta P_i^{(k)}, \Delta Q_i^{(k)}$: Active/Reactive power mismatch at bus i at iteration k

$P_i^{sch}, Q_i^{sch}$ : Scheduled active/reactive power injection at bus i (given or target value).

$P_i^{(k)}, Q_i^{(k)}$: Calculated active/reactive power injection at iteration k

The new estimates of the generator nodes are [29]:

$$\delta_i^{(k+1)} = \delta_i^{(k)} + \Delta\delta_i^{(k)} \quad \text{(II.38)}$$

$$|V_i^{(k+1)}| = |V_i^{(k)}| + \Delta|V_i^{(k)}| \quad \text{(II.39)}$$

The calculation steps are as follows:

1- From the system data, we take the bus admittance matrix $Y_{bus}$.

2- We estimate the initial values $|V_i^{(0)}|$ and $\delta_i^{(0)}$ for the load nodes, and $\delta_i^{(0)}$ for the control nodes.

3- We calculate $P_i$, $Q_i$ which give us $\Delta P$, $\Delta Q$.

4- Formation of the Jacobian matrix $J$.

5- We find the inverse of the Jacobian matrix.

6- We calculate.

$$\begin{bmatrix} \Delta\delta \\ \Delta|V| \end{bmatrix} = [J]^{-1} \begin{bmatrix} \Delta P \\ \Delta Q \end{bmatrix}$$

We obtain:

$$\delta_i^{(k+1)} = \delta_i^{(k)} + \Delta\delta_i^{(k)}$$

$$|V_i^{(k+1)}| = |V_i^{(k)}| + \Delta|V_i^{(k)}|$$

7- The process repeats until the following tolerance condition is met

$$max|\Delta P^k| \leq \varepsilon$$

$$max|\Delta Q^k| \leq \varepsilon \text{ [17]}$$

### II-8-1-1. Advantages of the Newton-Raphson Method

- Faster, more reliable and yields accurate results, [25]
- requires less number of iterations.
- The number of iterations required in this method is almost independent of system size.
- It possesses quadratic convergence and thus overall time for iterative process is short especially when the solution point is close.[30]

### II-8-1-2. Disadvantages of the Newton-Raphson Method

Program as well as memory is more complex.

- The computation time per iteration is larger.
- It needs a larger computer memory requirement. The need of additional storage space since it involves calculation of Jacobian matrices
- Difficult solution method; the code is more complicated

### II-8-1-3. Flowchart of the Newton-Raphson Method

The flowchart of the Newton-Raphson method is illustrated in Figure II.3 as follows [31].

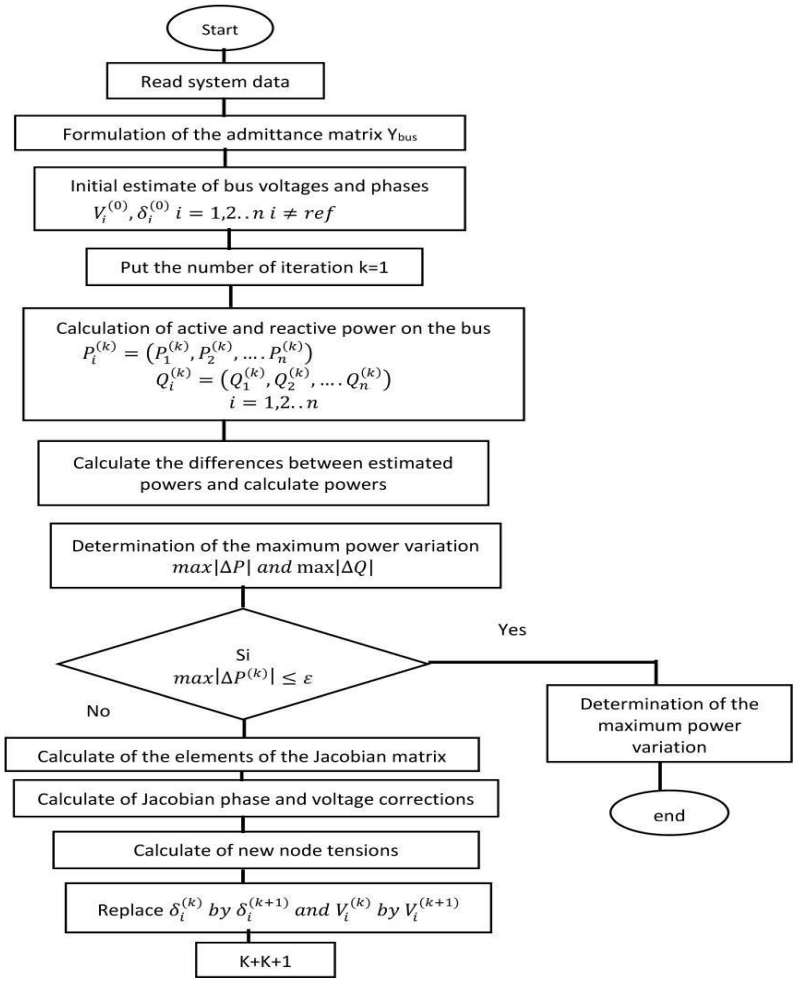


*Figure (II.3) Flowchart of Newton-Raphson method.*

## II-8-2. Gauss Seidel Method

Although the Newton–Raphson method is generally more efficient, the Gauss–Seidel algorithm one of the simplest iterative techniques was selected for the following reasons:

1. It holds reliable scientific value due to its simplicity.
2. It is used in low-power systems where programs are uncomplicated.
3. It is applied in large systems to obtain an approximate solution [32].

- Firstly, Forming the bus admittance matrix of the network via figure 2 (Nodal admittance), Where we will use diagonal and non-diagonal elements and substitute them in the equations:

$$[\mathbf{Y_{Bus}}] = \begin{bmatrix} Y_{11} & Y_{12} & \cdots & Y_{1n} \\ Y_{21} & Y_{22} & \cdots & Y_{2n} \\ \vdots & \vdots & \cdots & \vdots \\ Y_{1n} & Y_{n2} & \cdots & Y_{nn} \end{bmatrix}$$

- For the concrete case of power flow, the solution of the following nodal equation [33]:

$$I_i = Y_{i1}V_1 + Y_{i2} + \dots \dots \dots Y_{in}V_n = \sum_{K=1}^{N} Y_{ik}V_k \quad \text{(II.40)}$$

- The objective is to determine all $P_i$, $Q_i$, $|V_i|$ and $\delta_i$ for the $n$ nodes of an electrical network. The procedure consists of calculating $V_i$ and $\boldsymbol{\delta}_i$ for the PQ nodes, then $Q_i$ and $\delta_i$ for the PV nodes, and finally $P$ and $Q$ for the slack node [34]:

- *Noeuds PQ :*

For the load buses (PQ buses), the voltages $|V_i|$ and angles $\delta_i$ are obtained from the equation (II.41) ; at each iteration :

$$V_i^{(k+1)} = \frac{1}{Y_{ii}}\left[\frac{P_i - jQ_i}{V_i^{*(t)}} - \sum_{\substack{j=1 \\ j \neq i}}^{n} Y_{ij}V_i^{(k)}\right] \quad \text{(II.41)}$$

$$V_i^{(k)} = \left|V_i^{(k)}\right| \angle\delta_i^{(k)} \quad \text{(II.42)}$$

- $P_i$ , $Q_i$ : are the injected real and reactive power into bus $i$ respectively
- $Y_{ii}$: Diagonal elements; sum of admittances connected to bus $i$
- $Y_{ij}$: Off-diagonals, - (sum of admittances connected between busses $i$ and $j$)

- *Noeuds PV:*

For the generation buses (PV buses), and based on equations (II.43,44) we can calculate $Q_i$ and $\delta_i$ at each iteration as follows [30]:

$$Q_i^{(k)} = -Im\left[V_i^{(k)*}\left(\sum_{j=1}^{n} Y_{ij}V_i^{(k)}\right)\right] \quad \text{(II.43)}$$

$$\delta_i^{(k)} = arg\left[\frac{1}{Y_{ii}}\left(\frac{P_i - jQ_i}{V_i^*} - \sum_{\substack{j=1 \\ j \neq i}}^{N} Y_{ij}V_j^{(k)}\right)\right] \quad \text{(II.44)}$$

- *neaud Slack:* Here, just determine $P_i$ and $Q_i$ at iteration $k$ only:

$$P_s - jQ_s = V_s^* \sum_{j=1}^{n} Y_{sj}V_j^{(k)} \quad \text{(II.45)}$$

- $P_s$: Active power injected at the slack bus.

- $Q_s$ : Reactive power injected at the slack bus.
- $V_s^*$: The conjugate of the slack bus voltage.
- $Y_{sj}$ : Represents admittance connectivity between bus *s* and bus *j*.
- $V_j^{(k)}$ : Voltage at bus *j* at iteration *k*.

- Improvement of convergence by relaxation (using an acceleration factor) :

$$V_{i(\text{acceleration})}^{(k+1)} = V_i^{(k)} + \alpha(V_i^{(k+1)} - V_i^{(k)}) \quad \text{(II.46)}$$
$$= V_i^{(k)} + \alpha \cdot \Delta V_i^{(k)}$$

α : Acceleration factor, generally taken between [1,4 ≤ α ≤ 1,6].

Sometimes the number of iterations required to converge can be significantly reduced by application

of a so-called *acceleration factor*. The correction in voltage from $\boldsymbol{V}_i^{(k)}$ to $\boldsymbol{V}_i^{(k+1)}$ is multiplied by such a factor in order to bring the new voltage closer to its final value.

- The iterative process stops when the following stopping criterion is met: [35]

$$\textbf{max}\left|V_i^{(k+1)} - V_i^{(k)}\right| \leq \varepsilon$$

- [36] Also the line flows and losses are found as phasor sum of $S_{ij}$ and $S_{ji}$ .The complex power $\boldsymbol{S_{ij}}$ from bus *i* to jand $\boldsymbol{S_{ji}}$ from bus *j* to *i* are

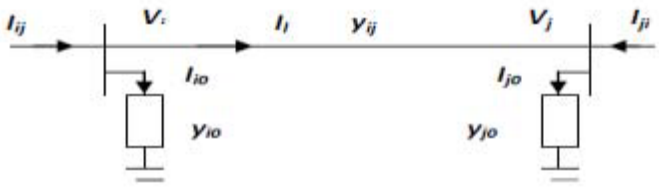


*Figure **II**.4 representation of line connected between*

$$S_i = P_i + jQ_i \quad \text{(II.47)}$$

$$S_i = S_{ij} + S_{ji} \quad \text{(II.48)}$$

$$S_{ij} = V_i I_{ij}^* \quad \text{(II.49)}$$

$$S_{ji} = V_j I_{ji}^* \quad \text{(II.50)}$$

$$I_{ij} = y_{ij}(V_i - V_j) + y_{i0}V_i$$

$$I_{ji} = y_{ji}(V_j - V_i) + y_{i0}V_j$$

### II-8-3. Fast Decoupled Power Flow Method

The Fast Decoupled Power Flow Method is one of the improved methods, which is based on a simplification of the Newton-Raphson method and reported by Stott and Alsac in 1974 [16]. This method, like the Newton-Raphson method, offers calculation simplifications, fast convergence and reliable results and became a widely used method in load flow analysis. However, fast decouple for some cases, where high resistance-to-reactance ($R/X$) ratios or heavy loading (low voltage) at some buses are present, does not converge well because it is an approximation method and make some assumption to simplify Jacobian matrix. For these cases, many efforts and developments have been made to overcome these convergence obstacles. Some of them targeted the convergence of systems with high $R/X$ ratios, and others with low voltage buses [28].

This method is a modification of Newton-Raphson, which takes the advantage of the weak coupling between real power flow-voltage angle $\boldsymbol{P-\delta}$ $((P = (V_1V_2 / X_1) \sin \delta))$ and reactive power flow-voltage magnitude $\boldsymbol{Q-V}$ $((Q = (V_1V_2/X) \cos \delta - (V_2^{(2)}/X_2)))$ due to the high $X$:$R$ ratios [25]. The Jacobian matrix of Equation (II.26) is reduced to half by ignoring the element of $J_2$ and $J_3$. Equation (II.26) is simplified as:

$$\begin{bmatrix} \Delta P \\ \Delta Q \end{bmatrix} = \begin{bmatrix} J_1 & 0 \\ 0 & J_4 \end{bmatrix} \begin{bmatrix} \Delta \delta \\ \Delta |V| \end{bmatrix} \tag{II.51}$$

Expanding Equation (II.51) gives two separate matrixes,

$$\Delta P = J_1 \Delta \delta = \left[\frac{\partial P}{\partial \delta}\right] \Delta \delta \tag{II.52}$$

$$\Delta Q = J_4 \Delta |V| = \left[\frac{\partial Q}{\partial |V|}\right] \Delta |V| \tag{II.53}$$

The elements of Jacobian matrix $\mathbf{J_1}$ are as follows [25].

The diagonal elements are

$$\frac{\partial P_i}{\partial \delta_i} = \sum_{j=1}^{n} |V_i| \, |V_j| |Y_{ij}| \sin(\theta_{ij} - \delta_i + \delta_j) - |V_i|^2 |Y_{ii}| \sin(\theta_{ii})$$

$$\frac{\partial P_i}{\partial \delta_i} = -Q_i - |V_i|^2 |Y_{ii}| \sin(\theta_{ii})$$

$$\frac{\partial P_i}{\partial \delta_i} = -Q_i - |V_i|^2 B_{ii}$$

Now, the diagonal elements of $J_1$ can be written as

$$\frac{\partial P_i}{\partial \delta_i} = -Q_i - |V_i|^2 B_{ii} \tag{II.54}$$

where $B_{ii} = |Y_{ii}| \sin \theta_{ii}$ is the imaginary part of the diagonal elements of the bus admittance matrix $Y_{bus}$.

Further simplifications can be applied to Eq. (II.54), by considering

$$B_{ii} \gg Q_i \text{ and } |V_i|^2 \approx V_i$$

$$\frac{\partial P_i}{\partial \delta_i} = -|V_i| B_{ii} \tag{II.55}$$

Also, as under normal operating conditions $\delta_j - \delta_i$ is quite small, therefor

$$\theta_{ij} - \delta_i + \delta_j \approx \theta_{ij} \; and \; |V_j| \approx 1$$

The off-diagonal elements of $\mathbf{J_1}$ can be written as

$$\frac{\partial P_i}{\partial \delta_j} = -|V_i||V_j||Y_{ij}| \sin(\theta_{ij} - \delta_i + \delta_j) \qquad \therefore \; |V_j| \approx 1$$

$$= -|V_i||Y_{ij}| \sin(\theta_{ij})$$

$$\frac{\partial P_i}{\partial \delta_i} = -|V_i| B_{ij} \tag{II.56}$$

Similarly, the diagonal elements of $\mathbf{J_4}$ may be written as

$$\frac{\partial Q_i}{\partial |V_i|} = -|V_i||Y_{ii}| \sin \theta_{ii} - \sum_{j=1}^{n} |V_j||Y_{ij}| \sin(\theta_{ij} - \delta_i + \delta_j)$$

Multiplying the above equation by $|V_i|$, we get

$$|V_i| \times \frac{\partial Q_i}{\partial |V_i|} = -|V_i|^2 |Y_{ii}| \sin \theta_{ii} - \sum_{j=1}^{n} |V_i||V_j||Y_{ij}| \sin(\theta_{ij} - \delta_i + \delta_j) = -|V_i|^2 B_{ii} + Q_i$$

Again, since $B_{ii} >> Q_i$, $Q_i$ may be neglected

$$\frac{\partial Q_i}{\partial |V_i|} = -|V_i| B_{ii} \tag{II.57}$$

Again assume $\theta_{ij} - \delta_i + \delta_j \approx \theta_{ij}$

$$\frac{\partial Q_i}{\partial |V_j|} = -|V_i||Y_{ij}| \sin \theta_{ij}$$

$$\frac{\partial Q_i}{\partial |V_j|} = -|V_i| B_{ij} \tag{II.58}$$

Applying these assumptions to Eqs. (II.52) and (II.53), we get

$$\frac{\partial P_i}{\partial \delta_i} = -|V_i| B_{ii} \quad \text{or} \quad \frac{\Delta P_i}{\Delta \delta_i} = -|V_i| B_{ii}$$

$$\frac{\Delta P_i}{|V_i|} = -B_{ii}\Delta\delta_i$$

$$\frac{\Delta P_i}{|V_i|} = -B'\Delta\delta_i \qquad \text{(II.59)}$$

Similarly,

$$\frac{\partial Q_i}{\partial|V_i|} = -|V_i|B_{ii} \quad \text{or} \quad \frac{\Delta Q_i}{\Delta|V_i|} = -|V_i|B_{ii}$$

$$\frac{\Delta Q_i}{\Delta|V_i|} = -B_{ii}\Delta|V_i|$$

$$\frac{\Delta Q_i}{|V_i|} = -B''\Delta|V| \qquad \text{(II.60)}$$

$B'$ and $B''$ are the imaginary parts of the bus admittance. It is better to ignore all shunt connected elements, as to make the formation of $J_1$ and $J_4$ simple. This will allow for only one single matrix than performing repeated inversion.The successive and voltage magnitude and phase angle changes are [28]

$$\Delta\delta = -\left[B'\right]^{-1}\frac{\Delta P}{|V|} \qquad \text{(II.61)}$$

$$\Delta|V| = -\left[B''\right]^{-1}\frac{\Delta Q}{|V|} \qquad \text{(II.62)}$$

**Fast Decoupled Load Flow Algorithm**

Step 1: Create the bus admittance matrix [$Y_{bus}$].

Step 2: Detect all kinds and numbers of buses and setting all bus voltages to an initial value of 1 p.u., all voltage angles to 0, and the iteration counter iter to 0.

Step 3: Create the matrices $B'$ and $B''$ according to Equations. (II.59) and (II.60).

Step 4: If max ($\Delta P$, $\Delta Q$) ≤ accuracy

$$\Delta P_i^{(k)} = P_i^{sch} - P_i^{(k)} \qquad \text{(II.63)}$$

$$\Delta Q_i^{(k)} = Q_i^{sch} - Q_i^{(k)} \qquad \text{(II.64)}$$

then go to Step 6

*else*

(i) Calculate $J_1$ and $J_4$ elements of Equations. (II.55), (II.56), (II.57) and (II.58).

$$\frac{\partial P_i}{\partial\delta_i} = -|V_i|B_{ii} \qquad \frac{\partial Q_i}{\partial\delta_j} = -|V_i|B_{ij}$$

$$\frac{\partial Q_i}{\partial|V_i|} = -|V_i|B_{ii} \qquad \frac{\partial Q_i}{\partial|V_j|} = -|V_i|B_{ij}$$

(ii) Check the limits of $Q_i$

$$if \quad Q_{i,min} < Q_i < Q_{i,max} \quad calculate\ P_i^{(k)}$$

$$if \quad Q_i^{(k)} > Q_{i,max} \qquad Q_{i,sch} = Q_{i,max}$$

$$if \quad Q_i^{(k)} < Q_{i,min} \qquad Q_{i,sch} = Q_{i,min}$$

(iii)Calculate the power residuals, $\Delta P$ and $\Delta Q$

$$\Delta P_i^{(k)} = P_i^{sch} - P_i^{(k)}$$

$$\Delta Q_i^{(k)} = Q_i^{sch} - Q_i^{(k)}$$

(iv) Calculate the bus voltage and voltage angle updates $\Delta V$ and $\Delta\delta$.

$$[\Delta\delta_i]^{(k)} = -[B']^{-1} \frac{\Delta P_i^{[k]}}{|V_i|}$$

$$[\Delta V_i]^{(k)} = -[B'']^{-1} \frac{\Delta Q_i^{[k]}}{|V_i|}$$

(v) Update the voltage magnitude $V$ and the voltage angle $\delta$ at each bus.

$$\delta_i^{(k+1)} = \delta_i^{(k)} + \Delta\delta_i^{(k)}$$

$$|V_i^{(k+1)}| = |V_i^{(k)}| + \Delta|V_i^{(k)}|$$

(vi) Increment of the iteration counter iter = iter + 1

Step 5: If iter ≤ maximum number of iterations

$$|\Delta P_i^{(k)}| \leq \varepsilon$$

$$|\Delta Q_i^{(k)}| \leq \varepsilon$$

then go to Step 4

*else* print out 'Solution did not converge' and go to Step 6.

Step 6: Print out of the power flow solution, computation and display of the line flow and losses.

This completes the load flow study.

## II-9. Optimal power flow

The optimal power flow (OPF) is an inevitable part of the energy management system for power system planning and operation over a couple of decades. The main objective of the OPF is to determine the most favourable operating conditions to meet the required demand by satisfying all the power system operational and security constraints [37].

Additionally, Optimal Power Flow (OPF) identifies the most efficient and secure operating point by optimizing chosen objectives—such as generation cost, voltage profile, stability,

transmission losses, and system security—while satisfying operational constraints. It does so by adjusting control variables (generator outputs, bus voltages, and transformer tap settings). Both classical and modern optimization techniques have been applied to solve the OPF problem [38].

Optimal Power Flow (OPF) aims to optimize a specified cost, planning, or reliability objective by controlling power flows within an electrical network, all while respecting power-flow constraints and equipment operating limits.

The general OPF problem is a nonlinear, non-convex, large-scale optimization problem which may contain both continuous and discrete control variables. Many different OPF formulations have been developed to address specific instances of the problem, using varying assumptions and select-ing different objective functions, controls, and system constraints. The resulting optimization formulations are referred to by different names, depending on the chosen objective function and the constraints applied. Regardless of the name, however, any power systems optimization problem that includes a set of power flow equations in the constraints may be classified as a form of OPF [39].

### II-9-1. Definition of Optimization

Optimization is selecting inputs of a physical system that will lead to the best possible outputs. Its process is to find the best possible solution that corresponds to the maximum or minimum value of an objective-function (OF) While respecting the conditions imposed by the system or the operator itself [40].

Furthermore, the "Objective" function can be a cost (minimize), profile (maximize), or production (maximize). Objective functions are diverse, as well as the constraints (conditions) depending on the problem to be optimized [41].

Moreover, Optimization may target either a single objective seeking one optimal solution that minimizes or maximizes a given function or multiple objectives identifying a set of trade-off solutions that best satisfy several criteria simultaneously [19].

### II-9-2. Optimization Problems

**An optimization problem** is defined by a state space, one or more objective function(s), and a set of constraints.

**The state space** is defined by the set of domains of definition of the problem's variables. In

most problems, this space is finite because the resolution method used needs to work in a restricted space (Examples: the Monte Carlo method, genetic algorithms). This limitation is not problematic because when a problem is posed, the decision-maker specifies a feasible range of values for each variable. Additionally, for operational reasons and computational time, it is preferable to work with finite domains.

**The problem's variables** can be of various types (real, integer, boolean, etc.) and can represent qualitative or quantitative data. There may also be difficulties in implementing certain methods if the variables are of different types.

**An objective function** represents the goal to be achieved by the decision-maker (minimization of cost, time, error, etc.). It defines a space of potential solutions to the problem.

**The set of constraints** defines conditions on the state space that the variables must satisfy. These constraints are often inequality or equality constraints and generally help to limit the search space.

In addition, although constraints and objectives both represent desired outcomes, they are conceptually distinct. Constraints restrict the search space by defining feasible regions, whereas objectives rank and evaluate solutions within that space. Moreover, most optimization techniques employ separate mechanisms for enforcing constraints and for optimizing objective functions.

**An optimization method** searches for the point or a set of points in the space of possible states that best satisfy one or more criteria. The result is called the optimal value or optimum.

### II-9-2-1. Choice of a Method

The nature of the variables, definition domains, and criteria to be optimized will influence the choice of the optimization method to use.

There are two main families of optimization methods: deterministic methods and stochastic methods [42].

### II-9-3. Global Optimum, Local Optimum

Global search methods for extrema are typically used to solve complex non-convex (non-linear) optimization problems by extensively exploring the domain to avoid local optima (traps) and thereby locate the global optimum.

Additionally, global methods are less dependent on initial conditions, but these techniques cannot take advantage of the local characteristics of the solution space like gradient-based methods, and their convergence will be slower. As shown in Figure II.5, the search space contains multiple local optima (traps) in addition to the global optimum. [41, 43].

- **Local optimization** is the search for a solution that is better locally (within a neighborhood of that solution). This solution is called a local optimum.
- **Global optimization** is the search for the best solution across the entire domain; that is, within the entire domain, there is no solution better than it while respecting the constraints. This solution is called the global optimum. By definition, the global optimum is also a local solution [44].

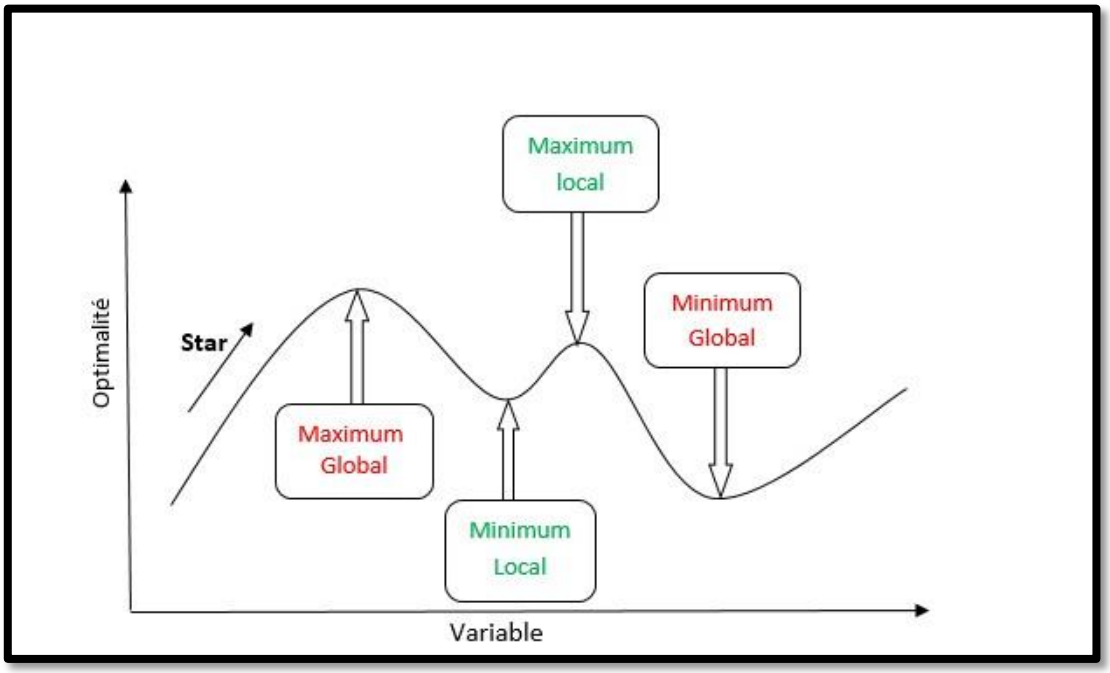


***Figure (II.5)*** *Local Optimum vs Global Optimum*

## II-9-4. Formulation of the ORPD

The optimal reactive power dispatch (ORPD) is an optimization problem recognized as an important tool in the electrical power engineering area, to manage reactive power in electrical networks. The main objective of ORPD is to assess the optimal operating state of the electrical power grid based on the criteria of economy, service quality and security [45].

Moreover, ORPD is a sub problem of optimal power flow calculation, which adjusts all kinds of controllable variables, such as generator voltages, transformer taps, shunt capacitors/inductors, etc, and handles a given set of physical and operating constraints to minimize transmission losses or other concerned objective functions [46].

The ORPD problem can be mathematically formulated as follows [47]:

$$Min\ f = Minimize(f_1, f_2) \tag{II.65}$$

$$\text{Subject to: } \begin{cases} g(x,\ u) = 0, & Equality\ Constraints \\ h(x,\ u) \le 0, & Inequality\ Constraints \\ u_j^{lower} \le u \le u_j^{upper} & Variable\ limits \end{cases} \tag{II.66}$$

Where $f_1$ *and* $f_2$ are the objective functions, $x$ represents the vector of dependent variables and $u$ represents the vector of control variables. They are represented as follows:

$$x^T = [V_L \ldots\ldots V_{NLB}, Q_{G1} \ldots\ldots Q_{G,NG}, S_1 \ldots\ldots S_{NTL}] \tag{II.67}$$

$V_L \ldots_{NLB}$ is the voltage magnitude of all load buses,

$Q_{G1} \ldots_{GN}$, $_{NG}$, is the reactive power generation, and

$S_{L1} \ldots_{NTL}$ is the transmission line capacity limit.

$$u^T = [V_{G1} \ldots\ldots V_{GNG}, T_1 \ldots\ldots T_{NT}, Q_{C1} \ldots\ldots Q_{CNC}] \tag{II.68}$$

$V_{G1}$ ,. . . $V_{GNG}$ represents voltage magnitude of generator bus, $Q_c$ . . . $Q_{cnc}$ depicts the shunt VAR compensator and $T_1$ . . . $N_T$ is the tap settings of transformers [37].

### II-9-4-1. Objective Functions

The three main objectives of the ORPD problem considered here consist of minimization of total active power losses, minimization of voltage deviation at load buses, and minimization of L-index [48], And we will discuss them in sequence :

#### II-9-4-1-1. Total Active Transmission Losses

With the increasing rate of energy consumption, the amount of power losses increased too, making the reduction of power losses as an important aim for system operators [47]. Subsequently, the transmission line loss can be calculated as:

$$f = min\ \sum_{k \in N_E} P_{kloss} = \sum_{k \in N_E} g_k \times (v_i^2 + v_j^2 - 2 \times v_i \times v_j \times cos\,\theta_{ij}) \tag{II.69}$$

where $P_{kloss}$ denotes the active power loss of $k$ branches, $g_k$ denotes the conductively of $k$

branches which conjoins bus $j$ and bus $k$, $N_E$ denotes all branches(transmission lines), $\theta_{ij}$ denotes the voltage phase difference, $v_i$ denotes the voltage amplitude of the $i$ node and $v_j$ denotes the voltage amplitude of $j$-node [49].

### II-9-4-1-2. Voltage Deviation

The second objective function aims to minimize the voltage deviation at the load busbars [50]. For stable power-system operation, bus voltages should be maintained as uniformly as possible. The effectiveness of the voltage adjustment can be evaluated through the total voltage deviation (TVD) index, which determines the voltage phase shift at the busbars compared to the reference voltage ($V_{ref}$) set at 1.0 [p.u].

The important to note that, if the minimum value of (TVD) implies that all bus voltages are close to $V_{ref}$, which makes it more level. And which can be formulated as follows [51, 52]:

$$\text{Min TVD} = \sum_{i \in N_L} |V_i - V_{refi}| \tag{II.70}$$

Where

$N_L$ is the number of load buses in the power system.

$V_i$ is the voltage magnitude of bus $i$

$V_{ref}$ is the voltage magnitude reference of the I'th bus (usually 1.0 pu)

### II-9-4-1-3. Voltage Stability Index

It's worth noting that, when the system subject to different operating situations such as disturbance or sudden load change, all buses should maintain acceptable bus voltage [53].The principal interest behind study of voltage stability index lies in the simplicity to provide the sufficient information's about the voltage instability or to quantify the vicinity of a power system to the voltage collapse (L-index is the voltage stability index that plays an important role in voltage stability analysis) [54]. This is can be achieved by the minimization of the voltage stability indicator L-index ($L_j$) at every bus of the electrical network, and consequently the total power system (Lindex), The values of the L-index is ranged from 0 to 1, where the lowest value refers to more stable system and vice versa. One widely used method in the literature is that proposed for the first time by Kessel P and Glavitsch H. The L-index of k'th bus is formulated as follows:

$$f(x, u) = VSI(x, u) = min(max(L_j)) \tag{II.71}$$

where $L_j$ of the $jth$ bus is formulated by the following equation:

$$L_j = \left| 1.0 - \sum_{i=1}^{N_{PV}} F_{ji} \times \frac{V_i}{V_j} \angle\theta_{ji} + \delta_i - \delta_j \right| \quad j=1,2,\ldots,N_{PQ} \tag{II.72}$$

With $F_{ji} = |F_{ji}|\angle\theta_{ji}$ , $V_i = |V_i|\angle\delta_i$ , $V_j = |V_j|\angle\delta_j$

$$F_{ji} = -[Y_1]^{-1} \times [Y_2] \tag{II.73}$$

where, $i$ and $k$ define the buses of generators and load, respectively. $Y_1$ and $Y_2$ depict the system sub-matrices for Y bus which obtained from the separation of generator PV and load buses PQ as shown in Eq [53, 54]:

$$\begin{bmatrix} I_{PQ} \\ I_{PV} \end{bmatrix} = \begin{bmatrix} Y_1 & Y_2 \\ Y_2 & Y_4 \end{bmatrix} \begin{bmatrix} V_{PQ} \\ V_{PV} \end{bmatrix} \tag{II.74}$$

### II-9-4-2. Operational Constraints

The ORPD subject to equality and inequality operational constraints of the system as presented follows:

#### II-9-4-2-1. Power flow Equality Constraints

The active and reactive power flow balance equation between the generated and absorbed power are generally referred to the equality constraints. These restrictions are one of the most important controlling parameters in the power system, while the load demands need to be satisfied by the generation [37]. The constraints are a reflection of the physical laws governing the electrical system. They are represented by the nonlinear equations of power flow. It is required that the sum of active and reactive powers injected into each bus set equals zero [24] . The equality constraints are formulated as follows [54] :

$$\begin{cases} P_{g,i} - P_{d,i} - \sum_{j=1}^{NB} |V_i| \times |V_j| \times |Y_{ij}| \times \cos \times (\theta_{ij} - \delta_i + \delta_j) = 0 \\ Q_{g,i} - Q_{d,i} - \sum_{j=1}^{NB} |V_i| \times |V_j| \times |Y_{ij}| \times \sin \times (\theta_{ij} - \delta_i + \delta_j) = 0 \end{cases} \tag{II.75}$$

where, $P_{g,i}$ and $Q_{g,i}$ are the output of active and reactive powers from the generator of bus $i$, respectively. $P_{d,i}$ and $Q_{d,i}$ are demand active and reactive powers of bus $i$, respectively [53].

#### II-9-4-2-2. Operational Inequality Constraints

The inequality constraints are also called power system operating and security constraints which include the power generation limit of generating units [37], Constraints related to

generator bus voltage magnitude, transformer tap settings, and other similar parameters are detailed as follows:

***a. Generator Constraints***

The voltages and reactive power outputs at all generating buses must be bounded within their upper and lower limits $V$ [53].

$$\begin{aligned} V_{Gi}^{min} \le V_{Gi} \le V_{Gi}^{max}, \quad & i=1, 2, 3..., N_G \\ Q_{Gi}^{min} \le Q_{Gi} \le Q_{Gi}^{max}, \quad & i=1, 2, 3..., N_G \\ P_{Gsl}^{min} \le P_{Gsl} \le P_{Gsl}^{max}, \quad & i=1, 2, 3..., N_C \end{aligned} \tag{II.76}$$

Where, $V_{Gi}^{min}$ , $V_{Gi}^{max}$ are the minimum and maximum generating voltages of bus generating i'th, $Q_{Gi}^{min}$ , $Q_{Gi}^{max}$ are the minimum and maximum generating reactive power of bus generator i'th and $P_{Gsl}^{min}$, $P_{Gsl}^{max}$ are the minimum and maximum active power output of slack bus i'th.

where $N_G$ denotes the set of buses where the generators are installed in the system.

***b. Capacitor Banks Constraints***

The reactive power compensated by the shunt capacitor banks is restricted within the upper and lower limits, as follows:

$$Q_{CB,i}^{min} \le Q_{CB,i} \le Q_{CB,i}^{max}, \forall i \in N_{CB} \tag{II.77}$$

where $N_{CB}$ represents the set of buses where the capacitor banks are connected [55].

***c. Constraints of Transmission Line Loading and Voltages at Load Buses***

The limits on apparent power transfer in transmission lines and power transformers are established to ensure system security against thermal losses in conductors and/or to maintain network stability [19].

$$S_{ij} \le S_{ij}^{max}, \ \forall i \ j \in N \tag{II.78}$$

Where $ij$ is the index for the transmission line connecting buses $i$ and $j$.

Under any condition, the bus voltage magnitude at each load bus $i$ must be maintained Within the permissible minimum and maximum limits, as expressed in the following formulation:

$$V_i^{min} \le V_i \le V_i^{max}, \ \forall i \in N_L \tag{II.79}$$

***d. Transformer Constraints***

Transformer's tap operation settings can vary between the minimum and maximum available value:

$$T_i^{min} \le T_i \le T_i^{max}, \ \forall i = 1 \dots N_T \tag{II.80}$$

where $N_T$ is the number of transformers [55].

Furthermore, to ensure that the dependent variables $V_i$, $Q_g$ , and $S_i$ remain within their prescribed limits, the penalty factor technique is applied. This method prevents the selected dependent variable from exceeding its boundaries by eliminating solutions that violate these constraints, even if they yield an optimal objective function value. To accomplish this, an augmented objective function is employed, as defined by the following equation:

$$F_{aug}=F(x,\,u)+\lambda_V\sum_{i=1}^{NLB}\Delta V_{Li}+\lambda_Q\sum_{i=1}^{NG}\Delta Q_{Gi}+\lambda_Q\sum_{i=1}^{NTL}\Delta S_{li} \tag{II.81}$$

Where $\lambda_V$ , $\lambda_Q$ are the penalty factors [20].

$$\Delta V_i\begin{cases}\left(V_i^{min}-V_i\right)^2 & if\quad V_i<V_i^{min}\\ (V_i-V_i^{max})^2 & if\quad V_i>V_i^{max}\\ 0 & if\quad V_i^{min}\le V_i< V_i^{max}\end{cases} \tag{II.82}$$

$$\Delta Q_i\begin{cases}\left(Q_i^{min}-Q_i\right)^2 & if\quad Q_i<Q_i^{min}\\ \left(Q_i-Q_i^{max}\right)^2 & if\quad Q_i>Q_i^{max}\\ 0 & if\quad Q_i^{min}\le Q_i< Q_i^{max}\end{cases} \tag{II.83}$$

$$\Delta S_i\begin{cases}(S_i-S_i^{max})^2 & if\quad S_i>S_i^{max}\\ 0 & if\quad S_i^{min}\le S_i< S_i^{max}\end{cases} \tag{II.84}$$

All three equations (II.82) - (II.84) are adapted from [33].

## II-10. Optimal Reactive Power Dispatch

The initial attempts to approach the ORPD problem resorted to linear programming, Newton based method, Gauss, and Fast decoupled method, interior point methods etc... Although these techniques are computationally fast they do not perform well when dealing with non-convex problems and discrete variables. Also they tend to converge to local minima and have difficulties handling a large number of decision variables [52].

## II-11. Conclusion

In summary, this chapter has provided a rigorous presentation of the foundational principles and numerical methods required for load flow, and optimal power flow analysis, ORPD in electrical power systems. Beginning with the mathematical formulation of the bus admittance matrix, we explored the essential iterative techniques that enable the resolution of nonlinear power flow equations, highlighting their strengths, limitations, and practical applications. Additionally, the discussion on Optimal Power Flow has underscored the significance of balancing system efficiency, stability, and security constraints within operational decision-making. As power systems continue to grow in scale and complexity, the need for

robust and sophisticated solution approaches becomes ever more critical. In the next chapter, we will further extend this study by focusing on metaheuristic, presenting advanced methodologies and predictive techniques that contribute to more reliable and optimized operation of electrical networks.

# CHAPTER III

# *CHAPITER 3*

# *The Meta-heuristics*

## III-1. Introduction

Optimization seeks the best solution to a problem within given constraints. Optimization algorithms fall into two categories: the deterministic approach and the stochastic approach. The deterministic approach uses gradient-restricted techniques to systematically approach the optimal value, while the stochastic approach uses gradient-free methods that employ randomized steps to generate diverse solutions. Stochastic techniques can be further divided into heuristic (HA) and metaheuristic (mHA) algorithms. A heuristic is a process that uses trial and error to quickly find good solutions, but it risks local trapping. Metaheuristic algorithms (mHAs) were developed due to the shortcomings of heuristic algorithms. Each MHA uses special techniques to guide the search process, effectively exploring the search location to find close-to-optimal solutions. Furthermore, they are non-greedy, enabling them to extensively discover the search region and possibly lead to the best solution, which occasionally coincides with the global optimum.

Meta-heuristic algorithms typically contain two key attributes: exploration and exploitation. Exploration refers to an algorithm's potential to globally search at numerous sections of the region, to avoid becoming trapped in local optima. Exploitation refers to the potential to locally discover for possible options in all promising areas to boost solution accuracy. A great performance is obtained when balancing between these two, exploration and exploitation to get the optimal or near-to-optimal solutions. Accordingly, MHAs are into four groups evolutionary-based, swarm-based, physics-based, and human-based methods as shown in Figure III.2 [56].

In this chapter we will present three special algorithms which are Genetic Algorithm (GA), Grey Wolf Algorithm (GWO), and proposed one Tunicate Swarm Algorithm (TSA), that categorized in metaheuristic as Evolutionary-based, and the last two methods as Swarm-based respectively.

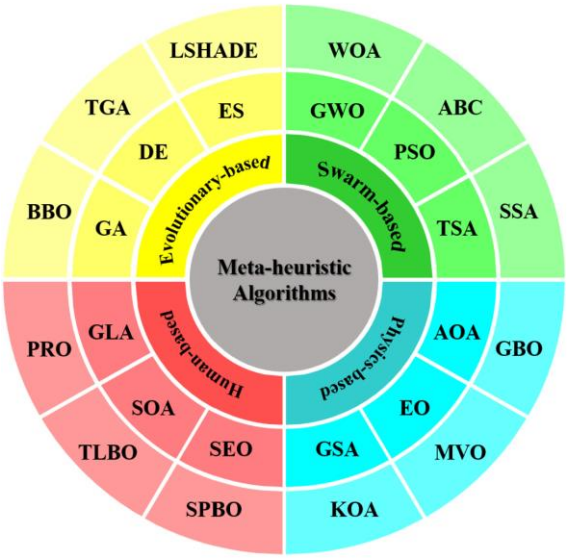


***Figure (III.1)*** *Classification of Metaheuristic Algorithm*

## III-1. Genetic Algorithm (GA)

### III-1-1. Inspiration

Genetic algorithms are search and optimization algorithms based totally on the concepts of natural evolution, which were first introduced through john Holland in 1970. Genetic algorithm additionally enforce the optimization techniques by simulating evolution of species via natural selections. Genetic algorithm is usually compared of two processes. First process is selection of individual for the production of next generation and 2$^{nd}$ manner is manipulation of the selected individual to structure the next generation by using crossover which individual strategies. The selection mechanism determines which individual are chosen for reproduction and how many offspring every chosen individual produce. The main principle of selection strategy is the better is an individual; the greater is its chance of being parent [57].

### III-1-2. Genetic Operators

**Initial Population**

The GA algorithm starts with a random population. This population includes multiple solutions, which represent chromosomes of individuals. Each chromosome has a set of variables, which simulates the genes. The main objective in the initialisation step is to spread the solutions around the search space as uniformly as possible to increase the diversity of population and have a better chance of finding promising regions [58].

Operations perform in GA:

- Selection

- Crossover
- Mutation [59]

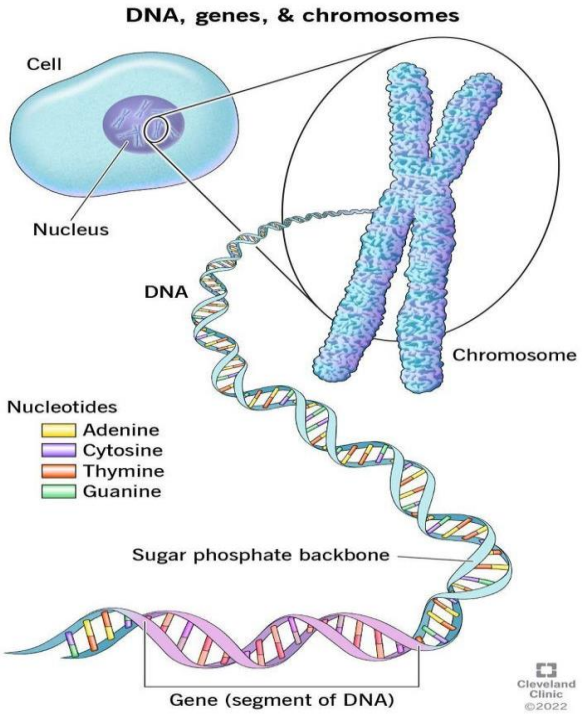


***Figure (III.2)*** *DNA, gene, & chromosome*

**a)** ***Selection Operation***

In the field of Genetic Algorithms (GAs), selection constitutes a foundational process that determines the chromosome or string (a sequence of genes) selected to participate in the reproduction phase [60]. In addition, in nature, the fittest individuals are more likely to get food and mating opportunities. This causes their genes to contribute more in the production of the next generation of the same species. Inspired by this concept, the Genetic Algorithm uses a roulette-wheel mechanism to assign selection probabilities to each chromosome based on its fitness value and select them for creating the next generation proportional to their fitness (objective) values [58].

- A chromosome is a full candidate solution (binary string).
- A string is how that solution is represented (usually as a sequence of numbers, bits, or other values)
- Each position in the string is called a gene.
- An allele is the value at that position (0 or 1) [60].

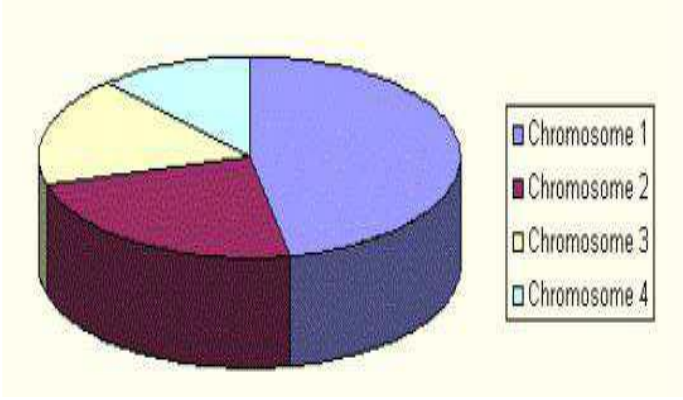


***Figure (III.3)*** *Roulette Wheel Selection*

Parents are selected in proportion to their fitness. Each chromosome occupies a segment on a roulette wheel that is sized according to its fitness value (see Fig. III.3). Chromosomes with higher fitness have a greater probability of being chosen and thus reproduce more frequently [57].

It is worth noting that, for a chromosome $ch_i$ or $x_i$ with fitness $f(ch_i)$, the probability of its selection into a new population of size $N$ is given by [61]:

$$P(ch_i)=\frac{f(ch_i)}{\sum_{j=1}^{N} f(ch_j)} \qquad \text{(III.1)}$$

Where

$f(ch_i)$ : Is the fitness of the chromosome number $i$

$f(ch_j)$ : The sum of chromosomes fitness

$P$ : the Probability of selection

**b) *Crossover Operations***

Once individuals have been selected by the selection operator, they are used to form the new generation. In nature, chromosomes from male and female individuals combine to form a new chromosome. Analogously, the GA simulates this process by selecting two parent chromosomes ( $ch_1$ and $ch_2$), via roulette-wheel selection and recombining them to produce two offspring chromosomes (children solutions $ch'_1$ and $ch'_2$. There are different techniques for the crossover operator in the literature of which two (single-point and double-point [16]) are shown in FigureIII.5.a, and b [58].

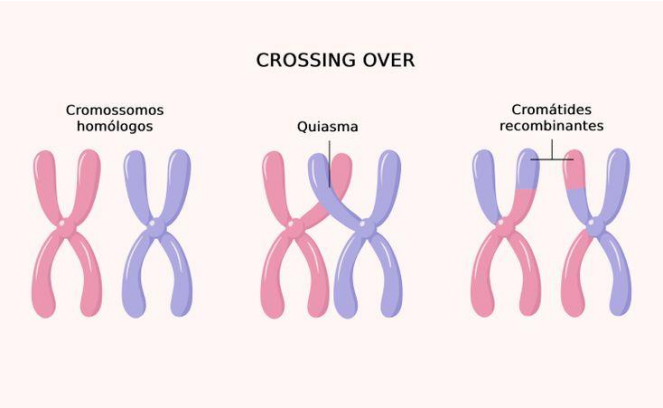


***Figure (III.4)*** *Crossing over of Chromosomes*

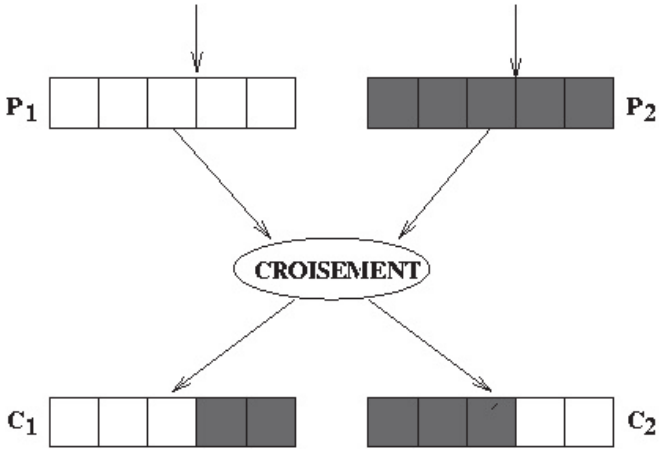


***Figure (III.5.a)*** *Single-Point Crossover*

**Single-point crossover:** a random cut-point is chosen along each parent's chromosome. The segment to the right of that cut in *Parent 1* is swapped with the corresponding segment in *Parent 2* (will be swaped with each other), This swap makes two children $C_1$, $C_2$ (New population)

**Two-point crossover:** two cut-points are selected, defining a middle segment on each parent. That middle portion of *Parent 1* is exchanged with the middle portion of *Parent 2,* and the same of exchange happen to *Parent 2* portion (It replaced the bits of both the parents), producing new offspring [60] as shown in figure III.5.b.

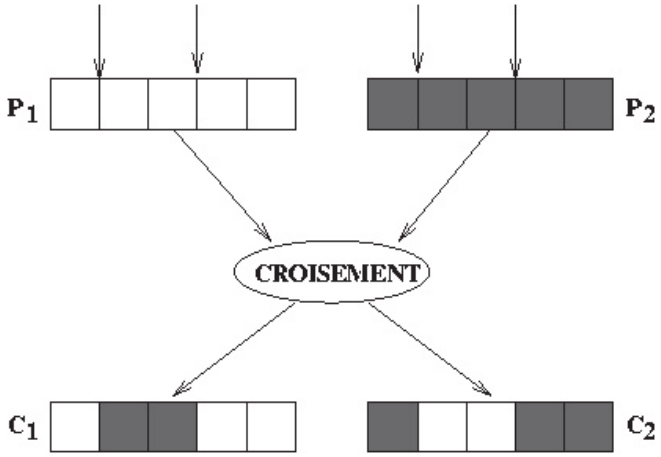


***Figure (III.5.b)*** *Two-Point Crossover*

| | |
|---|---|
| Chromosome 1 | 11011 \| 00100110110 |
| Chromosome 2 | 11011 \| 11000011110 |
| Offspring 1 | 11011 \| 11000011110 |
| Offspring 2 | 11011 \| 00100110110 |

***Figure (III.6)*** *Crossover of chromosome in binary*

Importantly, they generate two new chromosomes, $ch'_1(i)$ and $ch'_2(i)$, through a linear combination:

$$\begin{cases} ch'_1(i) = a \times ch_1(i) + (1 - a) \times ch_2(i) \\ ch'_2(i) = (1 - a) \times ch_1(i) + a \times ch_2(i) \end{cases} \quad \text{(III.2)}$$

- α: is a random weighting parameter that normally takes its values in the interval [−0.5, 1.5] [61].

**c)** ***Mutation***

At this stage, A gene may be replaced by another within a chromosome randomly. a mutation rate typically set between 0.001 and 0.01 (Probability of mutation $P_m$) [62].


***Figure (III.7)*** *Gene mutation 1 to 0 (example).*

For example, as illustrated in Figure III.7.a mutation occurred on the fourth gene of chromosome, changing that gene from 1 to 0

### III-1-3. Flowchart of GA

The Genetic Algorithm procedure for searching the space of candidate solutions is as follows:

***Procedure***:

1. [***Start***] Generate random population of n chromosomes (suitable solutions for the problem).

2. [***Fitness***] Evaluate the fitness f(x) of each chromosome x in the population.

3. [***New population***] Create a new population by repeating following steps until the new population is complete

a. [***Selection***] Select two parent chromosomes from a population according to their fitness (the better fitness, the bigger chance to be selected).

b. [***Crossover***] With a crossover probability cross over the parents to form a new offspring (children). If no crossover was performed, offspring is an exact copy of parents.

c. [***Mutation***] With a mutation probability mutate new offspring at each locus (position in chromosome).

d. [***Accepting***] Place new offspring in a new population.

4. [***Replace***] Use new generated population for a further run of algorithm.

5. [***Test***] If the end condition is satisfied, stop, and return the best solution in current population.

6. [***Loop***] Go to step 2.[57]

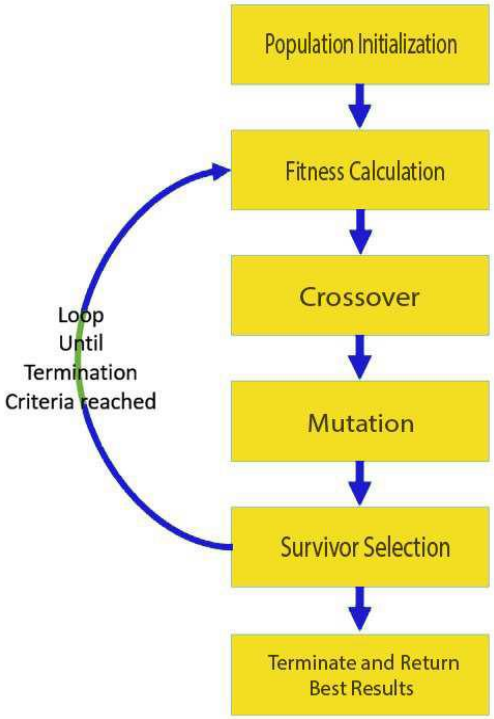


***Figure (III.8)*** *Flowchart of GA System*

### III-1-4. Strengths & Weaknesses

#### Strengths

A number of advantages made GAs to be applicable in multiple areas

- Having a satisfactory answer for the problems, which improves with time
- Works best in cases of large search space area possessing multiple parameters into it.
- Aims at delivering best solutions instead of a single solution
- Enhancing both continuous as well as distinct functions along with multi-purpose problems [59]

#### Weaknesses

- Can take long time to convergence
- No guarantee of finding global maxima [63].

### III-2. Grey Wolf Optimizer (GWO)

### III-2-1. Inspiration

In 2014, Seyedali Mirjalili and colleagues proposed the Grey Wolf Optimization (GWO) algorithm technique, inspired by the natural hunting strategies and social leadership hierarchy of grey wolves (Canis lupus). These grey wolves belong to the Canidae family, are regarded as apex predators [64].

Typically, grey wolves prefer to live in groups, with pack sizes ranging from 5 to 12 members. Interestingly, they follow a strict hierarchical social structure, as illustrated in Fig. (III.9) [65]. They categorize themselves into four groups: alpha wolf ($\alpha$) the first level, beta wolf ($\beta$) in the second level, delta wolf ($\delta$) represents the third level, then comes omega wolf ($\omega$) in the lowest position:

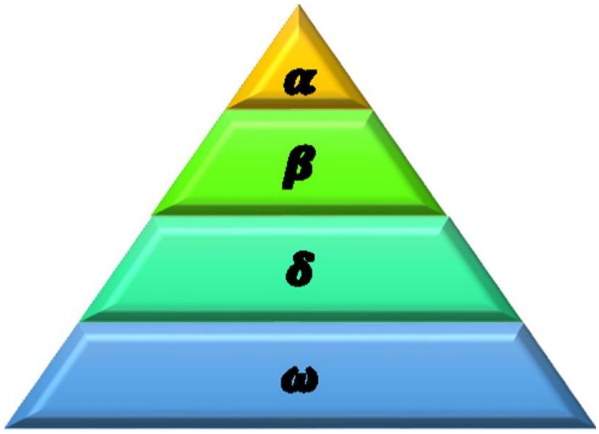


***Figure (III.9)*** *Social Dominant Hierarchy of Grey Wolves.*

The leader alpha (male or female) assumes leadership by making key decisions and maintaining order, though not necessarily being the strongest. The beta wolves serve as second in command, advising and helping alpha wolves to make a decision. Delta wolves are subordinates who assist the alphas and betas in a variety of roles, including scouts (watching the territory and warning the pack in case of danger), hunters, and sentinels, caretaker (caring the weak, ill, and wounded wolves). The omega wolf occupy the lowest in rank, plays a pivotal role in relieving stress for the pack by doing their responsibilities. This wolf frequently submits to the dominance of other wolves, they are the last wolves that are allowed to eat. on occasion, the omega assumes the role of scapegoat, also guarding young wolves [65, 66].

Hunting is significantly aided by using the alpha, beta, and delta wolves. They are the most effective wolves. These three wolves are totally accountable for tracking, pursuing, surrounding, and attacking the prey, as demonstrated in Figure III.10. The three principal stages of the grey wolf hunting mechanism are listed as follows:

- Tracking, chasing, and getting close to the prey
- Pursuing, encircling, and harassing the prey until it stops moving
- Attacking the target Prey [64]


***Figure (III.10)*** *Hunting behaviour of grey wolves: (A) chasing, approaching, and tracking prey (B-D) pursuiting, harassing, and encircling (E) stationary* [1]

### III-2-2. Mathematical Model and Algorithm

This part will talk about social hierarchy, and also explaining the behaviors of tracking, encircling, and attacking, and searching the prey mathematically:

#### III-2-2-1. Social hierarchy:

When designing the social hierarchy of wolves in Grey Wolf Optimization, we consider:

- The fittest solution as the alpha ($\alpha$)
- The second best solution is the beta ($\beta$)
- The third best solution as delta ($\delta$)

And the remaining candidate solutions are assumed to be omega ($\omega$), which the rest of these wolves follow the guides of the hunting (optimization) ($\alpha$), ($\beta$), ($\delta$) [1].

#### III-2-2-2. Encircling prey:

Wolves surround their target, and this encircling behavior can be modeled mathematically using equations (III.3) and (III.4) [67]:

$$\vec{D} = |\vec{C}.\vec{X}_P(t) - \vec{X}(t)| \quad \text{(III.3)}$$

$$\vec{X}(t+1) = \vec{X}_p(t) - \vec{A}.\vec{D} \quad \text{(III.4)}$$

The distance between the prey and the wolf here is $\vec{D}$. $X_p$ is the position vector of the prey, and $X$ implies the position vector of a grey wolf. [64] $t$ indicates the current iteration number and $T$ incidate the total iterations. $A$ and $C$ are random (coefficient) vectors that are determined in Equations. (III.5) and (III.6).

$$\vec{A} = 2\vec{a}.\vec{r}_1 - \vec{a} \quad \text{(III.5)}$$

$$\vec{C} = 2 \times \vec{r}_2 \quad \text{(III.6)}$$

$$a = 2 - 2 \times (\frac{t}{\mathrm{T}}) \quad \text{(III.7)}$$

The random vectors in the range of [0, 1] are $r_1$ and $r_2$. Vector $a$ regulates the GWO algorithm phenomenon for approaching the solution (prey) by decreasing it and is used as a foundation for $A$ computations, $A \in [-a, a]$. Vector $a$ is linearly decreased from 2 to 0 over the course of iterations [1, 68].

### III-2-2-3. Hunting:

The pack updates its positions according to the optimal positions of the three wolves, "$\alpha$","$\beta$", *and* " $\delta$ " (saving first best three solutions [1] ), as shown in Figure III.11. They believe that $\alpha$ , $\beta$, $\delta$ have more information about the location of the prey. This updating is articulated in the following equations [64, 68]:

$$\vec{D}_\alpha = |\vec{C_1}.\vec{X}_\alpha - \vec{X}|,\ \vec{D}_\beta = |\vec{C_2}.\vec{X}_\beta - \vec{X}|,\ \vec{D}_\delta = |\vec{C_3}.\vec{X}_\delta - \vec{X}| \quad \text{(III.8)}$$

$$\vec{X}_1 = \vec{X}_\alpha - \vec{A}_1.(\vec{D}_\alpha),\ \vec{X}_2 = \vec{X}_\beta - \vec{A}_2.(\vec{D}_\beta),\ \vec{X}_3 = \vec{X}_\delta - \vec{A}_3.(\vec{D}_\delta) \quad \text{(III.9)}$$

$$\vec{X}(t+1) = \frac{\vec{X}_1 + \vec{X}_2 + \vec{X}_3}{3} \quad \text{(III.10)}$$

In this context, $A_1$, $A_2$, and $A_3$ are like A. while, $C_1$, $C_2$, and $C_3$ are random vectors with values between 0 and 1. Finally, $X_1$, $X_2$, and $X_3$ represent the positions of the alpha, beta, and delta wolves, respectively.

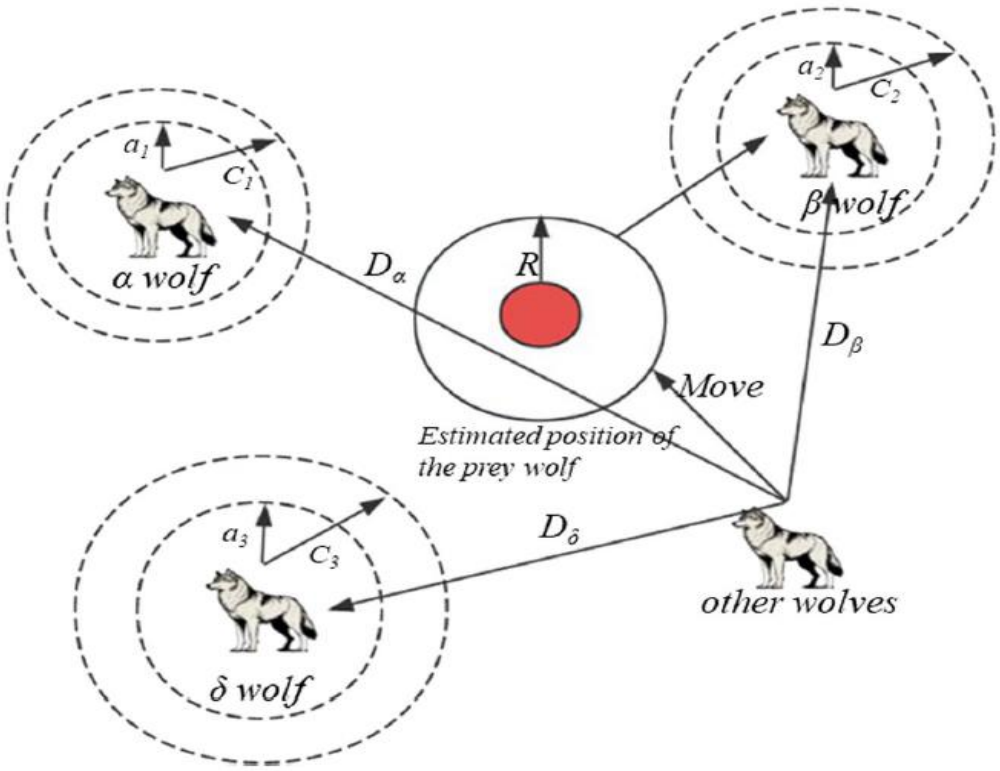


***Figure (III.11)*** *Position update of wolf groups in GWO algorithm* [2]

### III-2-2-4. Exploitation (Attacking the prey) and exploration (searching the prey) phase:

In the above equations, vectors *A* and *C* control exploitation and exploration in each iteration. When *A* and *C* are less than 1, the wolves focus on attacking prey, representing the exploitation phase. When *A* and *C* are greater than or equal to 1, the wolves explore more areas of the search space, representing the exploration phase [64]. Figure III.12 (a) shows that when $|A| < 1$, the wolves move to attack the prey.

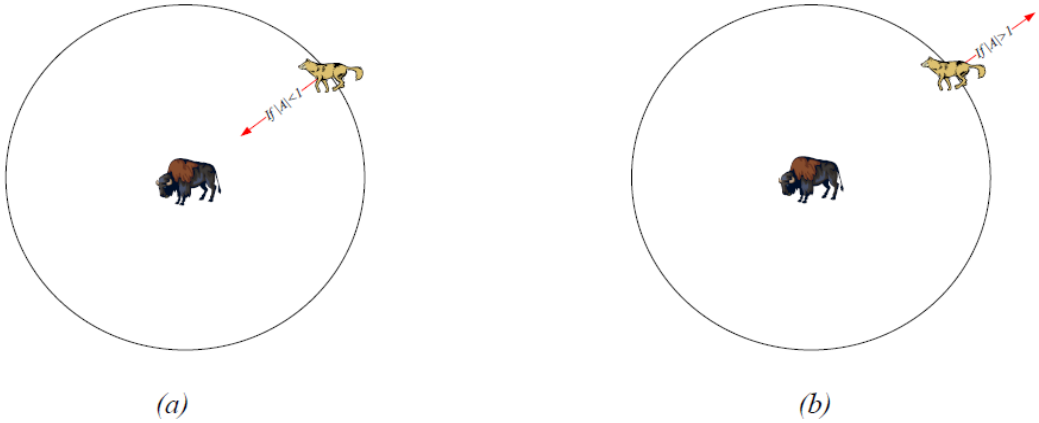


***Figure (III.12)*** *Attacking prey versus searching for prey*

### III-2-3. Flowchart of Grey Wolf Algorithm

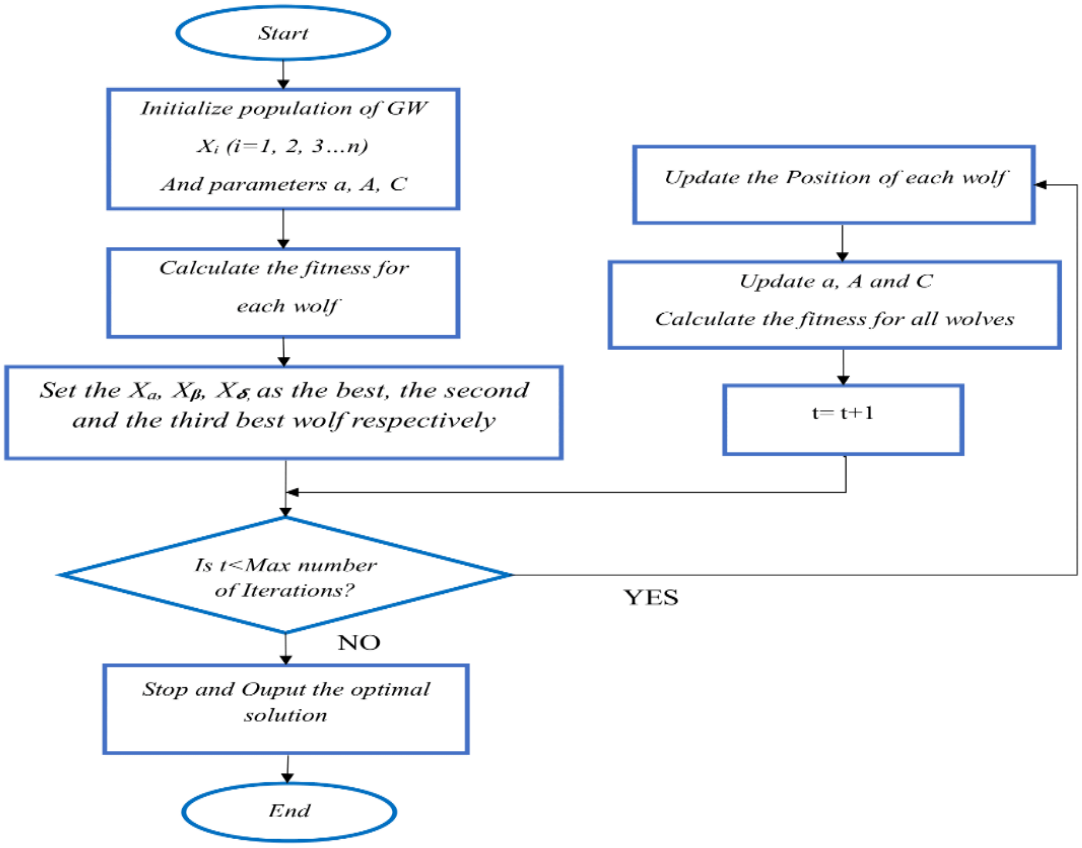


***Figure (III.13)*** *Flowchart of the grey wolf optimization algorithm* [1, 69, 70]

### III-2-4. Strengths & Weaknesses

#### Strengths

- Fewer parameters
- Implementing easily
- Simple principles

### Weaknesses

- Slow convergence speed
- Easy to fall into the local optimum
- Low solution accuracy [71]

## III-3. Tunicate Swarm Algorithm

### III-3-1. Inspiration

The Tunicate Swarm Algorithm (TSA) is a recently developed swarm-based metaheuristic inspired by the collective navigation and foraging behavior of tunicates. The TSA was first introduced in 2020 by S. Kaur, L.K. Awasthi, and G. Dhiman. The objective behind its development was to address nonlinear constrained optimization problems Its effectiveness has been validated through extensive testing on 74 benchmark functions encompassing a variety of problem types [72].

Tunicates, also known as sea squirts, are a group of marine animals that spend most of their lives connected to docks, rocks or the undersides of boats. The name, "tunicate" comes from the firm, but flexible body covering, referred to as a tunic. They have the form of a small barrel, and have two openings, known as siphons, enabling water to circulation through them so that they can feed on planktons. The tunicate moves via the ocean by using jet propulsion, this is achieved by expelling water through their siphons [73].

On the other hand, each tunicate is cylindrical in shape and has a gelatinous tunic that assists in connecting all the other tunicates. However, the TSA was inspired by two distinct behavioral patterns of tunicates in the deep sea: jet propulsion and swarm intelligence for locating the food source (the optimal solution) [73]. Furthermore, jet propulsion is the propulsion of something in one direction, produced by ejecting a jet of fluid in the obverse direction. Also in fact, Swarm intelligence relies on the collective behavior between individuals of the swarm [72]. As illustrated in Figures. III.14 and 15, respectively the visual representation of these patterns

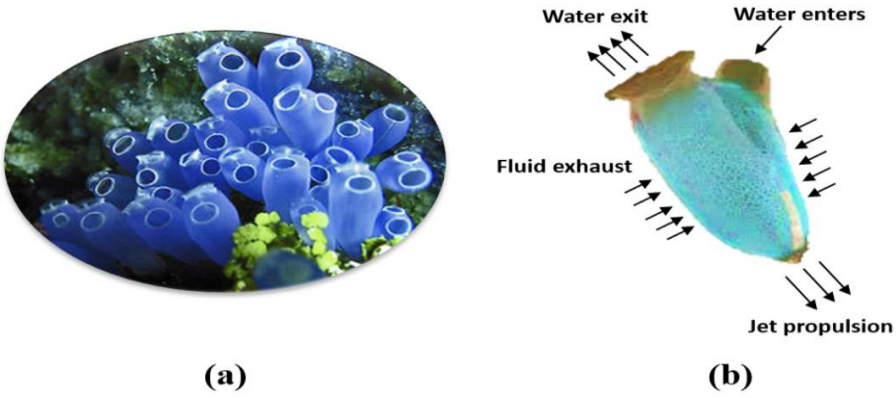


***Figure (III. 14)*** *Jet propulsion behavior of tunicates.*

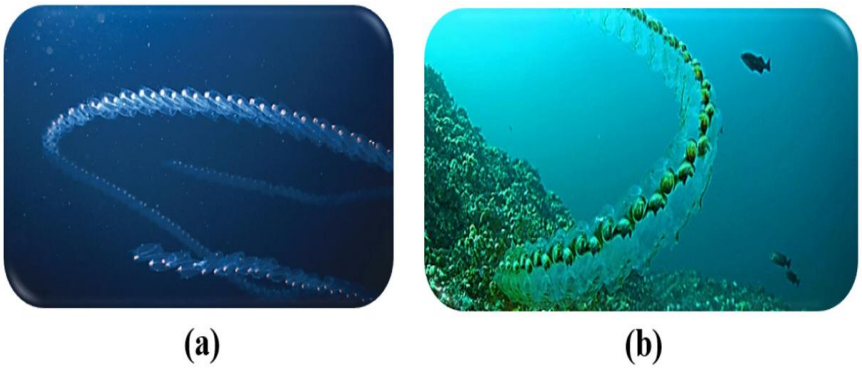


***Figure (III. 15)*** *Swarming behavior of tunicates.*

It is worth noting that, in order to find the optimal solution in the solution space the algorithm is based on four conditions, which are:

• Avoiding Conflicts Between Tunicate Individuals.

• Moving in the Direction of the Best Neighbor.

• Movement Towards the Best Tunicate

• Swarm Intelligence [74, 75].

### III-3-2-1. Avoiding Conflicts Between Tunicate Individuals

Firstly, tunicates (search agents, tunicate individuals) prevent conflicts between each other, by using a control vector $\vec{A}$. This vector calculates the position of new tunicates, as determined in equation III.16, also Figure (III.4) illustrates how tunicate individuals avoid conflicts [76, 77]

$$\vec{A} = \frac{\vec{G}}{\vec{M}} \quad \text{(III.11)}$$

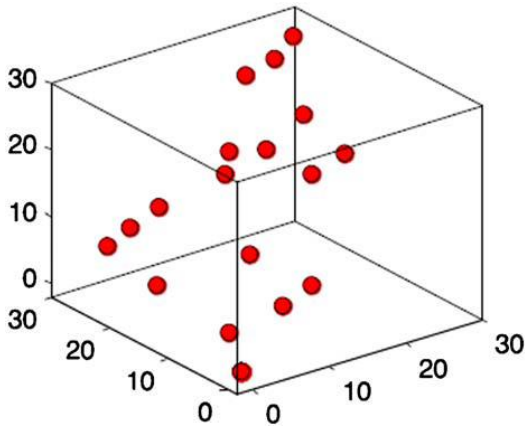


***Figure (III.16)*** *Conflict avoidance between search agents* [75]

$$\vec{G} = c_2 + c_3 - \vec{F} \quad \text{(III.12)}$$

$$\vec{F} = 2 \times c_1 \quad \text{(III.13)}$$

Notably, $\vec{G}$ is the gravity force, $\vec{F}$ represents the water flow advection in the deep ocean. $c_1$, $c_2$, and $c_3$ are the variables in the range of [0, 1]. $\vec{M}$ refers to the social forces between the search agents by the equation as follows:

$$\vec{M} = [\, P_{min} + c_1 \times P_{max} - P_{min} \,] \quad \text{(III.14)}$$

Where, $P_{min}$ and $P_{max}$ are the initial speed and inferior speed to make social communication. In this algorithm, the values of $P_{min}$ and $P_{max}$ are set to 1 and 4, respectively [78].

### III-3-2-2. Moving in the Direction of the Best Neighbor

After avoiding search conflicts among tunicate agents (search individuals), each individual in the population moves toward its best-performing neighbor, as illustrated in Figure III.17. This behavior can be formalized as [75]:

$$\overrightarrow{PD} = \left| \vec{FS} - rand \times \vec{P}_p(x) \right| \quad \text{(III.15)}$$

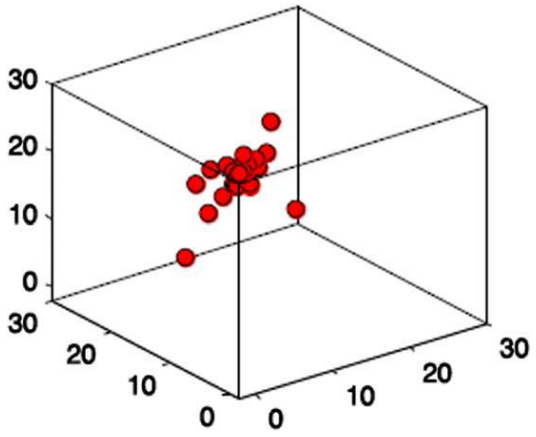


***Figure (III.17)*** *Search agent's movement towards the best neighbor.*

As well $\overrightarrow{PD}$ denotes the distance between the food source and the tunicate individual, $\overrightarrow{FS}$ is the location of the food source, $\vec{P}_P(x)$ is the current location (position) of the tunicate individual, $x$ is the number of current iterations, and random number between [0, 1] is denoted by *rand, rand* ∈ [0,1] [75].

### III-3-2-3. Movement Towards the Best Tunicate

After determining the distance between the food source and a tunicate individual, the tunicates, as illustrated in Fig. (III.18), move toward the current best tunicate individual according to Equation (III.16) [74].

$$\vec{P}_p(x') = \begin{cases} \vec{FS} + \vec{A} \times \vec{PD}, & if\ rand \geq 0.5 \\ \vec{FS} - \vec{A} \times \vec{PD}, & if\ rand < 0.5 \end{cases} \qquad \text{(III.16)}$$

- Where $\vec{P}_P(x')$ is the position of tunicate after updating regarding the position of food source $\overrightarrow{FS}$ [78]

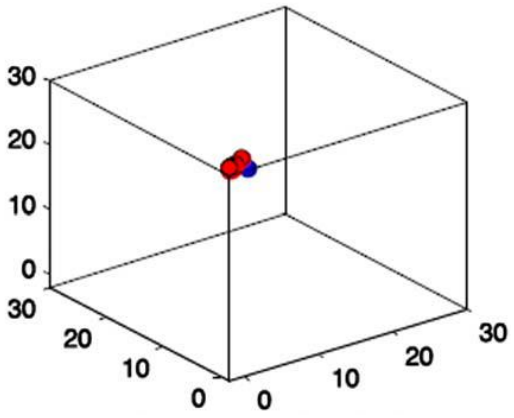


***Figure (III.18)*** *Converge towards best search agent position.*

### III-3-2-4. Swarm Intelligence (Swarm Behavior)

In the swarm intelligence mechanism, the Tunicate Swarm Algorithm (TSA) retains the two best solutions identified during the optimization process and updates the positions of the remaining tunicates accordingly [25]. The following equation is an illustration of this behavior:

$$\vec{P}_p(x+1) = \frac{\vec{P}_p(x) + \vec{P}_p(x')}{2 + c_1} \quad \text{(III.17)}$$

Where $_P = 1, 2, \ldots N$ , $N$ is the population size of tunicates, $\vec{P}_P(x+1)$ is the updated position of the current search individual, $P_P(x)$ is the position of the preceding search individual, and $P_P(x')$ is determined by Equation (III.16) [56].

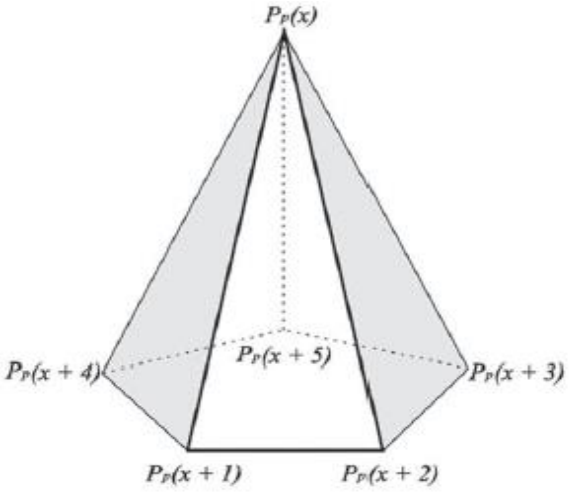


***Figure (III.19)*** *3D tunicate position.*

As demonstrated in Figure (III.19), the positions of the search agents are updated based on the location of the vector $P_P(x)$. And Tunicate position specifies an arbitrary location within a cone-shaped structure for the final position [76].

### III-3-2-5. Time Complexity of TSA

Assuming the size of the Tunicate swarm is N, the dimension size of the problem is D, and the maximum iteration is T. The main steps in TSA are as follows.

• Tunicate swarm initialization: $O(N \times D)$.

• Computational complexity for avoiding conflicts: $O(D)$.

• Computational complexity for moving towards the best neighbor: $O(N \times D)$.

• Computational complexity for moving towards the best tunicate: $O(N \times D)$.

• Computational complexity of swarm intelligence phase: $O(N)$.

In summary, the computational complexity of the Tunicate Swarm Algorithm (TSA) is expressed in this following Equation [74]:

$$O(N\times D+T\times(D+N\times D+N\times D+N)) = O(T\times N\times D) \quad \text{(III.18)}$$

- This means that the time increases linearly with each of the following: the number of iterations $T$, the number of individuals N, and the problem dimension D, and the number of behavioral operations. which makes it applicable over a wide range. However, it requires increasing computations in cases with high-dimensional problems or when using large swarms.

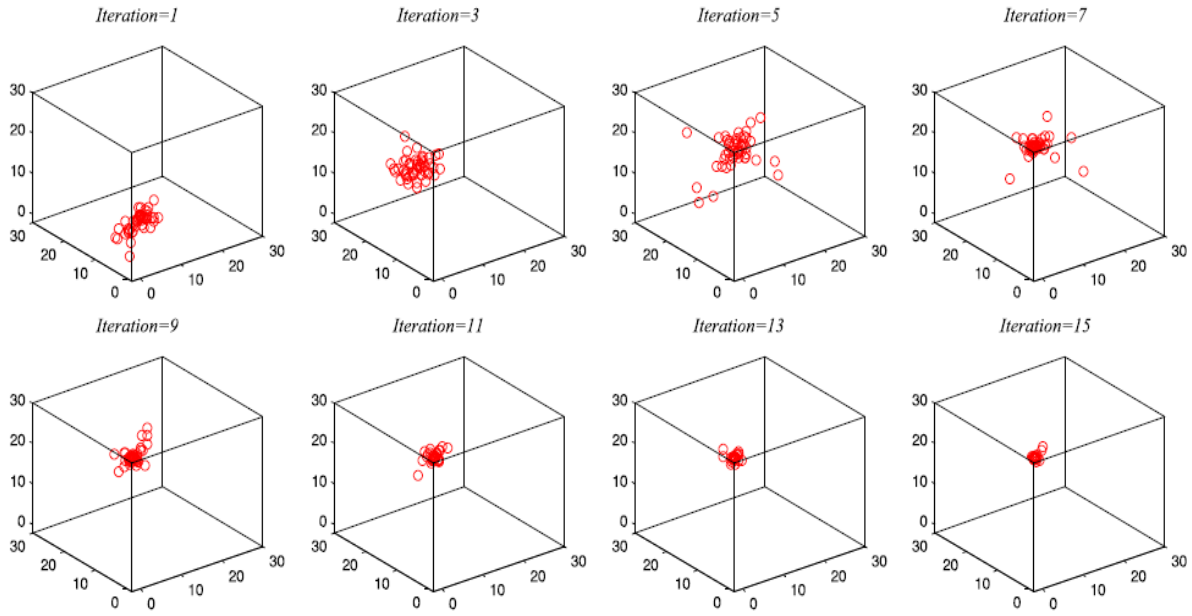


***Figure (III.20)*** *Jet propulsion and swarm behaviors of tunicate in two-dimensional environment*

## III-3-3. TSA Algorithm

In summary, the flowchart of TSA, and its pseudocode as presented in Algorithm 1.

### III-3-3-1. Pseudo-code

**Algorithm 1** Tunicate Swarm Algorithm

**Input:** Tunicate population $\vec{P}_p$
**Output:** Optimal fitness value $\vec{FS}$

**procedure** TSA
Initialize the parameters $\vec{A}, \vec{G}, \vec{F}, \vec{M}$, and $Max_{iterations}$
  Set $P_{min} \leftarrow 1$
  Set $P_{max} \leftarrow 4$
  Set $Swarm \leftarrow 0$
  **while** $(x < Max_{iterations})$ **do**
    **for** i ← 1 to 2 **do** /* Looping for compute swarm behavior */
      $\vec{FS} \leftarrow$**ComputeFitness(**$\vec{P}_p$**)** /* Calculate the fitness values of each search agent using **ComputeFitness** function*/
/* Jet propulsion behavior */
      $c_1, c_2, c_3, r_{and} \leftarrow Rand()$ /* Rand() is a function to generate the random number in range [0, 1] */
      $\vec{M} \leftarrow \left| P_{min} + c_1 \times P_{max} - P_{min} \right|$
      $\vec{F} \leftarrow 2 \times c_1$
      $\vec{G} \leftarrow c_2 + c_3 - \vec{F}$
      $\vec{A} \leftarrow \vec{G} / \vec{M}$
      $\vec{PD} \leftarrow \text{ABS}(\vec{FS} - r_{and} \times \vec{P_p}(x))$
/* Swarm behavior */
      **if**$(r_{and} \leq 0.5)$ **then**
        $Swarm \leftarrow Swarm + \vec{FS} + \vec{A} \times \vec{PD}$
      **else**
        $Swarm \leftarrow Swarm + \vec{FS} - \vec{A} \times \vec{PD}$
      **end if**
    **end for**
    $\vec{P_p}(x) \leftarrow Swarm/(2 + c_1)$
    $Swarm \leftarrow 0$
    Update the parameters $\vec{A}, \vec{G}, \vec{F}$, and $\vec{M}$
    $x \leftarrow x + 1$
  **end while**
return $\vec{FS}$
**end procedure**

**procedure** ComputeFitness($\vec{P}_p$)
  **for** i ← 1 to n **do** /* Here, n represents the dimension of a given problem */
    $FIT_p[i] \leftarrow FitnessFunction(P_p(\vec{i}, :))$ /* Calculate the fitness of each individual */
  **end for**
  $FIT_{Pbest} \leftarrow$ **BEST**$(FIT_p[])$ /* Calculate the best fitness value using **BEST** function */
return $FIT_{Pbest}$
**end procedure**

**procedure** BEST$(FIT_p)$
  $Best \leftarrow FIT_p[0]$
  **for** i ← 1 to n **do**
    **if**$(FIT_p[i] < Best)$ **then**
      $Best \leftarrow FIT_p[i]$
    **end if**
  **end for**
return $Best$ /* Return the best fitness value */
**end procedure**

### III-3-3-2. Flowchart

As illustrated in figure (III.21), the flowchart of the proposed algorithm, which showing the steps of TSA:

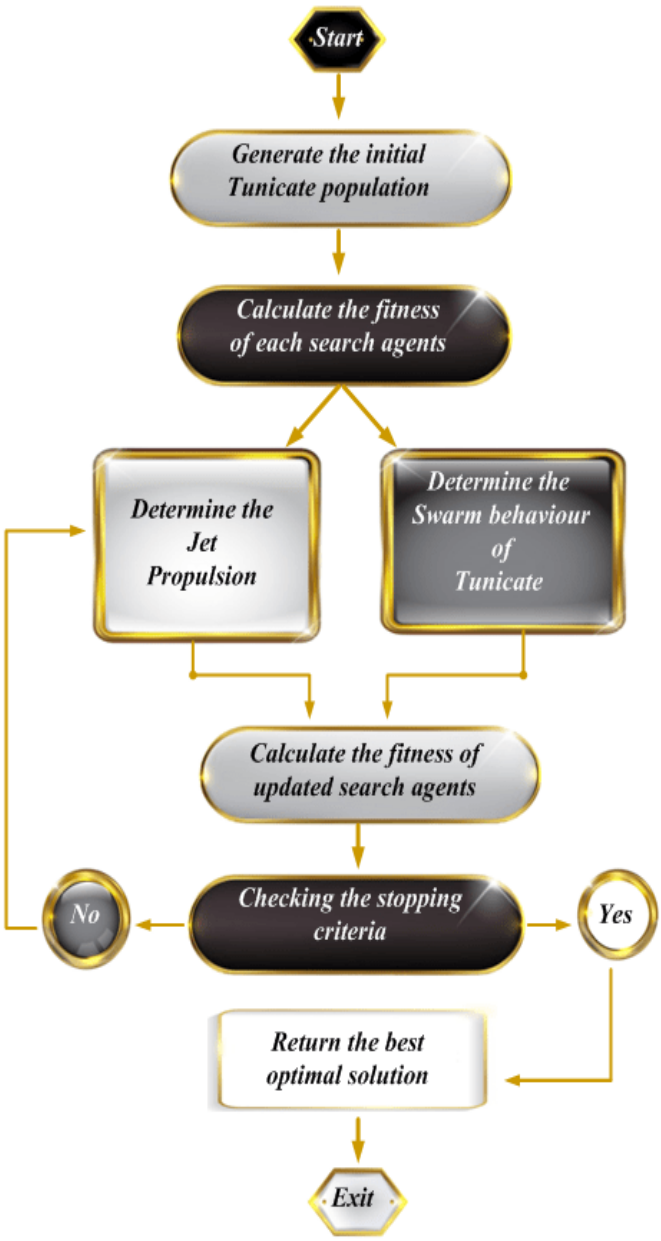


***Figure (III.21)*** *Flowchart of the proposed TSA algorithm.*

### III-3-4. Variants of Tunicate Swarm Algorithm

Due to its extensive application in addressing optimization problems of various sizes and complexities across multiple domains, TSA has been modified or hybridized to navigate the challenging search spaces of real-world optimization issues effectively. A multi-objective version of TSA has been developed also to address problems with multiple objectives [74].

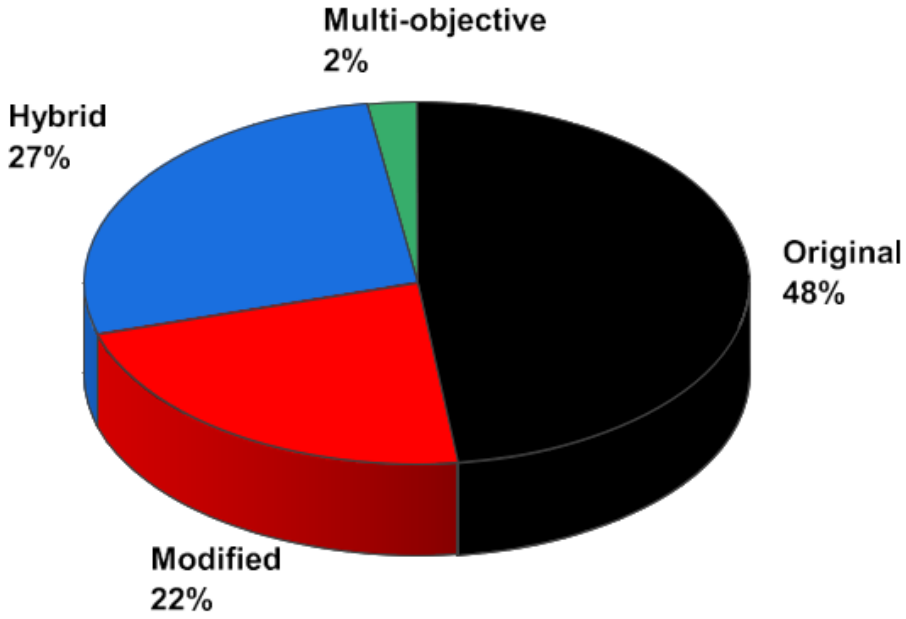


***Figure (III.22)*** *Percentage of applying TSA variants in diverse domains*

### III-3-5. Strengths of the Tunicate Swarm Algorithm

- **Simplicity & Few Parameters:** TSA requires only population size, iteration count, and a handful of coefficients, making it easy to configure and tune compared to many metaheuristics **SpringerLink.**
- **Robust Benchmark Performance:** Extensive testing on 74 standard functions (unimodal, multimodal, composite, CEC-2015/2017) shows TSA often ranks among the top two algorithms in mean best-fitness and stability ScienceDirect.
- **Real-World Applicability:** TSA has been successfully applied to six constrained and one unconstrained engineering design problems (e.g., pressure vessel, spring, beam, gear train), consistently finding feasible or superior solutions under complex constraints ScienceDirect.

### III-3-6. Applications of Tunicate Swarm Algorithm (TSA)

1. **Optimization of PEMFC Model Parameters (Power & Energy)**

   Menesy et al. applied TSA to extract optimal parameters of Proton Exchange Membrane Fuel Cell (PEMFC) mathematical models across three different stack types. By fitting the model to experimental polarization curves, TSA reliably identified parameter sets under varying operating conditions, demonstrating superior stability and precision compared to other metaheuristic.

2. **Energy-Centric Routing in Mobile Ad Hoc Networks (Networks)** Sudha et al. developed an Energy-Centric TSA (ECTSA) for sustainable multipath routing in MANETs. ECTSA selects routes by optimizing a cross-layer objective-minimizing total energy consumption while satisfying delay constraints—thus significantly prolonging network lifetime and improving overall throughput compared to traditional AODV-based approaches
3. **3D Dental Image Segmentation & Classification (Medical Imaging)** Awari et al. proposed 3DDISC-DLTSA, a deep-learning pipeline for automatic tooth segmentation and classification within 3D CAD models. TSA optimizes the hyperparameters of DenseNet-169 feature extractors and U-Net segmenters, achieving segmentation accuracies of 96.67% on one dataset and 97.48% on another—outperforming state-of-the-art CNN-only baselines [74]
4. Also, its efficiency in application is confirmed by solving some constrained and unconstrained engineering design problems such as pressure vessel, welded beam, speed reducer, 25-bar truss, tension/compression spring, displacement of loaded structure and rolling element bearing [72].

## III-3-7. Conclusion

In this chapter, an overview of optimization and its various approaches is provided, with a particular focus on metaheuristic algorithms. Among the different categories discussed, we highlighted three specific methods: Genetic Algorithm (GA), Grey Wolf Optimizer (GWO), and the Tunicate Swarm Algorithm (TSA). A particular focus was allocated to TSA, a novel algorithmic framework inspired by the collective behavior of tunicates. In the subsequent chapter, the results of the simulation will be presented, and a comparative analysis of TSA will be conducted against other state-of-the-art optimization techniques across different test systems.

# CHAPTER IV

# *CHAPITER 4*

## *Simulation Results and Analysis*

This chapter covers results tests of the introduced algorithm TSA and comparisons with other new algorithms in power systems.

### IV-1. Simulation results and discussions

To evaluate the proposed TSA for the ORPD problem, two standard test systems are considered which are IEEE 30 bus, IEEE 57 bus. The mono-objective optimization aims to minimize total active power losses ($P_{loss}$), total voltage deviation (TVD). The test-system parameters are listed in Table IV.1. Simulations were carried out in MATLAB 2022b computing environment and applied on 3.20 GHz Pentium IV personal computer with 8GB RAM. The population size ($N_P$), the maximum number of iterations (Max_iteration), and penalty factors $\lambda_V$ ,$\lambda_Q$. for each test power system appear in Table IV.2. The optimal solution achieved by the algorithm (TSA) is selected for the best solution over thirty runs independently executed.

***Tableau IV.1*** *Description of test power systems.*

| **Description** | **IEEE 30 bus** | **IEEE 57 bus** |
|---|---|---|
| **Number of control variables** | 19 | 25 |
| **Number of Generators** | 6 | 7 |
| **Number of Taps** | 4 | 15 |
| **Number of Q-shunt** | 9 | 3 |
| **Equality constraints** | 60 | 114 |
| **Inequality constraints** | 125 | 245 |
| **Discrete variables** | 13 | 18 |
| **Ploss (MW)** | **4.6725** | **22.6222** |
| **TVD (pu)** | **0.0976** | **0.7403** |

***Tableau IV.2*** *Description of Control variables and their values limits*

| **Control variables** | **Limits** | |
|---|---|---|
| | **Minimum** | **Maximum** |
| **Generator voltage $V_g$ (pu)** | 0.95 | 1.1 |
| **Transformer tap ratio T (pu)** | 0.9 | 1.1 |
| **Capacitor banks $Q_c$ (MVAR)** | 0 | 5000 |

***Tableau IV.3*** *Control parameter settings of TSA algorithm for test power systems*

| **Algorithm** | **TSA** | | | |
|---|---|---|---|---|
| **Parameters** | $\lambda_V$ | $\lambda_Q$ | $N$ | Max_iteration or MaxCycle |
| **IEEE 30 bus** | 0.2 | 0.2 | 80 | 150 |
| **IEEE 57 bus** | 10 | 5 | 150 | 300 |

## IV-2. IEEE 30 bus System

The first test system considered for the ORPD problem is the IEEE 30-bus network. It comprises 19 control variables: six generator voltage magnitudes at buses 1, 2, 5, 8, 11, and 13; four transformer tap settings on branches 6–9, 6–10, 4–12, and 28–27; and nine shunt capacitor reactive power injections at buses 10, 12, 15, 17, 20, 21, 23, 24, and 29. All network data and control-variable limits are detailed in [79], and the total real power demand is 2.834 pu on a 100 MVA base.

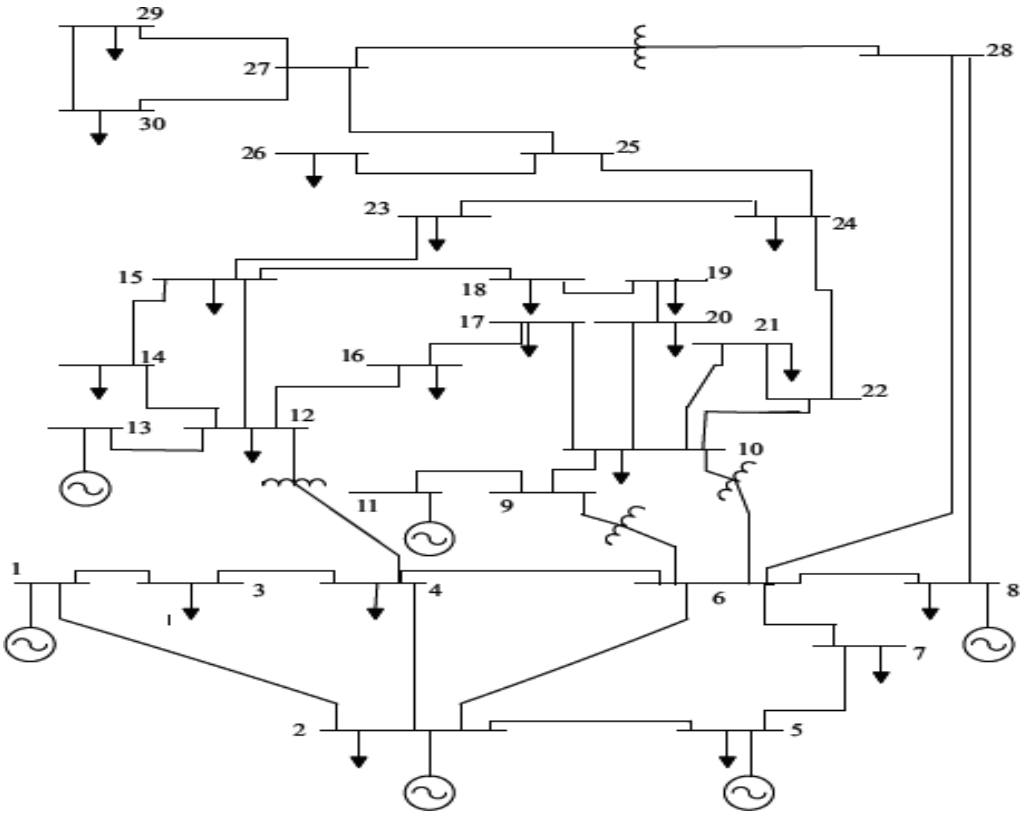


***Figure IV.1*** *Single line diagram of IEEE 30 bus power system*

### IV-2-1. Active Power Losses Minimization for IEEE 30 Bus System

In this case, $P_{loss}$ is selected as an objective function to minimize and the best control variables resulting from TSA computing code running are shown in Table IV.3. The results established after the simulation phase, by applying the TSA method are compared with those of other available methods as PDO[8], RSO[8], BWO[80], GJSO[81], CTFWO[82]. The minimum obtained $P_{loss}$ from the TSA algorithm is 4.6725 MW and it is less by 0.167 MW (3.57%) than PDO, which gives 4.8395 MW. A statistical comparison is performed based on Table IV.4 proving the capability of TSA to overcome other optimization techniques reported in the same table. The convergence curve for TSA method are illustrated in Figure IV.2, which had a stable convergence trend without significant oscillations demonstrates the robustness and reliability of TSA. From figure IV.3, it is observed that all the bus voltages optimized by TSA are within the limits of 1.028 p.u. to 1.1 p.u.

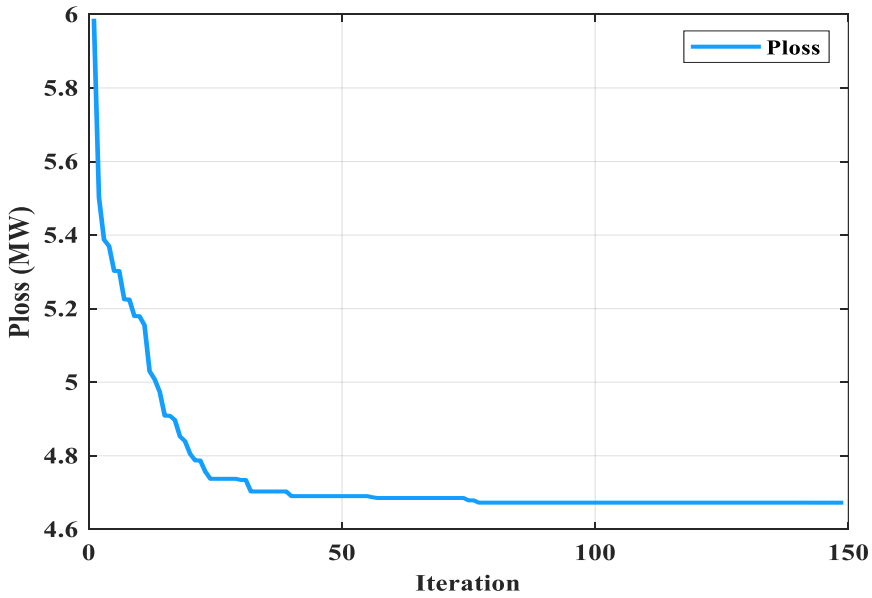


***Figure IV.2*** *Convergence curve for Active Power Losses of IEEE 30 Bus System*

***Table IV.3*** *Simulation results using TSA and other optimization techniques for Ploss minimization IEEE 30 bus.*

| **Control variables** | **TSA** | **PDO**[8] | **RSO**[8] | **BWO**[80] | **GJSO**[81] | **CTFWO** [82] |
|---|---|---|---|---|---|---|
| Generator voltage (pu) | | | | | | |
| $V_1$ | 1.1000 | 1.0736 | 1.0912 | 1.1 | 1.0727 | 1.0713 |
| $V_2$ | 1.0923 | 1.0638 | 1.0858 | 1.0885 | 1.0631 | 1.0621 |
| $V_5$ | 1.0729 | 1.0396 | 1.0737 | 1.1 | 1.0410 | 1.0397 |
| $V_8$ | 1.0738 | 1.0411 | 1.0387 | 1.0722 | 1.0417 | 1.0399 |
| $V_{11}$ | 1.1000 | 1.0986 | 1.0431 | 1.1 | 1.0300 | 1.0318 |
| $V_{13}$ | 1.1000 | 1.0941 | 1.0954 | 1.0851 | 1.0573 | 1.0623 |
| Transformer tap ratio (pu) | | | | | | |
| $T_{6-9}$ | 1.0481 | 0.9938 | 0.9620 | 1.1 | 0.9855 | 1.0134 |
| $T_{6-10}$ | 0.9639 | 0.9663 | 0.9688 | 0.9938 | 0.9882 | 0.9003 |
| $T_{4-12}$. | 1.0290 | 0.9831 | 1.0364 | 1.1 | 0.9700 | 0.9835 |
| $T_{28-27}$ | 0.9859 | 0.9541 | 0.9883 | 1.0195 | 0.9989 | 0.9871 |
| Capacitor banks (MVAR) | | | | | | |
| $Q_{C-10}$ | 0.1547 | 5.0000 | 3.8403 | 0.5 | 4.0683 | 0.0051 |
| $Q_{C-12}$ | 0.5189 | 5.0000 | 2.9197 | 0.5 | 0.6060 | 0 |
| $Q_{C-15}$ | 0.2840 | 0.0000 | 1.0707 | 0.5 | 1.3890 | 1.8709 |
| $Q_{C-17}$ | 3.2127 | 5.0000 | 0.7608 | 0.5 | 0.9269 | 0.7921 |
| $Q_{C-20}$ | 4.5097 | 0.0000 | 0.9202 | 0.5 | 1.9208 | 4.9785 |
| $Q_{C-21}$ | 4.3568 | 5.0000 | 3.4040 | 0.5 | 3.1220 | 2.3600 |
| $Q_{C-23}$ | 2.2588 | 4.0628 | 4.9810 | 0.5 | 1.0749 | 0.0028 |
| $Q_{C-24}$ | 0.5718 | 5.0000 | 3.5091 | 0.5 | 4.8484 | 3.7161 |
| $Q_{C-29}$ | 1.7683 | 0.0000 | 3.6373 | 0.18 | 1.9181 | 0 |
| **Power Losses (MW)** | **4.6725** | **4.8395** | **5.1328** | **4.7831** | **4.9450** | **4.9448** |
| TVD (pu) | 1.2666 | 1.2663 | 1.0240 | 0.9920 | - | - |

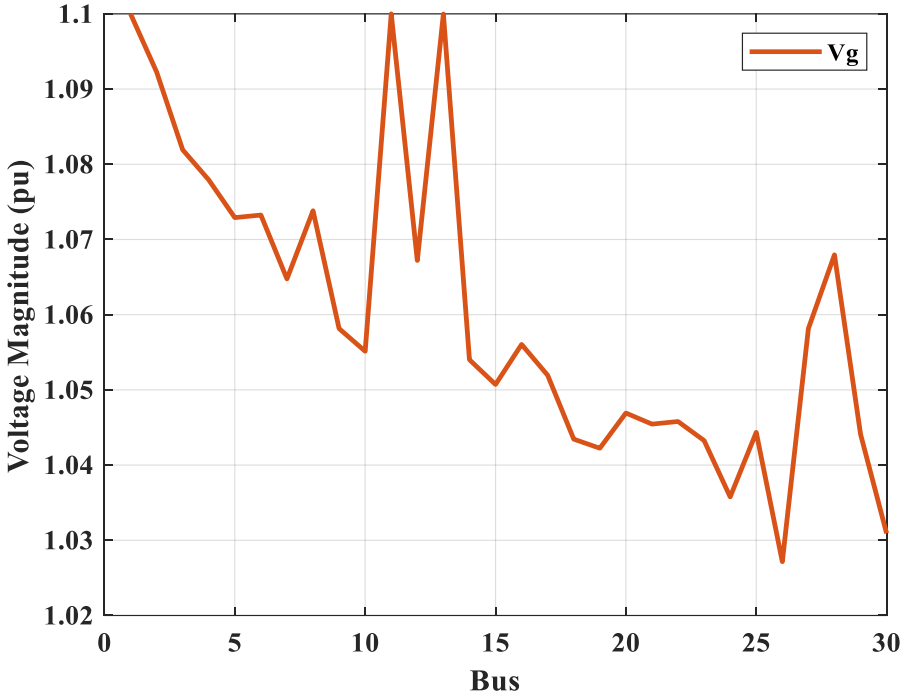


***Figure IV.3*** *Bus Voltage Profile for $P_{loss}$ IEEE 30 power System*

***Table IV. 4*** *Comparison of minimum real power losses for different methods for IEEE 30 bus system.*

| Algorithms | $P_{loss}$ MW | Algorithms | $P_{loss}$ MW |
|---|---|---|---|
| **TSA** | **4.6725** | **IMPAPSO**[83] | 5.0751 |
| **PDO**[8] | 4.8395 | **PSOGWO**[84] | 5.0903 |
| **RSO**[8] | 5.1328 | **OGWO**[85] | 6.99 |
| **BWO**[80] | 4.7831 | **ICOA**[86] | 4.7037 |
| **GJSO**[81] | 4.9450 | **AHA**[87] | 5.1461 |
| **CTFWO**[82] | 4.9448 | **EO**[81] | 4.9451 |

### IV-2-2. Total Voltage Deviation Minimization for IEEE 30 bus System

In this subsection, Total Voltage Deviation (TVD) is selected as the objective function to be minimized for the IEEE 30-bus test network. Table IV.5 presents a comprehensive compilation of the optimal TVD values achieved by the proposed TSA algorithm, alongside derived from the comparative methods of RSO [1], GJSO [3], GOA [10], AVOA [1], and SPO [1]. As illustrated in Table IV.6, a more clear presentation of the values of the algorithms is provided and more other algorithms to compare with. Where The TSA achieves the lowest TVD of 0.0976 pu, representing a notable improvement of (5.53%) over the obtained result of 0.1030 pu from AVOA [10]. It also demonstrated superior performance in comparison with the GOA algorithm

of 0.098 pu. As illustrated in Figure IV.4, the convergence curve of the TSA for TVD minimization demonstrates a rapid progression toward the global optimum. As illustrated in Figure IV.5, under the TVD objective, bus voltages demonstrate a tight clustering around 1.0 pu, predominantly ranging from 0.99 to 1.02 pu. This observation signifies the presence of stable control across the network.

***Table IV.5*** *Simulation results using TSA and other optimization techniques for TVD minimization IEEE 30 bus.*

| **Control variables** | **TSA** | **RSO**[8] | **GJSO** [81] | **GOA** [88] | **AVOA**[8] | **SPO**[8] |
|---|---|---|---|---|---|---|
| Generator voltage (pu) | | | | | | |
| $V_1$ | 1.0168 | 1.0498 | 1.0161 | 1.012 | 1.0088 | 1.0376 |
| $V_2$ | 1.0146 | 1.0369 | 1.0190 | 1.011 | 1.0037 | 1.0403 |
| $V_5$ | 1.0182 | 1.0104 | 1.0194 | 1.021 | 1.0184 | 1.0258 |
| $V_8$ | 1.0097 | 0.9851 | 0.9979 | 1.012 | 0.9996 | 0.9943 |
| $V_{11}$ | 1.0349 | 0.9751 | 0.9865 | 1.013 | 1.0873 | 0.9928 |
| $V_{13}$ | 1.0079 | 1.0925 | 1.0235 | 1.001 | 1.0051 | 1.0011 |
| Transformer tap ratio (pu) | | | | | | |
| $T_{6-9}$ | 1.0434 | 1.0513 | 1.0152 | 0.989 | 1.0907 | 0.9974 |
| $T_{6-10}$ | 0.9152 | 0.9279 | 0.9100 | 0.924 | 0.9193 | 0.9000 |
| $T_{4-12.}$ | 0.9807 | 1.0127 | 0.9704 | 0.967 | 0.9742 | 0.9398 |
| $T_{28-27}$ | 0.9539 | 0.9260 | 0.9665 | 1.079 | 0.9653 | 0.9393 |
| Capacitor banks (MVAR) | | | | | | |
| $Q_{C-10}$ | 4.6808 | 4.3980 | 4.0552 | 4.89 | 2.1842 | 2.3684 |
| $Q_{C-12}$ | 0.4675 | 0.4297 | 2.0334 | 0 | 4.9947 | 1.2804 |
| $Q_{C-15}$ | 5.0000 | 3.1278 | 2.0758 | 4.86 | 3.8551 | 1.2370 |
| $Q_{C-17}$ | 1.6357 | 3.8269 | 2.2702 | 5 | 4.6864 | 5.0000 |
| $Q_{C-20}$ | 5.0000 | 4.5900 | 4.8561 | 5 | 4.9868 | 4.7469 |
| $Q_{C-21}$ | 4.7249 | 4.0292 | 4.2384 | 5 | 4.2678 | 3.4785 |
| $Q_{C-23}$ | 5.0000 | 2.0630 | 3.3728 | 5 | 4.5073 | 4.2880 |
| $Q_{C-24}$ | 5.0000 | 1.4681 | 2.7978 | 4.781 | 4.9998 | 0.0000 |
| $Q_{C-29}$ | 1.0582 | 3.3382 | 2.6180 | 2.765 | 2.5337 | 1.8260 |
| Power Losses (MW) | 5.6609 | 5.7894 | - | - | 5.7946 | 5.8151 |
| **TVD (PU)** | **0.0976** | **0.2936** | **0.1221** | **0.098** | **0.1030** | **0.1247** |

***Table IV.6*** *Comparison of minimum Total Voltage Deviation for different methods for IEEE 30 bus system.*

| Algorithms | TVD (pu) | Algorithms | TVD (pu) |
|---|---|---|---|
| **TSA** | **0.0976** | **ROA**[8] | 0.1267 |
| **RSO**[8] | 0.2936 | **SCA**[80] | 0.1845 |
| **GJSO**[81] | 0.1221 | **PDO**[8] | 0.1410 |
| **AVOA**[8] | 0.1030 | **EO**[81] | 0.1234 |
| **GOA**[88] | 0.098 | **IMPAPSO**[89] | 0.2487 |
| **SPO**[8] | 0.1247 | **GWO-PSO**[84] | 0.2780 |

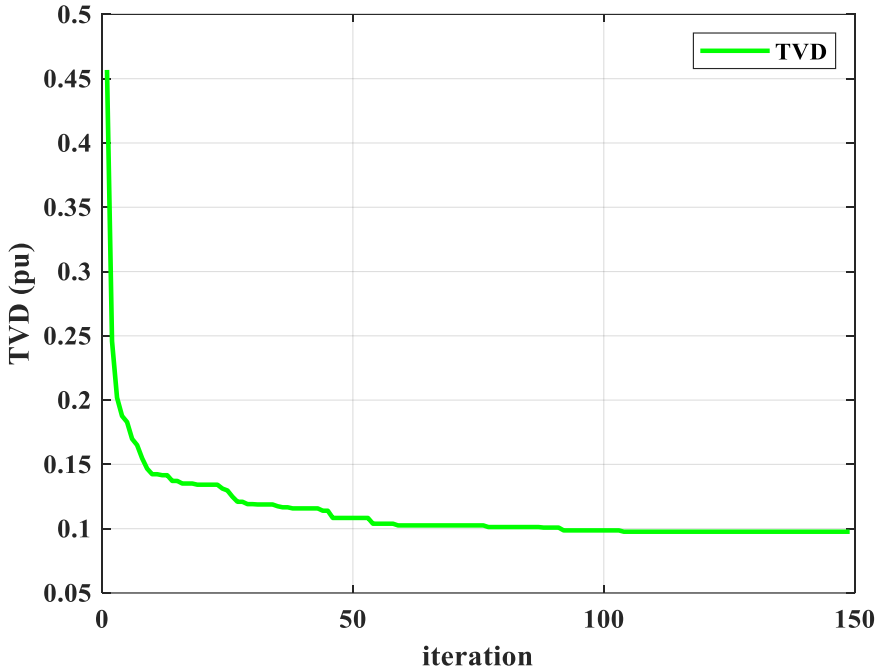


***Figure IV.4*** *Convergence curve for total voltage deviation of IEEE 30 Bus System*

***Table IV.7*** *Reactive power of generation in Ploss & TVD according to their min & max permissible limits for IEEE 30 Bus*

| PV Bus | Qmin MVAR | Qmax MVAR | Qg ($P_{loss}$) MVAR | Qg (TVD) MVAR |
|---|---|---|---|---|
| **1** | -20 | 200 | -1.3832 | -15.6170 |
| **2** | -20 | 100 | 18.9423 | 13.0482 |
| **5** | -15 | 80 | 28.2518 | 49.4877 |
| **8** | -15 | 60 | 37.4255 | 56.3001 |
| **11** | -10 | 50 | 22.4908 | 16.6787 |
| **13** | -15 | 60 | 25.988 | 0.6020 |

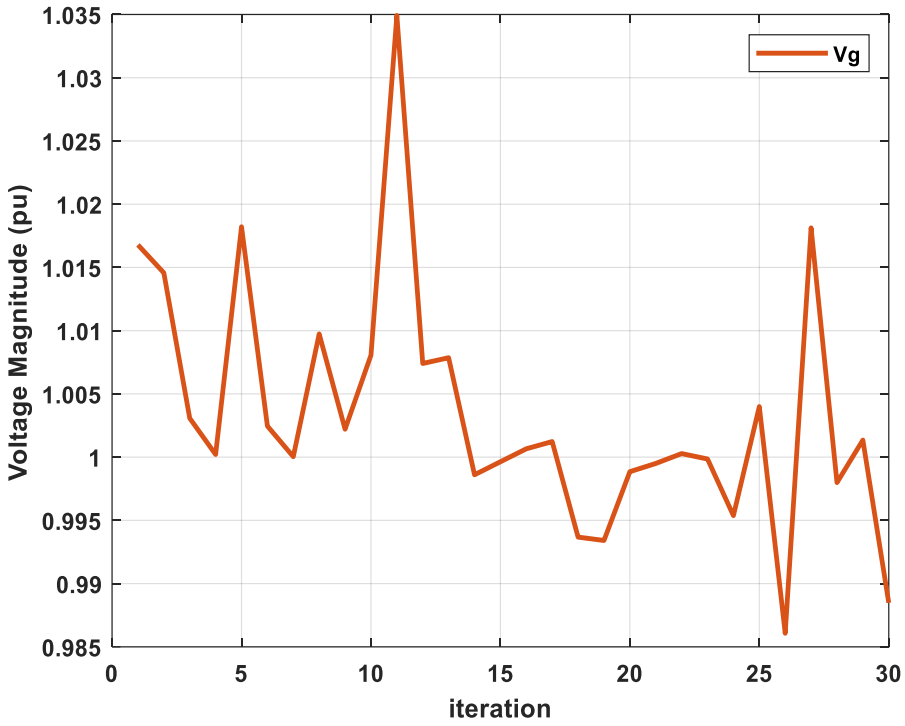


***Figure IV.5*** *Bus Voltage Profile for TVD IEEE 30 power System*

As illustrated in Figure IV.6, the reactive-power limits of each PV bus are overlaid with the actual injections determined by TSA for two objectives: Ploss (gray) and TVD (gold). A synthesis of salient points is as follows:

- All the generated reactive power of two objectives active power losses '$Q_g(P_{loss})$' and total voltage deviation '$Q_g$(TVD)' values remain strictly between their $Q_{min}/Q_{max}$ (the maximum and minimum generation of reactive power) bounds for every bus, confirming constraint compliance.

- As demonstrated in Figure IV.6, the gray $P_{loss}$ curve indicates relatively modest injections at the majority of buses. For instance, the injection at Bus 1 is approximately –1.4 MVAR, and the injection at Bus 2 is approximately 18.9 MVAR. These injections focus support where it is most effective in reducing $I^2R$ losses without exceeding the limits of the voltage-controlled bus (PV bus).

- The gold curve, representing $Q_g$ of TVD (reactive power generation for total voltage deviation), demonstrates that Buses 5 and 8 provide relatively high reactive-power injections of approximately 49.5 MVAR and 56.3 MVAR, respectively. While these values approximate the maximum limits, they remain well within the permissible $Q_g$ ranges defined for generator buses in Table IV.7.

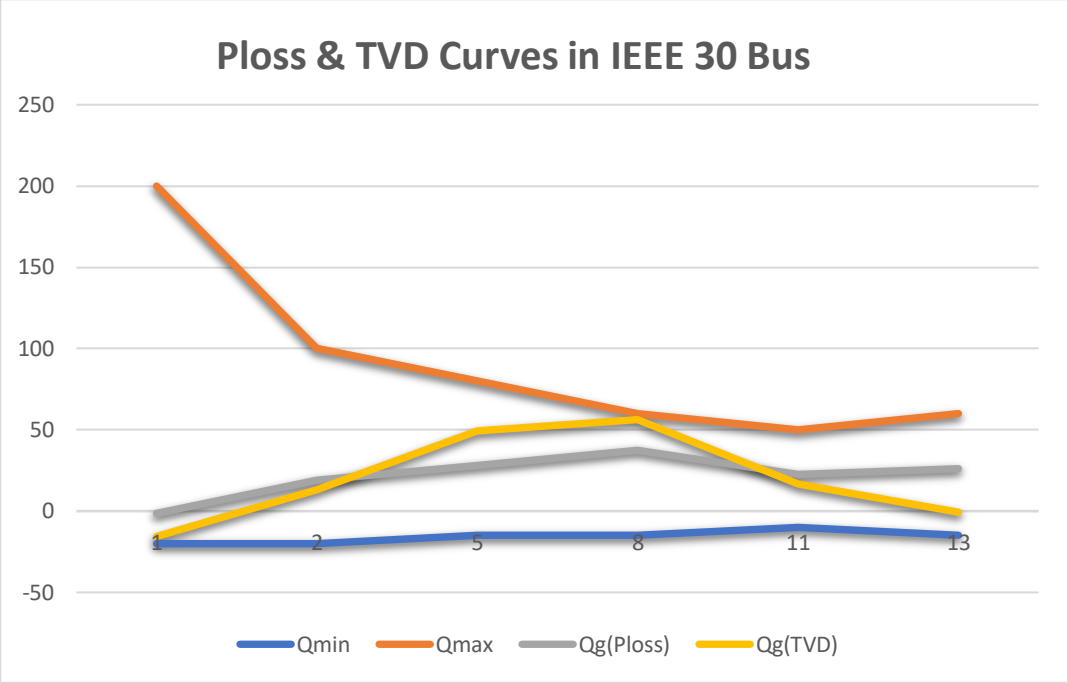


***Figure IV.6*** *Reactive of generation curves of $P_{loss}$ & TVD for IEEE 30*

## IV-3. IEEE 57 bus system

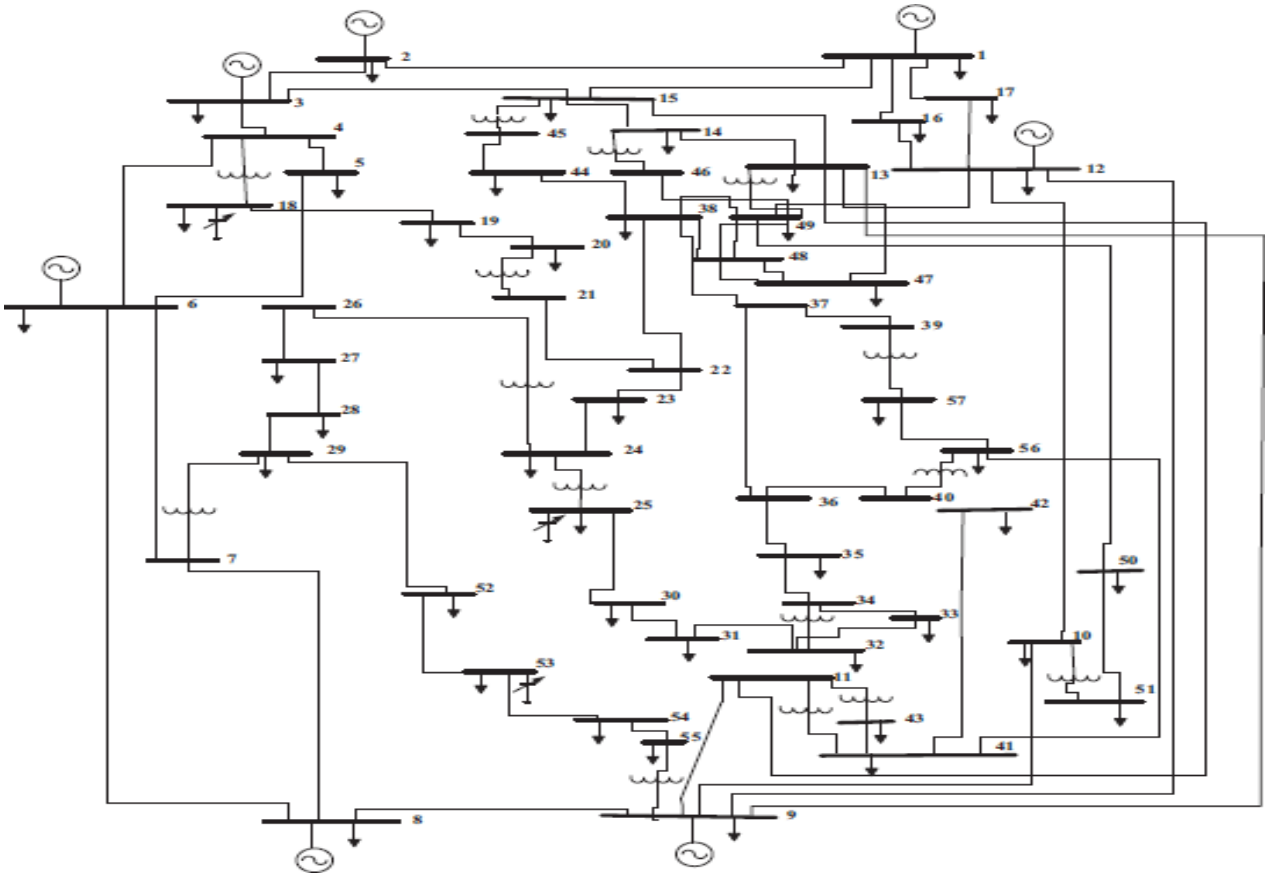

***Figure IV.7*** *Single line diagram of IEEE 57 bus test system*

The IEEE 57-bus system comprises 80 transmission lines and seven generators located at buses 1, 2, 3, 6, 8, 9, 12, and 15 branches under the transformer. Reactive shunt compensation is modeled at buses 18, 25, and 53. The total system demand is 12.508+j3.36412.508 pu on a 100 MVA base. the limits of the control variables are specified in [90].

### IV-3-1. Active Power Losses Minimization for IEEE 57 bus System

For the IEEE 57-bus test system, the proposed TSA minimizes active transmission losses by optimally adjusting all control variables. Table IV.8 summarizes the optimal objective value and corresponding control settings obtained via TSA. A comparative analysis against GSA [14], MFOA [15], and MVMO [16] demonstrates that TSA achieves the lowest losses (22.6222 MW), outperforming these methods and confirming its superior robustness. In particular, TSA delivers a 7.54 % reduction in losses relative to the best MVMO result. Table IV.9 demonstrates the results achieved in the same literature and the comparison with the TSA method. Figure IV.8 represents the convergence graph arising from TSA, it achieves a rapid improvement in the early iterations, gradually refines the solution, and stabilizes around 22.62 MW, demonstrating fast and stable convergence. This confirms the algorithm's robustness and efficiency in finding an optimal solution. Figure IV.9 shows the voltage profile for TSA method, when the optimal solution is reached for the current test system, noting that the voltage amplitude on all buses is within its allowed range with no violations beyond the allowed limits.

***Table IV.8*** *Comparison of simulation results for Ploss minimization in case of IEEE 57 bus system.*

| **Control variables** | **TSA** | **GSA**[91] | **MFOA** [92] | **MVMO** [93] |
|---|---|---|---|---|
| Generator voltage (pu) | | | | |
| $V_1$ | 1.1000 | 1.0600 | 1.0600 | 1.0594 |
| $V_2$ | 1.0884 | 1.0582 | 1.0600 | 1.0517 |
| $V_3$ | 1.0779 | 1.0462 | 1.0600 | 1.038 |
| $V_6$ | 1.0731 | 1.0391 | 1.0600 | 1.0352 |
| $V_8$ | 1.0975 | 1.0600 | 1.0600 | 1.0545 |
| $V_9$ | 1.0653 | 1.0432 | 1.0600 | 1.0336 |
| $V_{12}$ | 1.0697 | 1.0379 | 1.0600 | 1.0347 |
| Transformer tap ratio (pu) | | | | |
| $T_{4\text{-}18}$ | 0.9819 | 0.9054 | 0.9000 | 1.042 |
| $T_{4\text{-}18}$ | 1.0395 | 0.9978 | 0.9000 | 0.909 |
| $T_{21-20}$ | 1.0328 | 1.0021 | 0.9000 | 1.033 |
| $T_{24-26}$ | 1.0039 | 1.0180 | 0.9000 | 1.018 |
| $T_{7-29}$ | 0.9771 | 0.9712 | 0.9000 | 0.939 |
| $T_{34-32}$ | 0.9161 | 0.9692 | 0.9000 | 0.976 |
| $T_{11-41}$ | 0.9142 | 0.9683 | 0.9000 | 0.958 |
| $T_{15-45}$ | 0.9748 | 0.9717 | 0.9000 | 0.929 |

| | | | | |
|---|---|---|---|---|
| $T_{14-46}$ | 0.9565 | 0.9530 | 0.9000 | 0.917 |
| $T_{10-51}$ | 0.9702 | 0.9691 | 0.9000 | 0.967 |
| $T_{13-49}$ | 0.9281 | 0.9242 | 0.9000 | 0.922 |
| $T_{11-43}$ | 0.9695 | 1.0387 | 0.9000 | 0.924 |
| $T_{40-56}$ | 1.0091 | 1.0497 | 0.9000 | 1.06 |
| $T_{39-57}$ | 0.9396 | 1.0668 | 0.9000 | 0.959 |
| $T_{9-55}$ | 0.9857 | 0.9807 | 0.9000 | 0.956 |
| Capacitor banks (MVAR) | | | | |
| $Q_{C-18}$ | 2.3528 | 0.1863 | 0 | 4.200 |
| $Q_{C-25}$ | 5.0000 | 4.0488 | 0 | 4.200 |
| $Q_{C-53}$ | 1.7242 | 4.8099 | 0 | 4.900 |
| Ploss MW | **22.6222** | **24.4922** | **24.9314** | **24.3284** |
| TVD (pu) | 3.1584 | - | - | 0 |

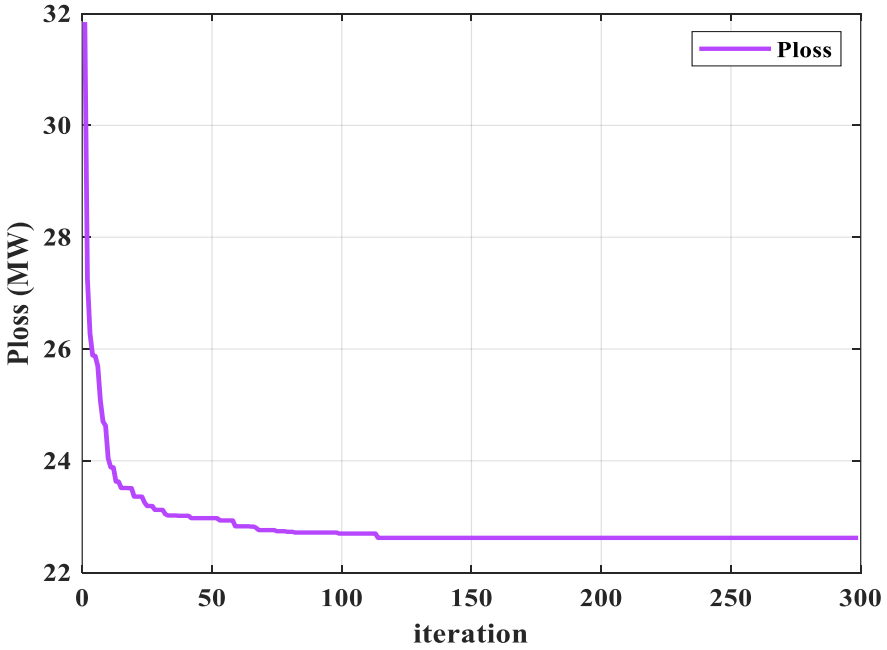


***Figure IV.8*** *Convergence curve for Active Power Losses of IEEE 57 Bus System*

***Table IV.9*** *Comparison of minimum real power losses for different methods for IEEE 57*

| Algorithms | $P_{loss}$ MW | Algorithms | $P_{loss}$ MW |
|---|---|---|---|
| **TSA** | **22.6222** | **ISMA**[94] | 24.7079 |
| **MVMO**[93] | 24.3284 | **ICOA**[86] | 24.9062 |
| **MFOA**[92] | 24.9314 | **SCA**[95] | 24.05 |
| **GSA**[91] | 24.4922 | **BSO**[96] | 24.37 |
| **IALO**[97] | 23.5429 | - | - |
| **mPFA**[98] | 22.9116 | - | - |

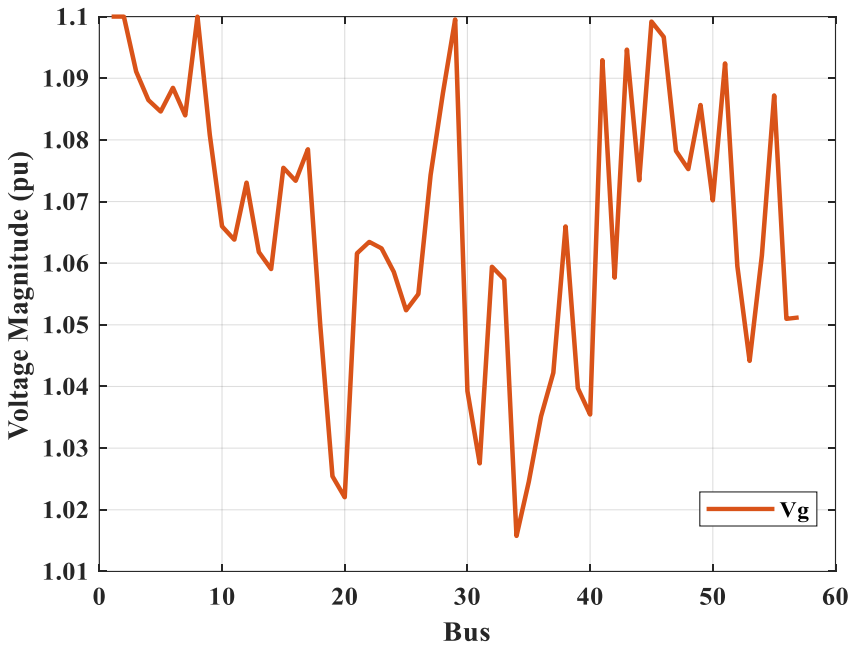


***Figure IV.9*** *Bus Voltage Profile for IEEE 57 power System*

### IV-3-2. TVD Minimization for IEEE 57 bus System

In this part, the proposed TSA algorithm is applied to minimize the Total Voltage Deviation (TVD) of the IEEE 57-bus power system. Detailed results for each algorithm are provided in Table IV.10, while a simplified comparison is presented in Table IV.11, including TSA and other methods such as APOPSO [22] and FOA [15]. The TSA algorithm outperforms the others in terms of TVD, achieving a 27.38% improvement compared to APOPSO [22]. As illustrated in Figure IV.10, TVD dropped quickly from about 2.1 to 0.8 over the first 50 iterations, showing strong global search capability. After that, the curve gently slopes down to 0.74pu by the time we reach iteration 300, showing the stable convergence of this algorithm.

***Table IV.10*** *Comparison of simulation results for Ploss minimization in case of IEEE 57 bus system.*

| **Control variables** | **TSA** | **APOPSO**[99] | **FOA**[92] |
|---|---|---|---|
| Generator voltage (pu) | | | |
| $V_1$ | 0.9580 | 1.02 | 0.94 |
| $V_2$ | 0.9550 | 1.009 | 0.94 |
| $V_3$ | 1.0428 | 0.9771 | 0.94 |
| $V_6$ | 0.9923 | 0.976 | 1.06 |
| $V_8$ | 1.0310 | 1.044 | 0.94 |
| $V_9$ | 1.0175 | 1.001 | 0.94 |
| $V_{12}$ | 1.0321 | 1.012 | 1.06 |

| | | | |
|---|---|---|---|
| Transformer tap ratio (pu) | | | |
| $T_{4-18}$ | 1.0035 | 0.998 | 1.1 |
| $T_{4-18}$ | 0.9954 | 0.944 | 0.9 |
| $T_{21-20.}$ | 0.9762 | 0.959 | 0.9 |
| $T_{24-26}$ | 1.0484 | 0.980 | 1.1 |
| $T_{7-29}$ | 0.9533 | 0.968 | 0.9 |
| $T_{34-32}$ | 0.9079 | 0.931 | 0.9 |
| $T_{11-41}$ | 0.9128 | 0.922 | 0.9 |
| $T_{15-45}$ | 0.9029 | 0.911 | 0.9 |
| $T_{14-46}$ | 1.0012 | 0.979 | 0.9 |
| $T_{10-51}$ | 1.0069 | 1.001 | 0.9429 |
| $T_{13-49}$ | 0.9082 | 0.882 | 0.9 |
| $T_{11-43}$ | 0.9474 | 0.871 | 0.9 |
| $T_{40-56}$ | 0.9945 | 0.966 | 0.9644 |
| $T_{39-57}$ | 0.9411 | 0.951 | 0.9 |
| $T_{9-55}$ | 0.9786 | 0.911 | 0.9 |
| Capacitor banks (MVAR) | | | |
| $Q_{C-18}$ | 0.2737 | 0.020 | 0.0800 |
| $Q_{C-25}$ | 5.0000 | 0.097 | 0.1600 |
| $Q_{C-53}$ | 1.7031 | 0.042 | 0.200 |
| Ploss (MW) | 38.8629 | 23.989 | - |
| TVD (pu) | **0.7403** | **0.943** | **1.2191** |

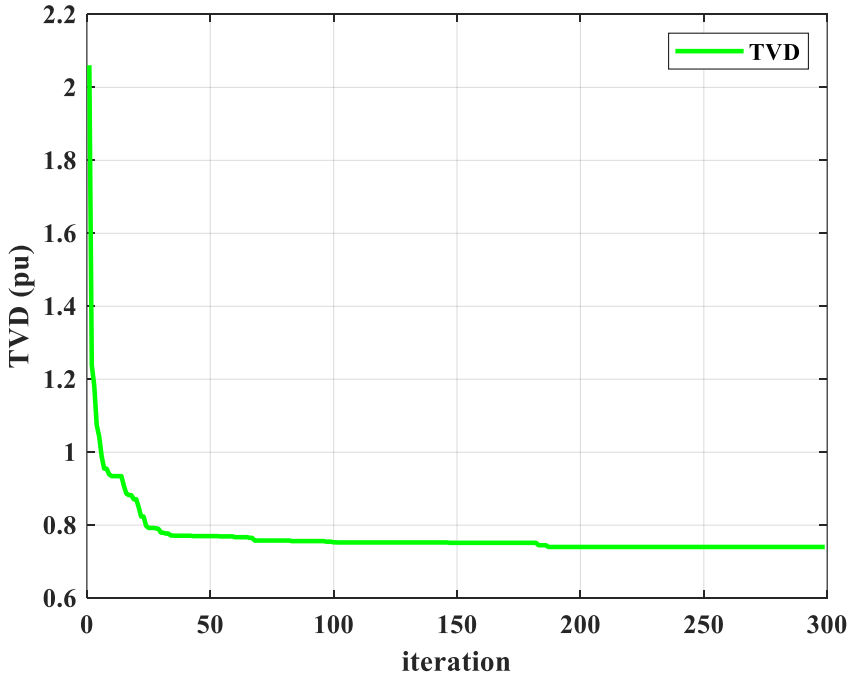


***Figure IV.10*** *Total voltage deviation convergence curve for IEEE 57 Bus System*

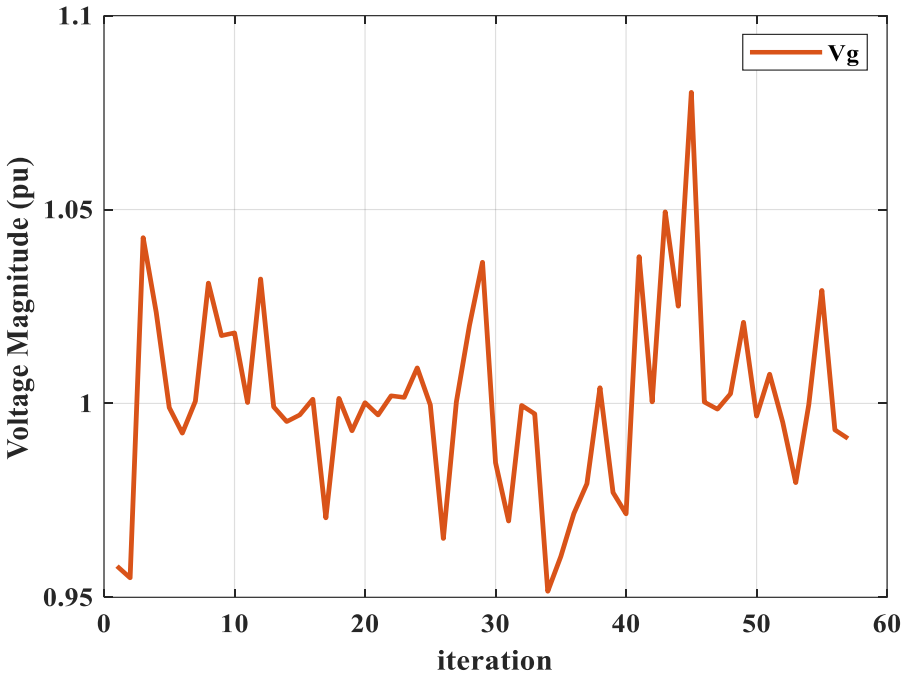


***Figure IV.11*** *Bus Voltage Profile for TVD IEEE 57 power System*

***Table IV.11*** *Comparison of minimum voltage deviation for different methods for IEEE 57*

| Algorithms | TVD (pu) |
|---|---|
| **TSA** | **0.7403** |
| **APOPSO**[99] | 0.943 |
| **ICOA[86]** | 0.7436 |
| **FOA**[92] | 1.2191 |

***Table IV.12*** *Reactive power of generation of Ploss & TVD according to their min & max permissible limits for IEEE 57 Bus*

| PV Bus | Qmin MVAR | Qmax MVAR | Qg (Ploss) MVAR | Qg (TVD) MVAR |
|---|---|---|---|---|
| **1** | -200 | 300 | -13.9025 | 129.862 |
| **2** | -17 | 50 | 44.395 | 20.14 |
| **3** | -10 | 60 | 54.4903 | 46.65 |
| **6** | -8 | 25 | 18.3036 | 10.71 |
| **8** | -140 | 200 | 39.388 | 62.5153 |
| **9** | -3 | 9 | 4.4673 | 6.12 |
| **12** | -150 | 155 | 48.2798 | 133.95 |

The entries of Table IV.12 in this regard illustrate the actual values of reactive power generations for both active losses (grey), total voltage deviation (gold) and in MVAR of the generating units versus the allowable limits, in which all generating reactive powers of both objectives are within their limits as shown in Figure IV.12.

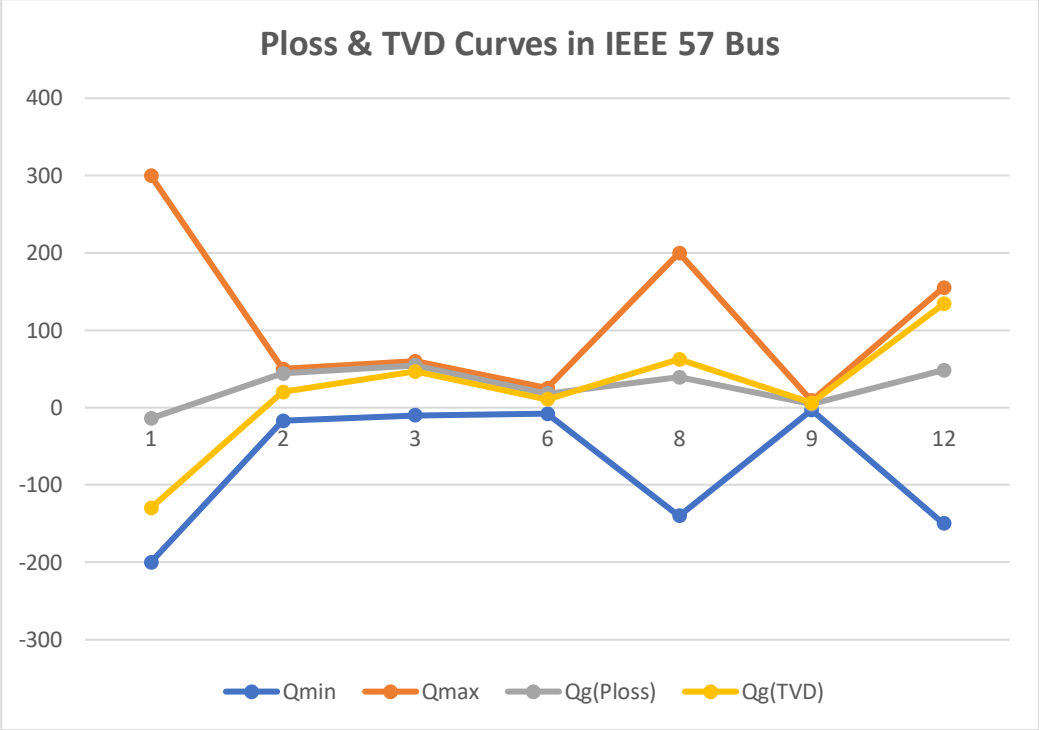


***Figure IV.12*** *Reactive of generation curves of $P_{loss}$ & TVD for IEEE 57*

## CONCLUSION

This chapter presented a comprehensive evaluation of the Tunicate Swarm Algorithm (TSA) for solving the Optimal Reactive Power Dispatch (ORPD) problem on two standard IEEE test systems: the 30-bus and 57-bus networks. The TSA was applied to two mono-objective functions minimizing active power losses and minimizing total voltage deviation (TVD). Simulation results demonstrated that TSA consistently outperformed several recent metaheuristic algorithms in terms of solution quality, robustness, and convergence speed.

# General Conclusion

In this thesis, we conducted a comprehensive study on the optimal management of reactive power in electrical power systems using modern metaheuristic techniques. We began by exploring the structure and components of electrical networks, including transmission lines, generators, transformers, and loads, with a focus on the role of power flow analysis in system planning and secure operation.

We then examined classical power flow calculation methods such as Newton-Raphson, Gauss-Seidel, and the Fast Decoupled method highlighting their strengths and limitations, particularly their inefficiency in solving complex and non-linear optimization problems like Optimal Reactive Power Dispatch (ORPD).

To address these limitations, we implemented metaheuristic techniques including Genetic Algorithm (GA), Grey Wolf Optimizer (GWO), and the proposed Tunicate Swarm Algorithm (TSA). These were applied and compared in terms of performance on IEEE 30-bus and 57-bus test systems with objective functions including active power loss minimization and voltage deviation reduction.

Simulation results demonstrated that the proposed TSA algorithm outperforms others in terms of convergence speed and optimization accuracy, proving its efficiency in solving ORPD problems.

In conclusion, the integration of computational intelligence and modern metaheuristic algorithms presents a promising direction for enhancing the performance, efficiency, and stability of electrical networks. Future work may focus on hybridizing these algorithms and integrating forecasting models to address uncertainties in renewable energy sources and load demands.

# References


[1] Mirjalili, S., S. Mirjalili, and A. Lewis, *Grey Wolf Optimizer.* Advances in Engineering Software, 2014. **69**: p. 46–61.

[2] Yu, M., et al., *Improved multi-strategy adaptive Grey Wolf Optimization for practical engineering applications and high-dimensional problem solving.* Artificial Intelligence Review, 2024. **57**(10).

[3] Muro, C., et al., *Wolf-pack (Canis lupus) hunting strategies emerge from simple rules in computational simulations.* 2011. **88**(3): p. 192-197.

[4] Islam, D.K.Y. *CONDUITE DES RESEAUX ELECTRIQUES*. SCRIBD, (2020).

[5] Nabila, S. and C. Samira, *Restructuration du réseau électrique moyenne tension 30 kv de la région Azazga*. 2010, Université Mouloud Mammeri.

[6] Nora, M. and M. Dahbia, *Etude des protections de réseau électrique THT à SONELGAZ*. 2012, Université Mouloud Mammeri.

[7] Belkacem, L. and K.M.J.M.d.F.d.E.p.l.o.d.D.d.I.d.E.e.E. Saber, Université Biskra, Promotion, *Compensation dynamique de l'énergie réactive dans les réseaux électrique.* 2005.

[8] Ali, M.H., et al., *A Novel Stochastic Optimizer Solving Optimal Reactive Power Dispatch Problem Considering Renewable Energy Resources.* 2023. **16**(4): p. 1562.

[9] Casazza, J. and F.J.U.E.P.S. Delea, *electric power systems.* 2004: p. 15-25.

[10] Shaik, D.K. *Difference between Active and Reactive Power*. SCRIBD, 2023.

[11] Alibi, A., *Contrôle des Réseaux Electriques par les Systèmes FACTS:(Flexible AC Transmission Systems)*. 2009, Université de Batna 2.

[12] MERAHI, A. *Analyse des réseaux de transport et de distribution I. Polycopié du cours UEF-ELTF 214.* Département de Génie Électrique, Ecole Supérieure en Génie Electrique et Energétique d'Oran (ESG2EO), Algérie., (2018/2019).

[13] Lilien, J., *Transport et distribution de l'énergie électrique. Cours donné à l'Institut d'Électricité Montefiore, Université de Liège*. 2013.

[14] Chiheb Eddine, Z.S., & Siradj Eddine , R. O. (n.d.). *Les Méthodes de l'écoulement de puissance.* . 2020/2021.

[15] Zohuri, B., *Gas Turbine Working Principles*. 2015. p. 147-171.

[16] Moniruzzaman, E., *Hydroelectric Power Generation system*. 2019.

[17] Mohamed Vall, M.A., & Chouki, M. (Encadreur). *Étude des systèmes facts (SVC) et de Leur comportement sur le contrôle des puissances et des tensions dans les Réseaux de transport.* Accueil de DSpace, 2021/2022.

[18] Sari, L., & Diabi, C *Étude d'un réseau de transport d'énergie à haute tension 90 kV (Master's thesis).* Université Badji Mokhtar, Annaba, Algérie., (2017).

[19] Mouassa, S. and T. Bouktir, *Optimisation de l'écoulement de puissance par une méthode métaheuristique (technique des abeilles) en présence d'une source renouvelable (éolienne) et des dispositifs FACTS*. 2012.

[20] Salhi, S. *Contribution to power flow optimization by enhanced artificial intelligence methods [Doctoral dissertation*. Mohamed Khider University of Biskra]. Mohamed Khider University Repository, (2023).

[21] Albadi, M., *Power Flow Analysis*. 2019.

[22] Sami Rashid, M. and S. Gheorghe, *Power Flow Analysis in Power System Planning. Case Study*. 2019. 142-146.

[23] Chakrabarti, K.C.a.A., *Soft Computing Techniques in Voltage Security Analysis*. 2015: Springer.

[24] Bouktir, T., *APPLICATION DE LA PROGRAMMATION ORIENTEE OBJET A L'OPTIMISATION DE L'ECOULEMENT DE PUISSANCE*. 2004.

[25] P. Venkatesh, B.V.M., S. Charles Raja, A. Srinivasan, *Electrical Power Systems: Analysis, Security and Deregulation*. 2012: PHI Learning Pvt. Ltd.

[26] Yao, Y. and M. Li, *Designs of Fast Decoupled Load Flow for Study Purpose.* Energy Procedia, 2012. **17**: p. 127–133.

[27] Saadat, H., *system analysis*. 1999, United States of America: Bobbi Simanjuntak.

[28] Afolabi, O., et al., *Analysis of the Load Flow Problem in Power System Planning Studies.* Energy and Power Engineering, 2015. **07**: p. 509-523.

[29] Khaled, D.G., *Modélisation et Optimisation des Réseaux Électriques*. 2021/2022, Esgee Oran.

[30] BELAYATI Abderraouf, B.M.A., Pr. A. KHELDOUN, *Power Flow Analysis For Ac Islanded Microgrids*. 2021, Université M'hamed Bougara - Boumerdes.

[31] Filbert Amigue, F., S. Ndjakomo Essiane, and A. Nelem, *Optimal Placement and Sizing of Distributed Energy Generation in an Electrical Network Using the Hybrid Algorithm of Bee Colonies and Newton Naphson.* Journal of Power and Energy Engineering, 2020. **08**: p. 9-21.

[32] Othmani Ali, k.M., Hebri.K, Chaalal.M, *Application des techniques d'optimisation dans un système électrique de puissance*. 2015/2016, Mémoire de Master, Université Ibn Khaldoun - Tiaret.

[33] BOUDOUANI Med Ryadh, K.N.-e., *Ecoulement de puissanceàcourant . Continue (DC)*. 2014-2015, Département du Génie Électrique et de l'Informatique, Université Dr YAHIA FARES MEDEA.

[34] Naoual KHATTAR, S.K., Dr. karim. SBAA & Abdelhalim. TLEMCANI, *Ecoulement de puissance optimal avec HVDC* (2016), [Mémoire de Master, Université Yahia Fares - Médéa].

[35] Djamel, S.H.L., *Amélioration de l'Ecoulement des Puissances à Travers les Systèmes FACTS Pour les Réseaux Electriques* 2019, [Thèse de Doctorat, Université Frères Mentouri - Constantine 1].

[36] Kapse, S.S.S., M.B. Diagavane, and N.G. Bawane. *A novel genetic algorithm approach to achieve steady state power flow solution*. in *2013 6th International Conference on Emerging Trends in Engineering and Technology*. 2013. IEEE.

[37] Islam, M.Z., et al., *Marine predators algorithm for solving single-objective optimal power flow.* PLOS ONE, 2021. **16**(8): p. e0256050.

[38] Nassef, A.M., M.A. Abdelkareem, and M. Louzazni, *Optimal power flow using recent red-tailed hawk optimization algorithm.* Results in Engineering, 2025. **25**: p. 104005.

[39] Frank, S., I. Steponavičė, and S. Rebennack, *Optimal power flow: a bibliographic survey I.* Energy Systems, 2012. **3**.

[40] Souhil, M., *Optimisation de l'écoulement de puissance par les méthodes non-conventionnelles dans les réseaux électriques intelligents (Smart Grid)* 2021, [Autre, Université Ferhat Abbas - Sétif 1].

[41] Abdelmadjid, A.A.D., *Optimisation et contrôle de l'écoulement de puissance dans réseau électrique*. 2020, [Mémoire de Master, Université Saad Dahleb - Blida].

[42] Berro, A., *Optimisation multiobjectifs et stratégies d'évolution en environnement dynamique*. 2001, ANRT [diff.].

[43] Nagi, A.O., *Optimisation De L'écoulement De Puissance Par Algorithmes : Ag Et Pso-tvac*. 2014, [Mémoire de Master, Université Mohamed Khider - Biskra].

[44] Nadia, B.H.H.A.M., *Application De L'algorithme D'optimisation Chaotique*. 2022, [Mémoire de Master, Université Saad Dahleb - Blida].

[45] Salhi, S., et al., *A novel hybrid approach based artificial bee colony and salp swarm algorithms for solving ORPD problem.* Indonesian Journal of Electrical Engineering and Computer Science, 2021. **23**: p. 1825_1837.

[46] Pany, P.K., S. Ghoshal, and V. Mukherjee. *Collective animal behavior algorithm for optimal reactive power dispatch problems*. in *2017 IEEE International Conference on Power, Control, Signals and Instrumentation Engineering (ICPCSI)*. 2017. IEEE.

[47] Nagarajan, K., P. a.k, and A. Rajagopalan, *Multi-Objective Optimal Reactive Power Dispatch using Levy Interior Search Algorithm.* International Journal on Electrical Engineering and Informatics, 2020. **12**: p. 547-570.

[48] Duong, T., et al., *Optimal Reactive Power Flow for Large-Scale Power Systems Using an Effective Metaheuristic Algorithm.* Journal of Electrical and Computer Engineering, 2020. **2020**: p. 1-11.

[49] Zhang, J., et al., *Using the Whale Optimization Algorithm to Solve the Optimal Reactive Power Dispatch Problem.* Processes, 2023. **11**(5): p. 1513.

[50] MANCER, N., *Contribution à l'optimisation de la puissance réactive en présence de dispositifs de compensation dynamique (FACTS)*. 2012, [Mémoire de Master, Université Mohamed Khider - Biskra].

[51] Chamba, A., C. Barrera-Singaña, and H. Arcos *Optimal Reactive Power Dispatch in Electric Transmission Systems Using the Multi-Agent Model with Volt-VAR Control*. Energies, 2023. **16**, DOI: 10.3390/en16135004.

[52] Villa-Acevedo, W.M., J.M. López-Lezama, and J.A. Valencia-Velásquez, *A Novel Constraint Handling Approach for the Optimal Reactive Power Dispatch Problem.* Energies (Basel), 2018. **11**(9): p. 2352.

[53] Elsayed, S.K., et al., *An improved heap-based optimizer for optimal reactive power dispatch.* 2021. **9**: p. 58319-58336.

[54] Mouassa, S., T. Bouktir, and A. Salhi, *Ant lion optimizer for solving optimal reactive power dispatch problem in power systems.* Engineering Science and Technology, an International Journal, 2017. **20**(3): p. 885-895.

[55] Tudose, A.M., et al., *Solving Single- and Multi-Objective Optimal Reactive Power Dispatch Problems Using an Improved Salp Swarm Algorithm.* Energies (Basel), 2021. **14**(5): p. 1222.

[56] Chandran, V. and P. Mohapatra, *A novel multi-strategy ameliorated quasi-oppositional chaotic tunicate swarm algorithm for global optimization and constrained engineering applications.* Heliyon, 2024. **10**(10): p. e30757.

[57] Haldurai, L., T. Madhubala, and R.J.I.J.C.S.E. Rajalakshmi, *A study on genetic algorithm and its applications.* 2016. **4**(10): p. 139-143.

[58] Mirjalili, S., *Genetic Algorithm*, in *Evolutionary Algorithms and Neural Networks: Theory and Applications*, S. Mirjalili, Editor. 2019, Springer International Publishing: Cham. p. 43-55.

[59] Lambora, A., K. Gupta, and K. Chopra. *Genetic Algorithm- A Literature Review*. in *2019 International Conference on Machine Learning, Big Data, Cloud and Parallel Computing (COMITCon)*. 2019.

[60] Katoch, S., et al., *A review on genetic algorithm: past, present, and future.* 2021. **80**: p. 8091-8126.

[61] Hachimi, H., *Hybridations d'algorithmes métaheuristiques en optimisation globale et leurs applications.* 2013.

[62] Mohamed, L., *Identification Des Paramètres De La Machine Asynchrone Triphasée*. 2011-2012, [Mémoire de Master, Université Saad Dahleb - Blida].

[63] KHALIFA, B.A.D.M., *Playing Tetris Using Genetic Algorithms* 2016 [Autre, Université M'hamed Bougara - Boumerdes].

[64] Chandran, V. and P. Mohapatra, *Enhanced opposition-based grey wolf optimizer for global optimization and engineering design problems.* Alexandria Engineering Journal, 2023. **76**: p. 429-467.

[65] TRAIKIA Oussama, D.A.R., *Design of Elliptic Antenna arrays using Gray wolf optimization*. 2018, [Autre, Université M'hamed Bougara - Boumerdes].

[66] Touabi, C. and H. Bentarzi, *Photovoltaic Panel Parameters Estimation Using Grey Wolf Optimization Technique.* 2022. **14**(1): p. 3.

[67] Muro, C., et al., *Wolf-pack (Canis lupus) hunting strategies emerge from simple rules in computational simulations.* Behavioural Processes, 2011. **88**(3): p. 192-197.

[68] Purushothaman, R., S. Rajagopalan, and G.J.A.S.C. Dhandapani, *Hybridizing Gray Wolf Optimization (GWO) with Grasshopper Optimization Algorithm (GOA) for text feature selection and clustering.* 2020. **96**: p. 106651.

[69] Teng, Z.-j., J.-l. Lv, and L.-w.J.S.c. Guo, *An improved hybrid grey wolf optimization algorithm.* 2019. **23**: p. 6617-6631.

[70] Amirsadri, S., et al., *A Levy flight-based grey wolf optimizer combined with back-propagation algorithm for neural network training.* 2018. **30**: p. 3707-3720.

[71] Hou, Y., et al., *Improved Grey Wolf Optimization Algorithm and Application.* 2022. **22**(10): p. 3810.

[72] Rizk-Allah, R.M., et al., *Enhanced Tunicate Swarm Algorithm for Solving Large-Scale Nonlinear Optimization Problems.* International Journal of Computational Intelligence Systems, 2021. **14**(1): p. 189.

[73] Krstić, M., B. Milenković, and Đ. Jovanović, *APPLICATION OF THE METAHEURISTIC TUNICATE SWARM ALGORITHM IN SOLVING APPLIED MECHANICS PROBLEMS.* Journal of Production Engineering, 2021. **24**: p. 31-34.

[74] Zheng, R., et al., *A Comprehensive Review of the Tunicate Swarm Algorithm: Variations, Applications, and Results.* Archives of Computational Methods in Engineering, 2025.

[75] Liu, G., et al., *MSHHOTSA: A variant of tunicate swarm algorithm combining multi-strategy mechanism and hybrid Harris optimization.* 2023. **18**(8): p. e0290117.

[76] Memon, A.S., et al., *Tunicate Swarm Algorithm based Optimized PID controller for automatic generation control of two area hybrid power system.* 2023. **45**(2): p. 2565-2578.

[77] Ajayi, O., R. Heymann, and E. Okampo. *Marine predators algorithm and tunicate swarm algorithm for power system economic load dispatch*. in *Proceedings of the 11th annual international conference on industrial engineering and operations management*. 2021. Singapore.

[78] Si, T., et al., *Opposition-based chaotic tunicate swarm algorithms for global optimization.* 2024. **12**: p. 18168-18188.

[79] Mahadevan, K. and P.S. Kannan, *Comprehensive learning particle swarm optimization for reactive power dispatch.* Applied Soft Computing, 2010. **10**(2): p. 641-652.

[80] Jamal, R., et al., *Solution to the deterministic and stochastic Optimal Reactive Power Dispatch by integration of solar, wind-hydro powers using Modified Artificial Hummingbird Algorithm.* Energy Reports, 2023. **9**: p. 4157-4173.

[81] Abd-El Wahab, A.M., et al., *An effective gradient jellyfish search algorithm for optimal reactive power dispatch in electrical networks.* 2025. **19**(1): p. e13164.

[82] Abd-El Wahab, A.M., et al., *Optimal Reactive Power Dispatch Using a Chaotic Turbulent Flow of Water-Based Optimization Algorithm.* 2022.

[83] Shaheen, M.A., et al., *A novel application of improved marine predators algorithm and particle swarm optimization for solving the ORPD problem.* 2020. **13**(21): p. 5679.

[84] Shaheen, M.A.M., H.M. Hasanien, and A. Alkuhayli, *A novel hybrid GWO-PSO optimization technique for optimal reactive power dispatch problem solution.* Ain Shams Engineering Journal, 2021. **12**(1): p. 621-630.

[85] Raj, S. and B.J.I.T.o.E.E.S. Bhattacharyya, *Reactive power planning by opposition-based grey wolf optimization method.* 2018. **28**(6): p. e2551.

[86] Kien, L.C., C.T. Hien, and T.T. Nguyen, *Optimal Reactive Power Generation for Transmission Power Systems Considering Discrete Values of Capacitors and Tap Changers.* 2021. **11**(12): p. 5378.

[87] Almutairi, S.Z., E.A. Mohamed, and F.F.J.M. El-Sousy, *A novel adaptive manta-ray foraging optimization for stochastic ORPD considering uncertainties of wind power and load demand.* 2023. **11**(11): p. 2591.

[88] Das, P., et al., *Optimal Reactive Power Dispatch and Demand Response in Electricity Market Using Multi-Objective Grasshopper Optimization Algorithm.* 2024. **12**(9): p. 2049.

[89] Shaheen, M.A.M., et al., *A Novel Application of Improved Marine Predators Algorithm and Particle Swarm Optimization for Solving the ORPD Problem.* 2020.

[90] Villa-Acevedo, W.M., J.M. López-Lezama, and J.A.J.E. Valencia-Velásquez, *A novel constraint handling approach for the optimal reactive power dispatch problem.* 2018. **11**(9): p. 2352.

[91] Anbarasan, P. and T. Jayabarathi. *Optimal reactive power dispatch problem solved by an improved colliding bodies optimization algorithm*. in *2017 IEEE International Conference on Environment and Electrical Engineering and 2017 IEEE Industrial and Commercial Power Systems Europe (EEEIC/I&CPS Europe)*. 2017. IEEE.

[92] Das, T., R. Roy, and K.K. Mandal. *Optimal reactive power dispatch based on modified JAYA algorithm*. in *2020 international conference on computer, electrical & communication engineering (ICCECE)*. 2020. IEEE.

[93] Londoño Tamayo, D.C., J.M. López Lezama, and W.M. Villa Acevedo, *Algoritmo de Optimización de Mapeo de Media Varianza Aplicado al Despacho Óptimo de Potencia Reactiva.* Inge CuC, 2021. **17**(1): p. 239-255.

[94] Wei, Y., et al., *Optimal reactive power dispatch using an improved slime mould algorithm.* Energy Reports, 2021. **7**: p. 8742-8759.

[95] Saddique, M.S., et al., *Optimal Solution of Reactive Power Dispatch in Transmission System to Minimize Power Losses Using Sine-Cosine Algorithm.* IEEE Access, 2022. **10**: p. 20223-20239.

[96] Shaheen, A.M., R.A. El-Sehiemy, and S.M.J.I.S.J. Farrag, *Integrated strategies of backtracking search optimizer for solving reactive power dispatch problem.* 2016. **12**(1): p. 424-433.

[97] Li, Z., et al., *Finding Solutions for Optimal Reactive Power Dispatch Problem by a Novel Improved Antlion Optimization Algorithm.* 2019. **12**(15): p. 2968.

[98] Yapici, H.J.E.O., *Solution of optimal reactive power dispatch problem using pathfinder algorithm.* 2021. **53**(11): p. 1946-1963.

[99] Aljohani, T.M., A.F. Ebrahim, and O. Mohammed, *Single and Multiobjective Optimal Reactive Power Dispatch Based on Hybrid Artificial Physics–Particle Swarm Optimization.* 2019. **12**(12): p. 2333.